



Nonlinear optics of liquid crystalline materials

Iam Choon Khoo *

Department of Electrical Engineering, 121 Electrical Engineering East, Pennsylvania State University, University Park, PA 16802, USA

ARTICLE INFO

Article history:

Accepted 28 January 2009
Available online 10 February 2009
editor: G.I. Stegeman

PACS:

42.65.-k
42.70.DF
42.65.Pc
42.79.-e

ABSTRACT

Liquid crystals occupy an important niche in nonlinear optics as a result of their unique physical and optical properties. Besides their broadband birefringence and transparency, abilities to self-assemble into various crystalline phases and to conform to various flexible forms and shapes, liquid crystals are compatible with almost all other optoelectronic materials and technology platforms. In both isotropic and ordered phases, liquid crystals possess extraordinarily large optical nonlinearities that stretch over multiple time scales. To date, almost all conceivable nonlinear optical phenomena have been observed in a very broad spectrum spanning the entire visible to infrared and beyond. In this review, we present a self-contained complete discussion of the optical nonlinearities of liquid crystals, and a thorough review of a wide range of nonlinear optical processes and phenomena enabled by these unique properties.

Starting with a brief historical account of the development of nonlinear optical studies of the mesophases of liquid crystals, we then review various liquid crystalline materials and structures, and their nonlinear optical properties. Emphasis is placed on the nematic phase, which best exemplifies the dual nature of liquid crystals, although frequent references to other phases are also made. We also delve into recent work on novel structures such as photonic crystals, metamaterials and nanostructures and their special characteristics and emergent properties. The mechanisms and complex nonlocal dynamics of optical nonlinearities associated with laser induced director axis reorientation, thermal, density, and order parameter fluctuations, space charge field formation and photorefractivity are critically reviewed as a foundation for the discussions of various nonlinear optical processes detailed in this paper.

© 2009 Elsevier B.V. All rights reserved.

Contents

1. Introduction and historical perspectives	222
2. Liquid crystals	227
2.1. Individual molecular electronic optical properties and birefringence	227
2.2. A survey of liquid crystalline materials	229
2.2.1. Nematics, cholesterics, and smectics	229
2.2.2. Dye doped and nanoparticle dispersed liquid crystals; metamaterials	230
2.2.3. Polymer dispersed liquid crystals	233
2.3. Liquid crystal cells and structures – Traditional and ‘exotic’	234
2.4. Liquid crystal optically addressed spatial light modulator [OASLM]	236
3. Optical nonlinearities of nematic liquid crystals	237
3.1. An introduction to nematogen theories – Order parameter, free energies and optical dielectric constants	237
3.2. Laser induced molecular reorientations in the isotropic phase – Ordinary optical nonlinearity	240

* Tel.: +1 814 8632299; fax: +1 814 8657065.

E-mail address: ick1@psu.edu.

3.3.	Steady State Laser induced molecular reorientations in the nematic phase – Giant optical nonlinearity	242
3.3.1.	More exact treatment – Plane wave and Gaussian laser beam; nonlocal dependence	243
3.3.2.	Director axis reorientation by pulsed lasers – Onset and relaxation dynamics	244
3.4.	Giant, supra and colossal orientational optical nonlinearities in doped nematic liquid crystals.....	246
3.5.	Photorefractivity in nematic liquid crystals.....	248
3.6.	Optical nonlinearities associated with order parameter changes, thermal and density effects	251
4.	Nonlinear optical phenomena observed in liquid crystals.....	252
4.1.	Self-phase modulation, focusing, defocusing and spatial solitons	252
4.2.	Stimulated orientation scatterings – Nonlinear dynamics	253
4.2.1.	Steady-state SOS	253
4.2.2.	Stimulated orientational scattering – Nonlinear dynamics	255
4.2.3.	Stimulated thermal scattering (STS)	257
4.3.	Optical wave mixing and image processing.....	257
4.4.	Passive optical switching – Laser hardening and optical limiting.....	260
4.5.	Concluding remarks and outlook.....	262
	Acknowledgements.....	262
	References.....	263

1. Introduction and historical perspectives

Once just some naturally occurring curious and colorful substances, liquid crystals (LCs) have now grown to be a major class of scientifically intriguing and technologically important materials. A good historical account of their discoveries dating back to 1888 [1], and subsequent technological advancements leading to present day worldwide utilization of liquid crystal displays may be found in [2]. Just as their semiconductor counterpart, liquid crystals possess wonderful electronics and optical properties by virtue of their molecular constituents and the myriad of physical mechanisms at work. One of the most fascinating properties is their ability to self-assemble into various phases that exhibit properties and responses not possible in crystals or liquids, while possessing all the fluid and solid state crystalline properties [3–6].

Among the three principal types of liquid crystals, namely, thermotropics, polymerics and lyotropics, perhaps the most widely investigated are thermotropic liquid crystals. As a function of temperature, they self-assemble in various ordered arrangement of their crystalline axis, the so-called director axis \mathbf{n} , c.f. Fig. 1.1. In nematics, \mathbf{n} has directional order but no position order; in cholesterics, which are also termed chiral nematics, \mathbf{n} spirals around an axis with a pitch; in smectic phases, \mathbf{n} exhibits layered structures with \mathbf{n} either normal to the layer as in smectic-A, or oriented at an oblique angle as in smectic-C or ferroelectrics. As a function of temperatures, these phases are manifested usually in the order solid-smectic-nematic-isotropic phases.

Situated between the highly ordered solid-smectic and the disordered isotropic phase, the crystalline axes of nematics are most susceptible to perturbation by external fields, resulting in their exceptional light scattering abilities. Light scatterings by dielectric constant changes associated with director axis fluctuations in nematic liquid crystals are many orders of magnitude stronger than all other mechanisms. As we will see presently, these unique characteristics are also responsible for the largest optical nonlinearities known to date. Since the underlying theoretical frameworks are quite similar [3–6], and the bulk of nonlinear optics studies have been conducted in nematics, this report is devoted mainly to this phase, but references and comparison to other phases will be made wherever possible.

Fig. 1.2 illustrates a typical light scattering geometry in which an incident polarized light wave with a wave vector \mathbf{k}_i is scattered into an orthogonally polarized outgoing wave with a wave vector \mathbf{k}_f . These cases naturally arise in aligned nematic liquid crystals for ordinary or extraordinary polarized incident light, where the director axis fluctuations depolarize the incident wave. For a uni-axial birefringent medium such as a liquid crystal, the dielectric constant tensor may be written as

$$\varepsilon_{\alpha\beta} = \varepsilon_{\perp} \delta_{\alpha\beta} + (\varepsilon_{\parallel} - \varepsilon_{\perp}) n_{\alpha} n_{\beta} \quad (1.1)$$

where n_{α} and n_{β} are the components of a unit vector \hat{n} along the optical axis. (In liquid crystals \hat{n} is the director axis.). Fluctuations in $\varepsilon_{\alpha\beta}$ arise from changes in ε_{\perp} and ε_{\parallel} due to density and temperature fluctuations and from fluctuations in the orientation of \hat{n} . Specifically, the differential scattering cross-sections $d\sigma/d\Omega$ for polarized incident light waves can be shown to be given by [3]:

$$\frac{d\sigma}{d\Omega} = \left(\frac{\Delta\varepsilon\omega^2}{c^2} \right)^2 V \sum_{\alpha=1,2} \frac{k_B T}{k_3 q_3^2 + k_{\alpha} q_1^2} \left[f_{\alpha} (\hat{i} \cdot \hat{n}_0) + i_{\alpha} (\hat{f} \cdot \hat{n}_0) \right]^2. \quad (1.2)$$

Here $\Delta\varepsilon$ is the dielectric anisotropy, k_B the Boltzmann Constant, $k_{1,2,3}$ are the elastic constants and q the scattering wave vectors, and \hat{i} and \hat{f} are the incident and outgoing optical field polarization directions.

On the other hand, in the liquid phase, i.e. in anisotropic fluids, light scattering is caused by density fluctuations. Denoting the average dielectric constant in the isotropic phase by ε and denoting the local change in the volume by $u(r)$, the dielectric

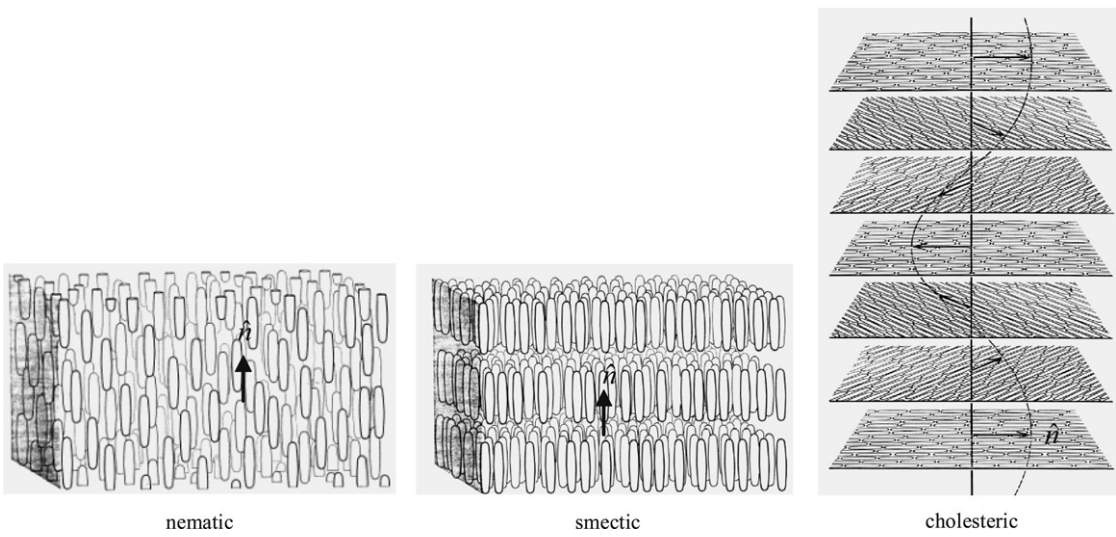


Fig. 1.1. Spatial arrangement of the director axis n in the nematic, cholesteric and smectic phases of thermotropic liquid crystals.

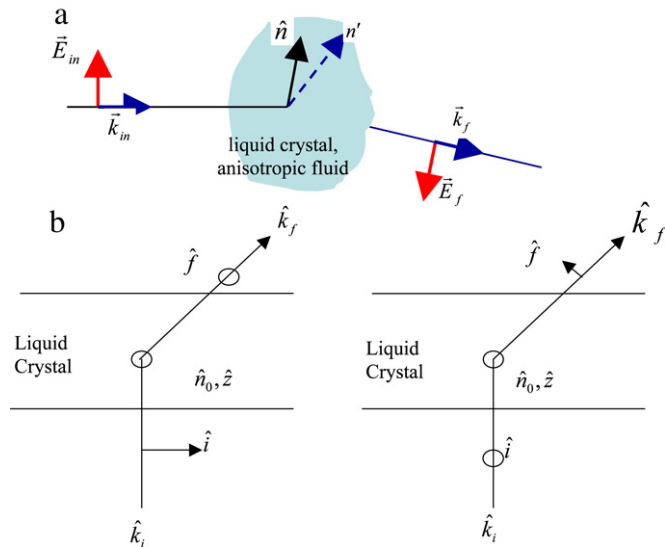


Fig. 1.2. Schematic depiction of two typical polarized light scattering in liquid crystals for the two cases (a) and (b) where the incident and scattered light are cross polarized.

constant can be written as:

$$\begin{aligned} \varepsilon &= \bar{\varepsilon} + \frac{d\varepsilon}{dV} u(\mathbf{r}) \\ &= \bar{\varepsilon} + \varepsilon' u(\mathbf{r}). \end{aligned} \quad (1.3)$$

The differential scattering cross-section is then of the form:

$$\left(\frac{d\sigma}{d\Omega} \right)_{iso} = V \left(\frac{\varepsilon' \omega^2}{c^2} \hat{f} \cdot \hat{i} \right)^2 \frac{k_B T}{W}. \quad (1.4)$$

The extraordinary light scattering abilities of nematics become crystal clear when we compare the two scattering cross-sections (1.1) and (1.3). Denoting the ratio of $d\sigma/d\Omega$ (nematic) from (1.2) to $d\sigma/d\Omega$ (isotropic) from (1.4) by σ_R , we arrive at a highly informative expression:

$$\sigma_R \sim \frac{\Delta\varepsilon}{\varepsilon'} \frac{W}{Kq^2}. \quad (1.5)$$

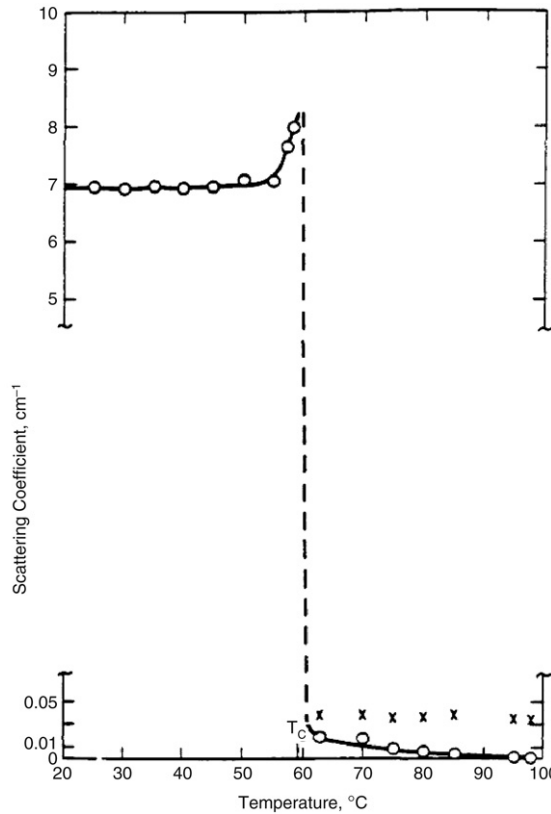


Fig. 1.3. Scattering coefficients of the liquid crystal E7 below and above the nematic–isotropic phase transition temperature T_c [after Khoo and Wu Ref. [6]].

Since $1/q \sim \lambda$ (optical wavelength), and $\Delta\epsilon/\epsilon' \sim 1$, $K \sim u/a$, $W \sim u/a^3$, we have $\sigma_R \sim (\lambda/a)^2 \sim 10^6$ for $\lambda \sim 5000 \text{ \AA}$ and $a \approx \text{a few \AA}$. In other words, the light scattering abilities of nematic liquid crystals are a million fold better than an anisotropic fluid, c.f. Fig. 1.3 which shows experimentally observed scattering coefficients of a widely used nematic liquid crystal E7 below and above T_c .

The easy susceptibilities of the director axis to external perturbations, leading to their extraordinary linear light scattering abilities, also apply to nonlinear optical scattering processes where the director axis fluctuations are caused by the optical electric field. Since the scattering process is nonlinearly dependent on the electric field intensity, one would expect that the nonlinear orientational optical responses of nematic liquid crystals to be many orders of magnitude larger than those obtainable from anisotropic fluids. As the following analysis would show, the nonlinear index coefficient characterizing a standard nonlinear optical effect, namely, the Kerr effect, is a trillion times larger than those obtainable in anisotropic fluids.

Consider a typical polarized light-LC interaction as depicted in Fig. 1.4. The energy density involved in reorienting the LC axis by an angle θ is given by:

$$U \approx K \left(\frac{\partial \theta}{\partial x} \right)^2 L \quad (1.6)$$

where L is the interaction length and K the LC elastic constant. In a wave mixing type of interaction geometry which leads to an interference pattern with periodicity Λ , the reorientation angle θ is of the form

$$\theta = \theta_0 \sin(qx) \quad (1.7)$$

where $q = 2\pi/\Lambda$. Therefore, we have

$$U_{LC} \sim 4K\pi^2\theta^2L/\Lambda^2. \quad (1.8)$$

On the other hand, the energy provided by the light beam is of the form:

$$E_{\text{light}} = I\tau(1 - e^{-\alpha L}) \sim \alpha L I \tau \quad (1.9)$$

where α is the light energy loss coefficient [associated with the light induced mechanisms that lead to an eventual reorientation of the director axis], and τ the response time. Writing $\eta E_{\text{light}} = U_{LC}$, i.e., assuming a conversion efficiency η of absorbed light energy to achieving reorientation, we get

$$K\pi^2\theta^2/\Lambda^2 \approx \eta\alpha L I \tau. \quad (1.10)$$

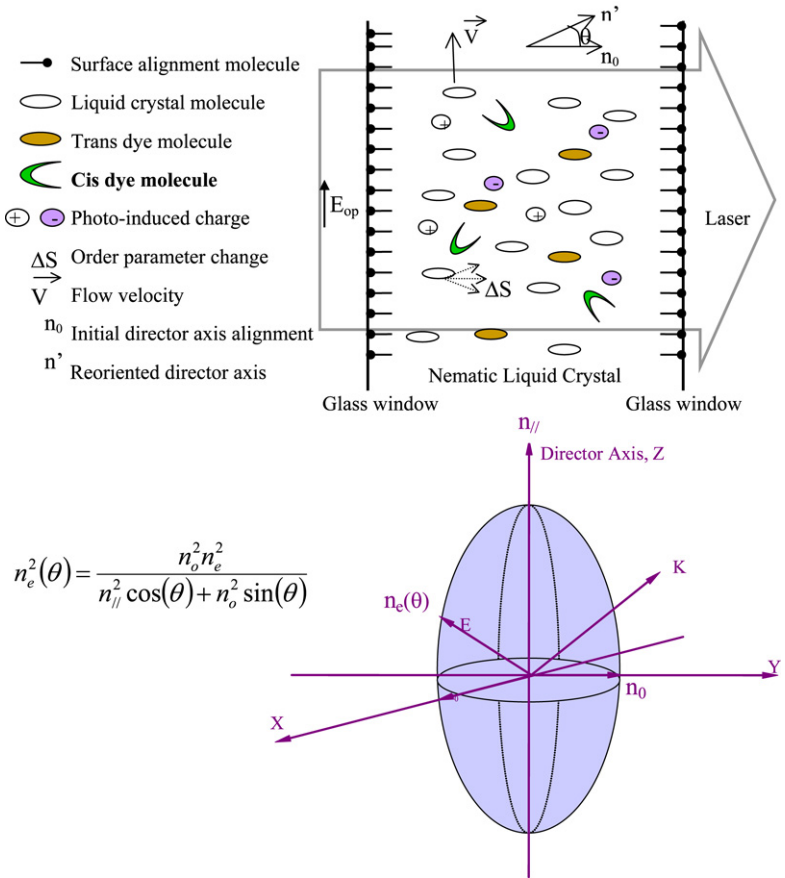


Fig. 1.4. Schematic depiction of the interaction of a polarized laser with the director axis of a nematic liquid crystal. Figure below shows the index ellipsoid for an extraordinary wave with a propagation wave vector k in an aligned nematic liquid crystal.

For an interaction geometry as depicted in Fig. 1.2, the change in index experienced by an incident e-wave

$$\Delta n \sim (n_e - n_0)\theta^2 \sim \eta(n_e - n_0)I\tau\alpha\Lambda^2/4\pi^2K. \quad (1.11)$$

Writing $\Delta n = n_2 I$ yields the nonlinear index coefficient n_2 :

$$n_2 \sim \eta(n_e - n_0)\tau\alpha\Lambda^2/4K\pi^2. \quad (1.12)$$

From (1.12), one may define a Figure of Merit $n_2/\alpha\tau$:

$$n_2/\alpha\tau \sim \eta(n_e - n_0)\Lambda^2/4K\pi^2. \quad (1.13)$$

For nematic liquid crystals, typical τ is on the order of 10's of millisecond (10^{-2} s), $\Lambda \sim 40 \mu\text{m}$ (the grating constant in a typical wave mixing process), elastic constant $K \sim 10^{-7} \text{ erg/cm}$, anisotropy $(n_e - n_0) \sim 0.2$, $\alpha \sim 100 \text{ cm}^{-1}$, $\eta \sim 1$ and we have $n_2 \sim 1 \text{ cm}^2/\text{W}$ [7]. This is more than 10 trillion times (10^{14}) larger than the orientation nonlinearity of anisotropic fluids such as CS_2 , the n_2 of which is $\sim 10^{-14} \text{ cm}^2/\text{W}$ [8].

The nonlinear coefficient n_2 given in (1.12) shows that such orientation mediated optical nonlinearity is primarily governed by the liquid crystalline birefringence $\Delta n = n_e - n_0$, the elastic constant K , the interaction geometry characterized by Λ , the actual nonlinear optical scattering processes characterized by the response time τ and the light conversion efficiency η . As a truly unique gift from nature, nematic liquid crystals possess the smallest elastic constants K , and the largest birefringence Δn among all known materials. Furthermore, the large birefringence spans the entire visible-infrared spectrum and beyond [5,6,9], c.f. Fig. 1.5. By virtue of their organic nature, they can be chemically synthesized and processed on a very large scale; they are also compatible with almost all technologically important optoelectronic materials, thus making them one of the most versatile and widely used optical materials.

Although such light scattering capabilities of nematics and the underlying physical theories had already been established in the late 60s, studies of laser induced molecular orientation processes conducted in the 70s were largely focused on isotropic phase liquid crystals [10,11], which behave like anisotropic fluids such as CS_2 . During this period, there were a few optics studies of the ordered mesophases (nematics and smectics) but they were centered on the small electronic

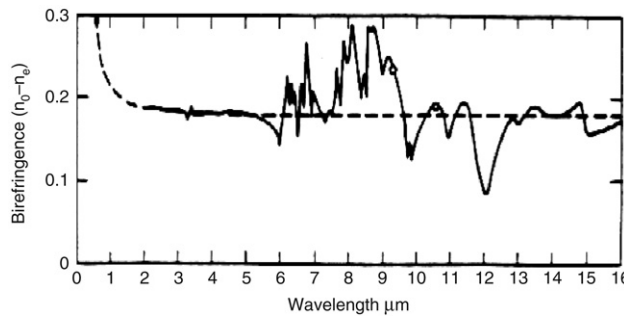


Fig. 1.5. Ultra-broadband birefringence of a typical nematic liquid crystal.

optical nonlinearities and anisotropies for harmonic generation [12–14]. In the studies of laser induced reorientations in the isotropic phase, it was observed that the nonlinear optical response increases dramatically as the temperature is lowered towards the phase transition temperature. Although this was a very obvious indication that on the other side of T_C , i.e. in the liquid crystal phase, an enormous optical nonlinearity awaited, it was not until 1979 and the early 80s that the giant optical nonlinearities of liquid crystals made their debut in several pioneering theoretical and experimental works [15–20].

A first quantitative theoretical calculation on the possibility of observing giant optical nonlinearity was presented in the work by Herman and Serinko [15] in 1979. These authors theorized that if the director axis of the nematic liquid crystals is pre-tilted by an external bias field, i.e. above the Freedericksz transition [3–6], it can be further reoriented by the optical electric field to result in a change in the effective refractive index. This process was confirmed in the nonlinear optical wave mixing study by Khoo [16] where a magnetic field is employed to create the Freedericksz transition. At about the same time, it was also recognized that the process can be enabled by a purely optical field since the frequency of the applied field is not involved in the interaction; the reorientation is dependent on a quadratic function of the applied fields, i.e., involving such terms as $\Delta\chi_m H^2$, $\Delta\epsilon_{ac} E^2$, $\Delta\epsilon_{op} E_{op}^2$, where $\Delta\chi_m$, $\Delta\epsilon_{ac}$, $\Delta\epsilon_{op}$ are the magnetic, ac dielectric and optical anisotropies, respectively. This is the central premise underlying the pioneering studies [17–20] of optically induced director axis reorientation that ushered in the era of the so-called Giant Optical Nonlinearities (GON) characterized by n_2 on the order of 10^{-4} – 10^{-3} cm²/W. A great deal of theoretical and experimental work immediately followed (see exemplary references quoted in the following sections), involving pure or specially doped liquid crystals with or without the use of external bias fields, and the observed nonlinearities approached 10^{-1} cm²/W in the next decade [see for example [21–23]]. A dramatic breakthrough occurred with the discovery of excited-dye (Methyl-Red)-assisted director axis reorientation [7], where the observed optical nonlinearity n_2 is $\gg 1$ cm²/W and is termed Supra Optical Nonlinearity (SON). The nonlinearity of Methyl-Red doped nematic liquid crystals was later measured to be $> 10^3$ cm²/W [24].

Paralleling these discoveries of giant and supra-optical nonlinearities, a host of nonlinear optical phenomena [5], old and new, have been observed or investigated, bringing forth at each juncture new definitions of ‘low optical thresholds’ as the laser powers involved precipitously dropped from kilowatt levels to micro- and nano-Watts. Almost all nonlinear optical processes have been observed in liquid crystalline media, including transient and steady state degenerate and non-degenerate wave mixings, optical bistabilities and instabilities, self-focusing and self-guiding, phase conjugation, stimulated scatterings, optical limiting, interface switching, beam combining and self-starting laser oscillations. With this review, we attempt to present a critical timely exposition of the unique material and physical properties of liquid crystals that mediate these novel nonlinear optical processes in established nonlinear optics ‘platforms’ as well as newly emergent fields such as nano and metamaterial sciences.

We close this section with some further remarks on another special aspect of liquid crystals as a preferred material for nonlinear optics applications. In their pure impurity- and moisture-free form, besides being transparent and chemically and physically stable, they are excellent laser-hardened materials capable of handling very intense pulsed lasers or continuous wave lasers. Studies have shown that common liquid crystals such as 5CB and E7 can withstand nanosecond laser pulses of over 10 J/cm² (corresponding to an intensity in excess of 10^{10} W/cm²), thus making them particularly useful for constructing high power laser optics such as polarization rotators, wave plates, optical isolators and laser blocking notch filters [25]. Pure nematic liquid crystals are also hardened against high power cw lasers; prolonged illumination of the liquid crystals with laser intensity of several kiloWatt/cm² does not produce any structural/chemical damages.

In Table 1, we list some of the observed nonlinearities of nematic liquid crystals, and compare and contrast them with other classes of materials [semiconductors and polymers] in which sizeable optical nonlinearities have also been observed [26–30]. It is to be noted that these tables of values are meant for quick reference purposes only, rather than as benchmarks for promoting one class of materials over the other. In nonlinear optics, nonlinearities are often expressed in terms of the nonlinear susceptibilities $\chi^{(n)}$; a laser induced intensity dependent refractive index change is associated with a third order nonlinear polarization of the form $P_{NL} = \chi^{(3)} EEE$, where $\chi^{(3)}$ is the third order nonlinear susceptibility. Because of the multitude of conventions and systems of units used in nonlinear optics, it is useful to note here that n_2 (in cm²/W) = $0.158\chi_{cgs}^{(3)}/n_o^2$; also, $\chi^{(3)}SI^{(3)}(m^2/V^2) = 1.39 \times 10^{-8}\chi_{cgs}^{(3)}$. From (1.13), we can also define a Figure of Merit (FOM) in

Table 1

Nonlinear refractive index coefficients of liquid crystals and some optoelectronics materials.

Materials	Order of magnitude of n_2 (cm^2/W)
Nematic liquid crystal	
Purely optically induced	$\sim 10^{-4}\text{--}10^{-3}$
Thermal and order parameter change	$\sim 10^{-5}\text{--}10^{-3}$
Excited dopant (dye molecule) assisted	$\sim 10^{-1}\text{--}10^{-3}$
Photorefractive – C60 doped	$\sim 10^{-3}\text{--}10^{-2}$
Methyl-red doped	$\sim 1\text{--}2000$
Azobenzene LC (BMAB) doped NLC	$> 10^{-2}\text{--}10^{-1}$
C60/nanotube doped film	$> 10^{-2}\text{--}10^{-1}$
OASLM-LC [estimated]	$\sim 10\text{--}200$
Electronic non-resonant nonlinearities	$\sim 10^{-13}\text{--}10^{-12}$
GaAs bulk [Ref. [26]]	$\sim 10^{-5}$
GaAs Multiple Quantum Well MQW [Ref. [27]]	$\sim 10^{-3}$
Photorefractive crystals/polymers [Refs. [28,29]]	$\sim 10^{-4}$
Bacteriorhodopsin [Ref. [30]]	$\sim 10^{-3}$

Table 2Switching efficiency $\chi^{(3)}/\alpha\tau$ of various materials.

Materials [Ref.]	$\chi^{(3)}/\alpha\tau$ ($10^{-10} \text{ m}^3 \text{ V}^{-2} \text{ s}^{-1}$)
GaAs bulk	30
GaAs MQW	300
Bacteriorhodopsin	0.05
Photorefractive crystals/polymers	10^{-1}
methyl-red doped LC film	> 100
C60/nanotube doped LC film	> 100
OALC SLM	> 100

terms of $\chi^{(3)}$:

$$\chi^{(3)}/\tau\alpha \sim \eta(n_e - n_o)n_o^2 n^2 \Lambda^2 / 4\pi^2 K. \quad (1.14)$$

As an example, For MRNLC, $\alpha = 150 \text{ cm}^{-1}$, $\tau = 10 \text{ ms}$, $\chi^{(3)} = 3.13 \times 10^{-6} (\text{m}^2/\text{V}^2)$, so $\chi^{(3)}/\alpha\tau = 209 (10^{-10} \text{ m}^3 \text{ V}^{-2} \text{ s}^{-1})$. Needless to say, the response times in all cases depend on the many factors involved such as the particular liquid crystal mesophases and dopants, ambient temperatures, interaction configurations, optical intensity, etc. Therefore the FOM values quoted in Table 2 are merely to serve as a quick general guide there. Also, for some applications such as telecommunication signal processing that require very short laser pulses, slower response materials are completely ruled out, even if the switching efficiency may be much higher than those of other optoelectronics materials. On the other hand, for visualization, display and other image processing purposes, a frame speed of 1 kHz is quite adequate.

2. Liquid crystals

2.1. Individual molecular electronic optical properties and birefringence

Liquid crystals are rodlike organic compounds. Fig. 2.1 depicts the molecular structure of a widely studied nematic liquid crystal 5CB (pentyl-cyano-biphenyl); it is comprised of a side chain with two or more aromatic rings, connected by linkage groups, and at the other end connected to a terminal group. More complex liquid crystals such as the banana-shaped LC and 'shuttle-cock' photosensitive LC depicted in Fig. 2.2 are but a few examples of the immense possibilities and variations afforded by chemical synthesis [31,32]. Physical properties of liquid crystals such as dielectric constants, elastic constants, viscosities, absorption spectra, phase transition temperatures, conductivity, photosensitivities and various optical properties are largely dictated by these constituent molecules.

Quantum chemical/physical theories for their optical properties are now fairly well established [33]. Since most liquid crystals are aromatic compounds, containing one or more aromatic rings, the energy levels or orbitals of aromatic rings play a major role. In particular, the $\pi \rightarrow \pi^*$ transitions in a benzene molecule correspond to the absorption of light in the near-UV spectral region ($\leq 200 \text{ nm}$) whereas the $\sigma \rightarrow \sigma^*$ transitions in liquid crystals containing saturated cyclohexane rings or bands correspond to absorption of light of shorter wavelength ($\leq 180 \text{ nm}$). In general, therefore, most liquid crystals are quite absorptive in the UV region; the linear absorption coefficient α is on the order of 10^3 cm^{-1} . Many liquid crystals are transparent in the visible and near-infrared regime (i.e., from $0.4 \mu\text{m}$ to $3 \mu\text{m}$). Further into the near-infrared ($\sim 3\text{--}5 \mu\text{m}$) and the infrared (e.g., $9 \mu\text{--}12 \mu\text{m}$), molecular rotational/vibrational transitions dominate, resulting in some strong absorption bands in these spectral regimes, with $\alpha \sim 10^2 \text{ cm}^{-1}$ c.f. Fig. 2.2.

Outside the far-infrared regime, e.g. in the 20–60 GHz microwave region, the birefringence of liquid crystals is still sizeable [9]; for a typical liquid crystal such as E7, the dielectric permittivities for extraordinary and ordinary waves have

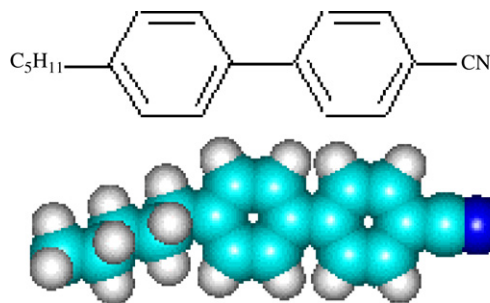


Fig. 2.1. Molecular structure of a typical liquid crystal – Pentyl-Cyano-Biphenyl 5CB.

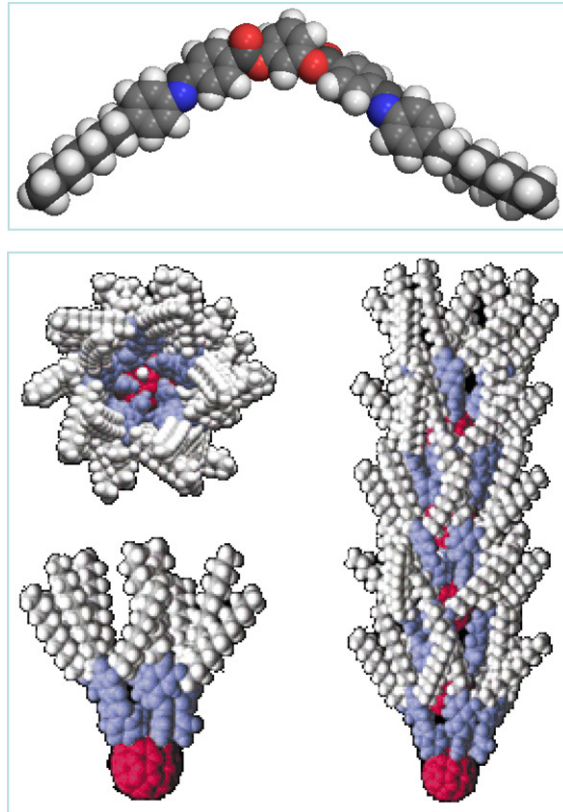


Fig. 2.2. Schematic depictions of the constituent molecules for (upper) 5CB, (middle) banana-shaped LC and (lower) 'shuttle-cock' LC.

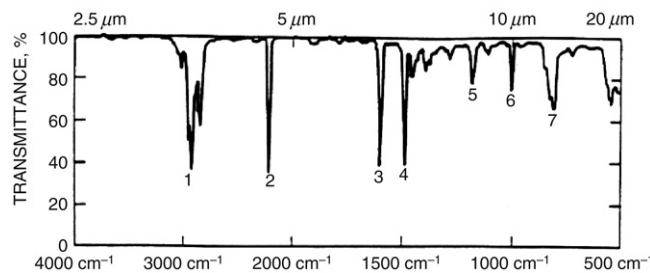


Fig. 2.3. Transmission spectra of nematic liquid crystals 5CB.

been measured to be $\varepsilon_e = 3.17$ [refractive index $n_e = 1.78$] and $\varepsilon_0 = 2.72$ [refractive index $n_0 = 1.65$], respectively, i.e. a birefringence $\Delta n \sim 0.13$. Such birefringence has been employed in recent studies of tunable negative permeability metamaterials in the microwave regime [34] (Fig. 2.3).

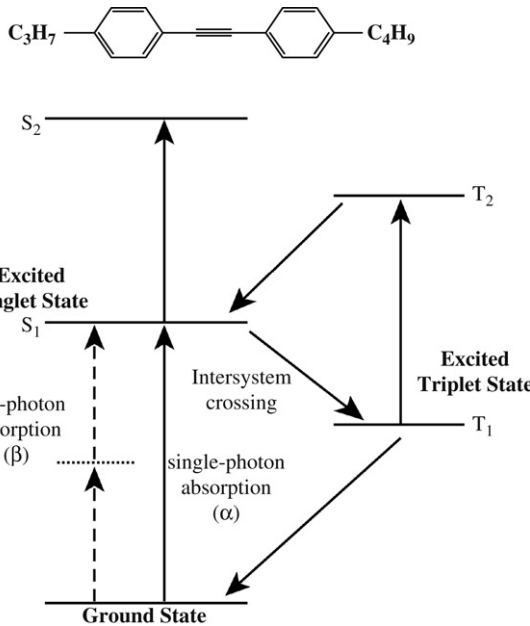


Fig. 2.4. Molecular level structure of a two-photon and excited state absorbing organic molecule. Inset shows the molecular structure of L34 [spell out the name].

Besides linear absorption, in recent years considerable interests have been focused on multi- or multiple-photon transition processes occurring in organic molecules [35–38], including liquid crystals [39,40]. Fig. 2.4 depicts the molecular structure of a room-temperature isotropic liquid crystal L34 (abbreviated name for 4-propyl4'-butyl diphenyl acetylene) that has been demonstrated in recent studies [41] to be an excellent neat liquid for optical limiting applications against visible nanosecond laser pulses. Just as other organic materials, L34 is transparent in the visible–near-infrared regime [400–1200 nm]. However, it possesses strong two-photon transitions in the visible spectrum to the S_1 , and more importantly, an excited state manifold capable of strong excited state linear absorption following the two-photon excitation from the ground state to the S_2 , c.f. Fig. 2.4. Such molecular electronic photonic energy level structures, quite commonly found in most liquid crystals and organic molecules, are highly desirable for extending the dynamic range of nonlinear absorption and optical limiting applications against sub-picosecond–nanosecond lasers [35–38,41].

2.2. A survey of liquid crystalline materials

2.2.1. Nematics, cholesterics, and smectics

Thermotropic liquid crystals are the most extensively studied LCs for their extraordinary linear, electro-optical and nonlinear optical properties. They exhibit various liquid crystalline phases as a function of temperature. In the continuum theory, their complex molecular structures are represented as rigid rods; these rigid rods interact with one another and form distinctive ordered structures [3–6]. Thermotropic liquid crystals can exhibit three mesophases: nematic, cholesteric, and smectic. In the nematic phase, the rodlike molecules are aligned in a general direction defined by a crystalline \hat{n} , which is often called the “director” axis; they are otherwise positionally random, very much like liquids. In fact, nematic liquid crystals flow like anisotropic liquids, with the flow dynamics controlled by various viscosity coefficients. Generally, nematic liquid crystals exhibit centro-symmetry on a macroscopic scale; their physical properties are the same in the $+\hat{n}$ and $-\hat{n}$ directions. In other words, if the individual molecules carry a permanent electric dipole (which most nematic liquid crystal molecules do), they will assemble in such a way that the bulk dipole moment vanishes.

Cholesterics are chiral nematic liquid crystal; they resemble nematic liquid crystals in all physical properties except that the molecules are aligned in a helical manner as depicted in Fig. 1.1(b). This property results from the synthesis process in which a chiral molecule is added to the nematic liquid crystal molecule. As a result of the 1D spatially periodic variation in the dielectric constant, the dispersion $w(\mathbf{k})$ exhibits bandgaps and other interesting and useful photonic crystal properties. Recent studies of cholesterics in the context of chiral photonic crystals, with or without defects, and cholesteric liquid crystal lasers are but a few examples of how these chiral structures have enabled novel nonlinear optical processes and photonic devices [42–48].

Smectic liquid crystals, unlike nematics, possess positional order. Several sub-phases of smectics have been “discovered”, differing in the arrangement or ordering of the molecules and their structural symmetry properties (3–6), c.f. Fig. 2.5. Besides smectic-A phase in which the director axis is normal to the layer, there are many other variations corresponding to smectic

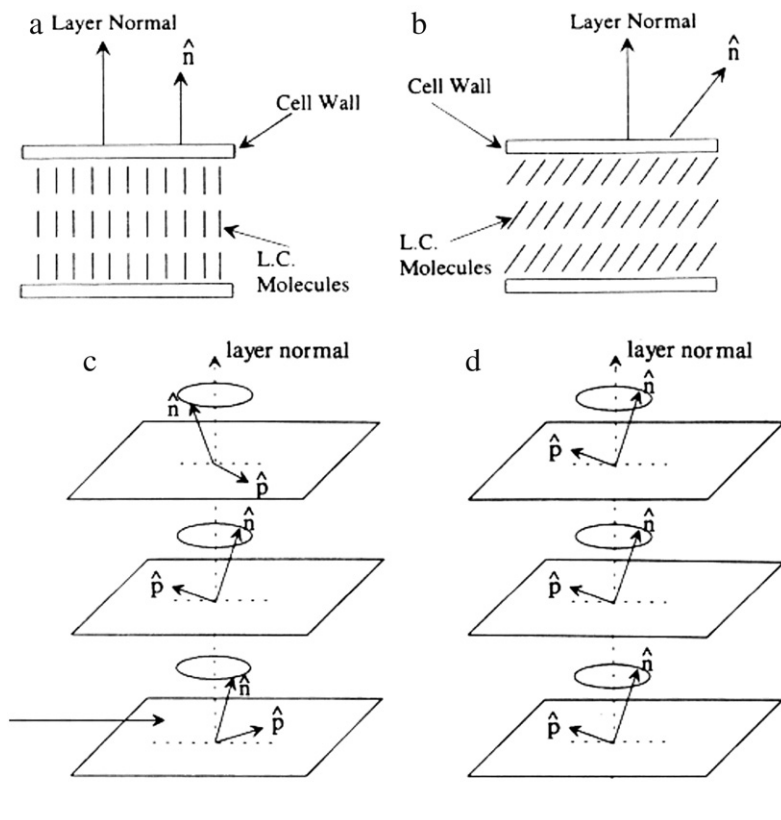


Fig. 2.5. Director axis orientation of various liquid crystalline phases.

phases C, C* or ferroelectric, G, H, I, F...Q, to name a few [3–6]. Similar to nematics, smectic-A liquid crystals are optically uniaxial; that is, there is a rotational symmetry around the director axis. The smectic-C phase is different from the smectic-A phase in that the material is optically biaxial, and the molecular arrangement is such that the long axis is tilted away from the layer normal \hat{z} , cf. Fig. 2.5.

In smectic-C* liquid crystals, the director axis \hat{n} is tilted away from the layer normal \hat{z} and “precesses” around the \hat{z} -axis in successive layers. This is analogous to cholesterics and is due to the introduction of optically active or chiral molecules to a smectic-C liquid crystal. Smectic-C* liquid crystals possess a spontaneous electric polarization \hat{p} ; if the helical structure is unwound and \hat{n} points in a fixed direction, as in Fig. 2.5(d), then \hat{p} will point in one direction [49]—this breaks the centro-symmetry. Clearly, this and other director axis reorientation processes are accompanied by considerable change in the optical refractive index and other system properties, and they can be utilized in practical electro- and opto-optical (nonlinear optical) modulation processes [6]. Such ‘broken symmetry’ is also necessary for second order nonlinear optical processes such as second harmonic generation [50–52]; nematics with a strong dc field to break the $+\hat{n}$ and $-\hat{n}$ symmetry, and ferroelectric [smectic-C*] liquid crystals have been studied for their second harmonic generation capabilities.

2.2.2. Dye doped and nanoparticle dispersed liquid crystals; metamaterials

While pure and transparent nematic liquid crystals are the preferred materials for linear and electro-optical applications, nonlinear optics frequently requires photosensitivity which is usually provided by appropriate doping of the liquid crystals. Perhaps the most frequently employed dopants are dye molecules. Dichroic dyes such as Methyl-red tend to disperse themselves in aligned nematic liquid crystals with their long axis parallel to the director axis. As a result, the sample will exhibit strong absorption anisotropies as exemplified in Fig. 2.6. Such absorption anisotropy underlies the supra-optical nonlinearities observed in methyl-red doped nematics [7,24] and other extremely nonlinear optical responses [53–62]. Some dyes, when excited, will produce the space charges and local fields necessary for enabling photorefractivity in liquid crystals; they could also give rise to intermolecular torques that enhance the optical reorientation efficiency of the liquid crystal director axis. Another effect of an azodye is to facilitate changes in the order parameter through laser excited conformational changes such as Trans–Cis isomerism and the resulting intermolecular interactions leading to disorder in the liquid crystal host.

Besides dye molecules, other dopants such as Fullerene C₆₀, carbon nanotubes, electron-donor and electron-acceptor groups, gold and silver nanospheres and other nanoparticulates of various shapes and forms have also been employed to

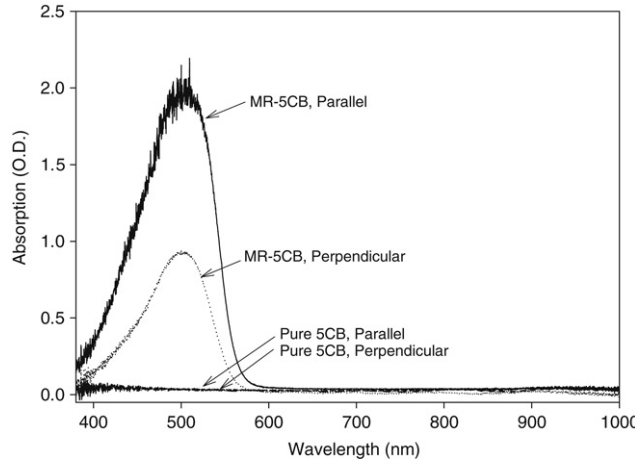


Fig. 2.6. Methyl-red dye doped 5CB absorption spectrum for light polarized along and perpendicular to the director axis.

create *metamaterials* that possess emergent properties and new functionalities [62–69]. In particular, these metamaterials can exhibit refractive indices which are sub-unity, zero and negative. As derived in [68], the complex refractive index n of a metamaterial can be expressed in terms of the complex permittivity ε_r and permeability μ_r by:

$$n = \text{sign} \left[\cos \left(\frac{\theta_\varepsilon - \theta_\mu}{2} \right) \cos \left(\frac{\theta_\varepsilon + \theta_\mu}{2} \right) \right] \sqrt{\varepsilon_r \mu_r} = \text{sign} (\cos \theta_\varepsilon + \cos \theta_\mu) \sqrt{\varepsilon_r \mu_r}. \quad (2.1)$$

Here θ_ε and θ_μ are defined in the interval $[-\pi, \pi]$ by:

$$\varepsilon'_N + i\varepsilon''_N = \frac{\varepsilon'_r}{|\varepsilon_r|} + i\frac{\varepsilon''_r}{|\varepsilon_r|} \equiv \cos \theta_\varepsilon + i \sin \theta_\varepsilon; \quad \mu'_N + i\mu''_N = \frac{\mu'_r}{|\mu_r|} + i\frac{\mu''_r}{|\mu_r|} \equiv \cos \theta_\mu + i \sin \theta_\mu. \quad (2.2)$$

The sign of the refractive index is given by $\text{sign} (\cos \theta_\varepsilon + \cos \theta_\mu)$. Fig. 2.7 shows 3D plots of the real and imaginary part of the refractive index in the phase space spanned by θ_ε and θ_μ . Clearly, for a particular value of the real part of the refractive index n , there are very many combination possibilities of θ_ε and θ_μ , corresponding to a wide ranging positive (loss) or negative (gain) values for the imaginary part of n ; there are also vast regions in the θ_ε – θ_μ phase space where the real part of refractive index can be zero or negative. The central issue in the development of a metamaterial is the ‘engineering’ of the permittivity and permeability of the metamaterial constituents in conjunction with specialized structures in order to realize a desired complex refractive index value.

An example involves the dispersion of core–shell nanospheres [67] in aligned nematic liquid crystals as depicted in Fig. 2.8. If the size of the nanospheres is much smaller than the optical wavelength, the light would ‘see’ an effective refractive index following the effective medium theory [70]. For the case reported in [67], the core is a polaritonic material with a permittivity of the form $\varepsilon_1 = \varepsilon(\infty) \left(1 + \frac{\omega_l^2 - \omega_T^2}{\omega^2 - \omega^2 - i\omega\gamma_1} \right)$ where $\varepsilon(\infty)$ is the high frequency limit of the permittivity, ω is the incident frequency, ω_T is the transverse optical phonon frequency, ω_L is the longitudinal optical phonon frequency, and γ_1 is the damping coefficient. The shell is a Drude [71] material with a permittivity $\varepsilon_2 = 1 - \frac{\omega_p^2}{\omega^2 + i\omega\gamma_2}$ where ω_p is the plasma frequency and γ_2 is the damping term. The optical permittivity of the host nematic liquid crystal (NLC) for a linearly polarized light incident at an oblique angle θ is given by $\varepsilon_3 = \frac{\varepsilon_e \varepsilon_o}{\varepsilon_e \cos^2 \theta + \varepsilon_o \sin^2 \theta}$ where ε_e and ε_o are the respective permittivities for light polarized parallel and perpendicular to the director axis \hat{n} , and θ is the angle made by the director axis with the optical wave vector k_0 .

Using the Maxwell–Garnett mixing rule [70], the effective permittivity and permeability $\varepsilon_r^{\text{eff}}$ and μ_r^{eff} can be calculated to give respectively:

$$\varepsilon_r^{\text{eff}} = \varepsilon_3 \left(\frac{k_3^3 + j4\pi Na_1}{k_3^3 - j2\pi Na_1} \right) \quad (2.3)$$

$$\mu_r^{\text{eff}} = \frac{k_3^3 + j4\pi Nb_1}{k_3^3 - j2\pi Nb_1} \quad (2.4)$$

where

$$k_3 = \sqrt{\varepsilon_3} k_0 = \left(\frac{\varepsilon_e \varepsilon_o}{\varepsilon_e \cos^2 \theta + \varepsilon_o \sin^2 \theta} \right)^{1/2} k_0. \quad (2.5)$$

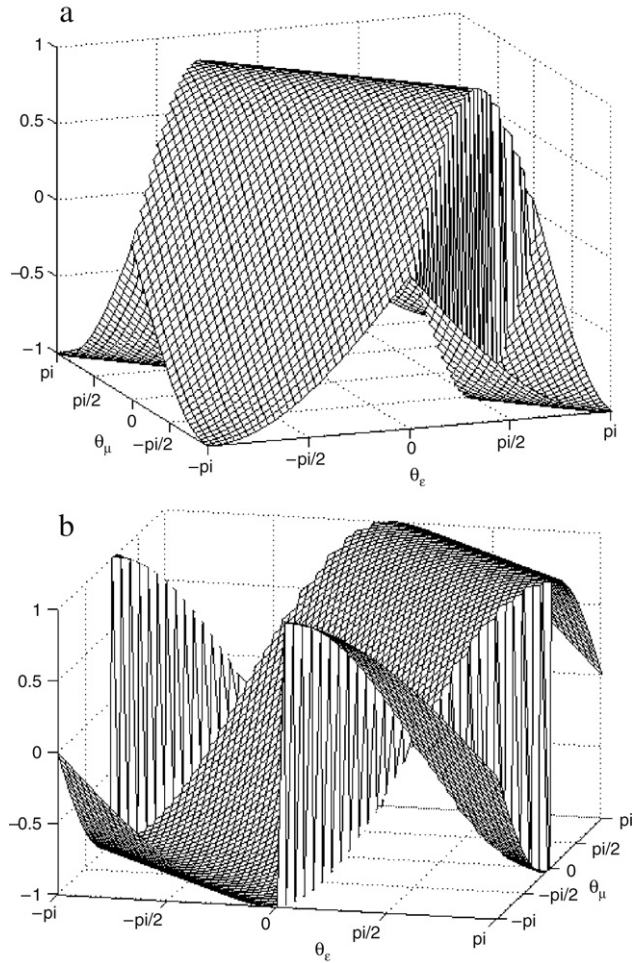


Fig. 2.7. Plot of the (a) real part and (b) imaginary part of the complex refractive index on the $\theta_e - \theta_\mu$ phase space. Note that in the convention used, a positive (>0) imaginary part corresponds to loss.

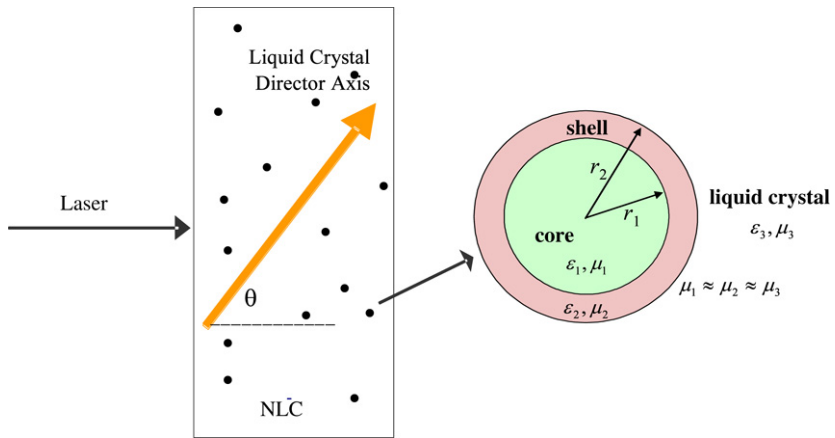


Fig. 2.8. Dispersion of core–shell nanoparticles in aligned nematic liquid crystal.

Here a_1 and b_1 are the MIE scattering coefficients of the coated dielectric sphere, N is the volume density of the spheres ($N = 3f/4\pi r_2^3$) and f is the filling fraction of the composite.

Fig. 2.9 shows a specific example for a filling fraction $f = 0.1$, $r_1 = 0.13 \mu\text{m}$, $r_2 = 0.143 \mu\text{m}$ and the following parameters for the constituent core, shell and host: $\epsilon(\infty) = 17$, $\omega_L/2\pi = 570 \text{ THz}$, $\omega_T/2\pi = 240 \text{ THz}$, $\gamma_1/2\pi = 2.5 \text{ THz}$,

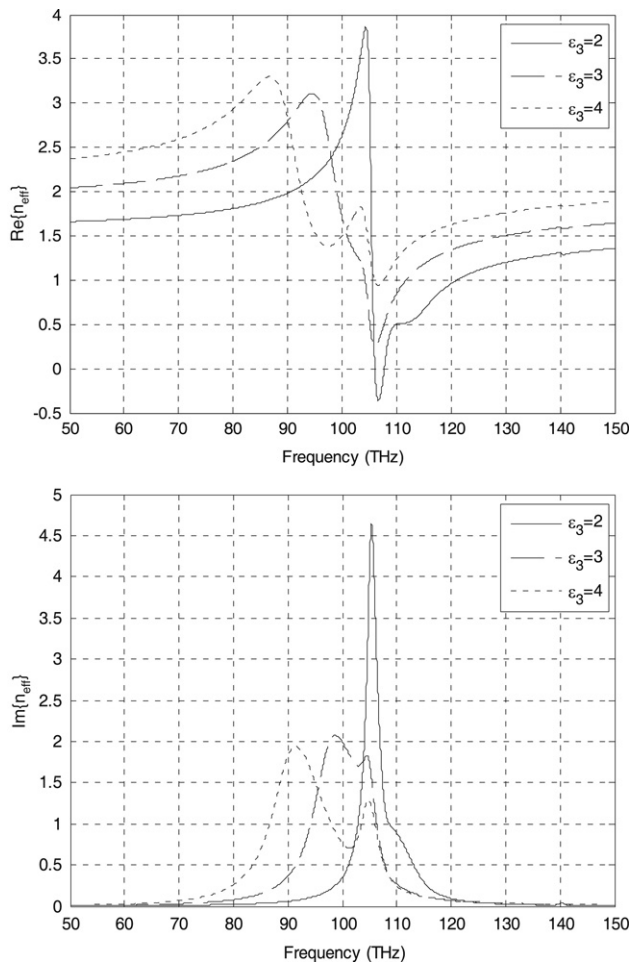


Fig. 2.9. Real part, $\text{Re}\{n_{\text{eff}}\}$, and Imaginary part, $\text{Im}\{n_{\text{eff}}\}$, of the complex effective refractive index n_{eff} of the nanospheres dispersed NLC in the 50–150 THz region. The dimensions and composition of the spheres can be scaled up/down for applications in other spectral region.

$\mu_1 = \mu_2 = \mu_3 = 1$, $\gamma_2 = \omega_p/60$, $\omega_p/2\pi = 134.0$ THz and the LC birefringence $\Delta n_{\text{LC}} = n_e - n_o \sim 0.6$, corresponding to the nematic host dielectric anisotropy of $\varepsilon_e - \varepsilon_o = 2$; $\varepsilon_e \sim 4$ and $\varepsilon_o \sim 2$. Such liquid crystalline metamaterials, by virtue of having these high dielectric constant constituent nanospheres, generally possess larger effective birefringence than the liquid crystal ‘host’, although in general they are also more absorptive due to the larger value of the imaginary part of the n_{eff} . Nevertheless, there are regions where the absorption is low, e.g. around 50–70 THz region, where the effective birefringence is still substantially higher than that of the host nematic (Δn_{eff} is ~ 0.75 at 50 THz, 0.9 at 70 THz, and at 80 THz region, compared to $\Delta n_{\text{LC}} = n_e - n_o \sim 0.6$). At 80 THz, where the loss is still low, the effective birefringence is as large as ~ 1.1 .

An interesting property of such core-shell nanosphere doped liquid crystals is that in some frequency interval around 107 THz, the effective refractive index can assume sub-unity (<0), zero or negative (<0) values as the dielectric constant of the host nematic liquid crystal is varied. Similar results have been obtained for Au- or Ag-nanoparticle dispersions in liquid crystals [69]. Since the ‘tuning’ of the refractive index of the host liquid crystal can be mediated by an optical field, i.e., by nonlinear optical means, such metamaterials would be prime candidates for studying nonlinear optics in the hitherto unexplored sub-unity, zero and negative refractive index regimes. Nevertheless, a major drawback of such ‘metamaterials’ is that in these spectral regimes, the corresponding imaginary part of n_{eff} is quite large, i.e. the material is highly absorptive. A major challenge is to search and identify constituent materials with the appropriate permeability and permittivity values such that their combination in the $\mu-\varepsilon$ space gives the desired index values. Another challenge is to realize the high concentration (or volume fraction) of nanoparticle dopants needed to effect sizeable changes in the effective refractive indices.

2.2.3. Polymer dispersed liquid crystals

Just as the presence of a resonant dye and other nanoparticles modifies the optical properties of liquid crystals, the presence of non-resonant dielectric material interdispersed in the liquid crystals of a different refractive index modifies the

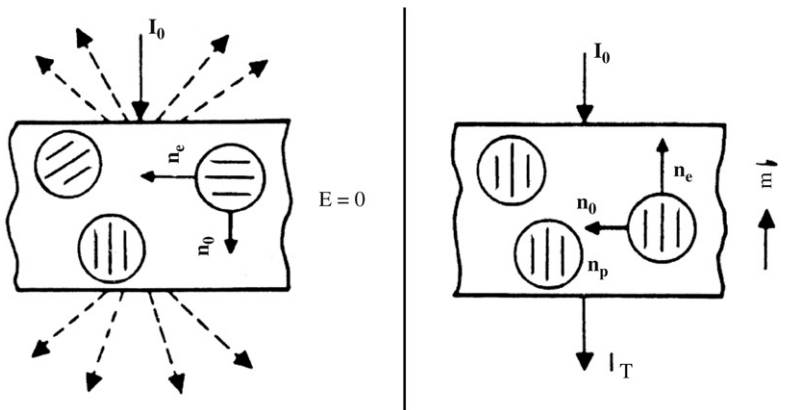


Fig. 2.10. Schematic depiction of polymer dispersed liquid crystal.

scattering properties of the resulting “mixed” system. Polymer dispersed liquid crystals are formed by introducing liquid crystals as microns or sub-micron sized droplets into a polymer matrix [72–79]. The optical indices of these randomly oriented liquid crystal droplets, in the absence of an external alignment field, depend on the liquid crystal–polymer interaction at the boundary, and therefore assume a random distribution (cf. Fig. 2.10(a)). This causes large scattering. Upon the application of an external field, the droplets will be aligned (Fig. 2.10(b)), and the system will become clear as the refractive index of the liquid crystal droplets matches the isotropic polymer backgrounds. Since the first introduction of polymer dispersed liquid crystals using phase separation and the encapsulation methods [72,73], now there are many techniques for preparing such composite liquid crystalline materials, including for example, optical holographic interference methods [74–79]. These latest PDLC structures possess excellent optical qualities that enable high diffraction efficiency as well as laser emission capabilities.

2.3. Liquid crystal cells and structures – Traditional and ‘exotic’

Liquid crystals, particularly nematics which are commonly employed in many electro-optical devices, behave physically very much like liquids. They therefore have to be enclosed (usually in flat thin cells) where their ordered crystalline properties are manifested. The alignment of the nematic liquid crystal axis in the bulk of these cells is controlled by the anchoring conditions on the enclosing surfaces. Two most commonly occurring surface alignments are the so-called homeotropic and homogeneous (or planar) configurations, corresponding to the director axis being perpendicular or parallel to the surface, respectively. Such nematic alignments are usually effected by surface treatment [5,6]. The cell preparation methods for a ferroelectric liquid crystal, smectic-C* for SSFLC operation (Surface Stabilized FLC) is more complicated as it involves surface stabilization [80,81]. These surface alignment processes become very challenging in confined geometries such as holey fibers and waveguides [82,83].

In recent years, with advances in nano and metamaterial technologies, more exotic ‘cell structures’ have been devised such as 3D photonic crystals [84–86]. In particular, Graugnard et al. [84] has reported using non-close-packed inverse opals that consist of overlapping air spheres in a TiO_2 matrix that was infiltrated with liquid crystal, c.f. Fig. 2.11. Because of the higher volume fraction for NLC infiltration, a larger electrical tuning range [$>20 \text{ nm}$] of the Bragg reflection peak can be achieved. Clearly, these structures are also capable of exhibiting optical nonlinearities and novel nonlinear optical phenomena as a consequence of the optical intensity dependent refractive indices (Fig. 2.11).

Another approach to making periodic planar metamaterial/structures has also been recently advanced. These planar structures are also termed Frequency Selective Structures FSS [87,88]. Basically they are 2D periodic arrays of metallic patches or aperture elements that possess low pass, high pass, band pass, or multi-band filtering properties for incident electromagnetic waves. Total reflection or total transmission will occur when the incident wavelength corresponds to the “resonant length” of the FSS screen elements. The planar geometry is particularly suitable for incorporating an aligned nematic liquid crystal over-layer. An example of an LC-cladded FSS unit cell [88] is shown in the inset of Fig. 2.12. It consists of polyimide blocks embedded in a layer of silica with an over-layer of liquid crystal. By electrically or optically changing the dielectric constants of the LC from 2 ($n_0 = 1.414$) to 4 ($n_e = 2$), the stop-band in the transmission response can be shifted from 92 THz ($\sim 3.26 \mu\text{m}$) to 83 THz ($3.64 \mu\text{m}$), corresponding to a tuning range of $\sim 380 \text{ nm}$. Since the birefringence of nematic liquid crystals span the entire spectrum from visible to far-infrared, LC-PFSS will allow one to devise broadband high-extinction-ratio tunable filters/switches. For nonlinear optics, such FSS structures obviously allow the possibilities of the optically self-activated counterpart devices/processes.

More recently, such planar structures have evolved into more complex bulk forms with new emergent properties such as tunable sub-unity, zero and negative index [89,90]. Fig. 2.13 shows an example of a tunable metamaterial nanostructure formed by periodic arrays of unit cells which are made up of a magnetic resonator and negative dielectric constant material

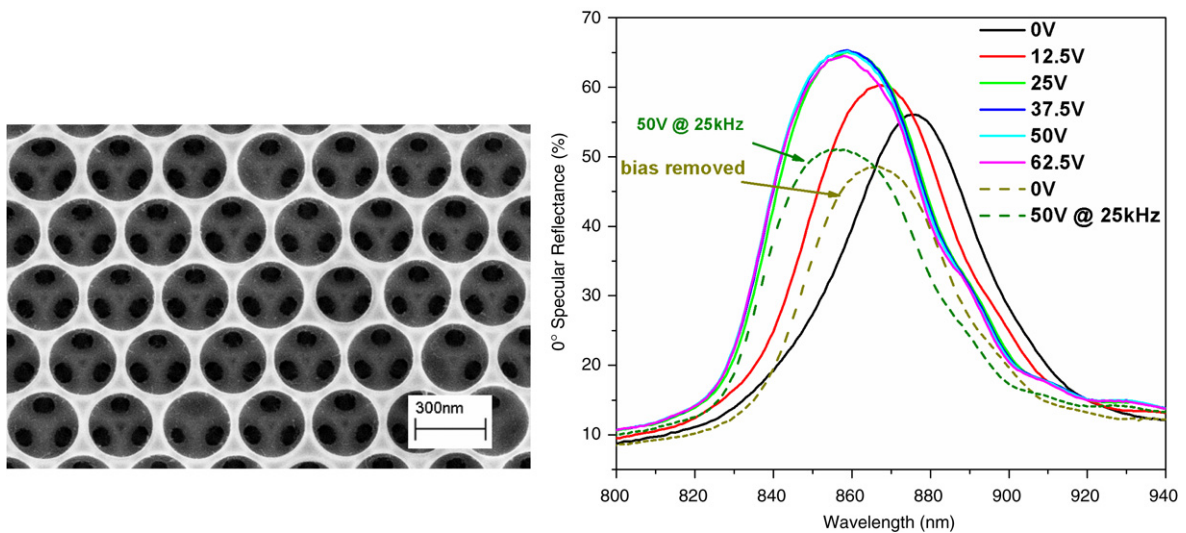


Fig. 2.11. Cross-sectional view of an inverse opal structure for fabricating liquid crystal filled photonic crystals. Figure at right shows the electrically tunable reflection bands from such liquid crystal infiltrated photonic crystals.

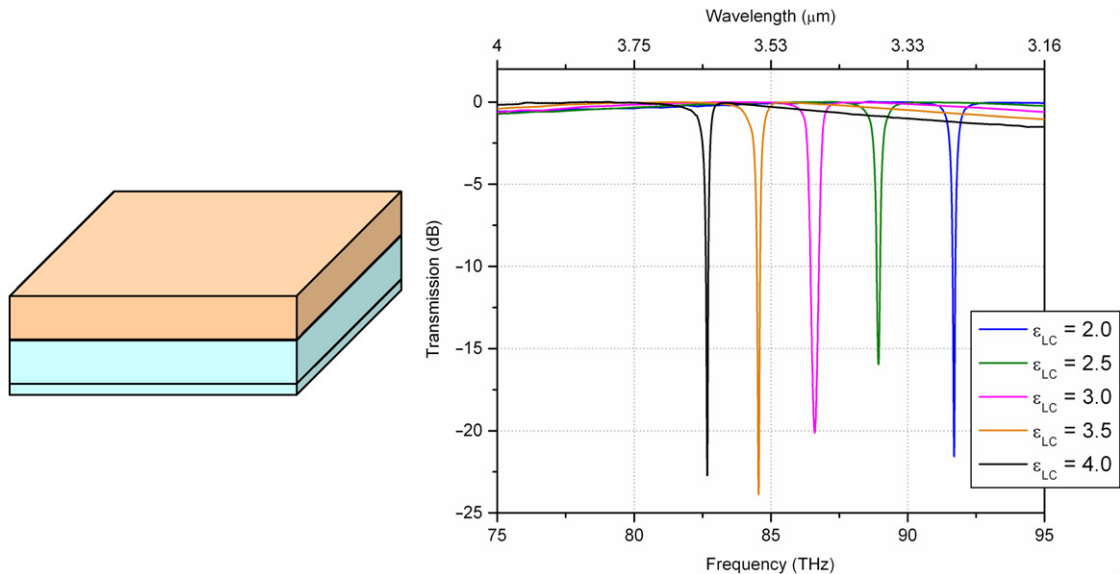


Fig. 2.12. Left: The unit cell make up of a planar Frequency Selective Surface (FSS). Right: The transmission of the FSS in the near-IR regime showing its tunable filtering capability.

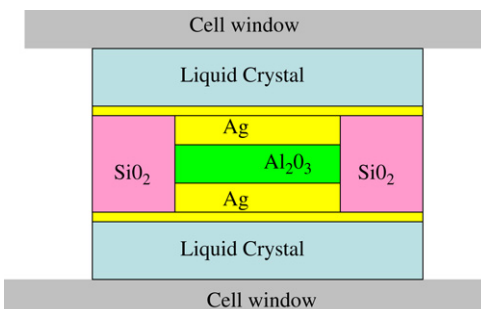


Fig. 2.13. The unit cell make up of a 'bulk' Frequency Selective Surfaces that possesses tunable negative-zero positive refractive indices.

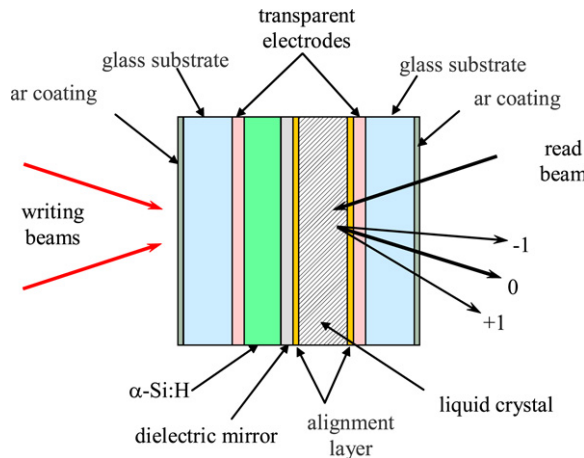


Fig. 2.14. Exploded view of a liquid crystal spatial light modulator operating in the reflective mode.

sandwiched between two aligned nematic liquid crystal layers. The unit cell of the FSS nanostructure is comprised of a magnetic resonator made of two strips of silver of thickness 30 nm separated by a thin layer of alumina of thickness 20 nm. Negative permittivity needed for negative-index behavior is provided by thin silver films bounding the periodic array of magnetic resonators. The space between neighboring magnetic resonators is filled with silica. These structures exhibit tunable refractive indices [as a consequence of the LC's tunable birefringence] in the near-infrared and longer wavelength regimes, depending on the size/dimension of the unit cell.

As in the case of the nanodispersed liquid crystal metamaterials discussed in the previous section, the main problems with these tunable negative index materials, besides the extreme difficulties in fabricating bulk size structures, are their large optical losses in the region where negative index is manifested.

2.4. Liquid crystal optically addressed spatial light modulator [OASLM]

An optically addressed spatial light modulator is an excellent example of a practical nonlinear optical device that integrates the unique physical properties of liquid crystals and optoelectronic materials. There are two types of LC spatial light modulators: transmissive and reflective. Fig. 2.14 shows the schematic construction of a typical Optically Addressed Liquid Crystal Spatial Light Modulator [OALCSLM] operating in the reflective mode [5,6,91–93]. It consists of an aligned liquid crystal layer sandwiched between transparent electrodes and adjacent to a photoconducting (PC) thin film (e.g. α -Si:H, CdS, ZnS, or CdSe) sensitive to the writing beams and a dielectric mirror coated to block the reading beam, and to reflect the reading light.

In the absence of the incident light, the PC film is highly resistive, and thus experiences the bulk of the voltage drop across the electrodes. When illuminated by light, the PC layer becomes conducting, and the voltage drop now takes place across the LC layer. This causes the liquid crystal's director axis to reorient and all the resulting optical property changes associated with it. Accordingly, the spatial distribution in the incident optical intensity (e.g. an image) will be recorded as an orientation distribution pattern and therefore a corresponding spatially varying optical phase shift for a reading beam that will sense this phase shift and reproduce the image on the other side. As illustrated in Fig. 2.14 the incident signal is in the form of an interference pattern (hologram) formed by interfering two coherent beams. The holographic interference pattern is transferred to the liquid crystal layer via the photoconducting layer and the bias field. When the hologram is illuminated with viewing light [the reading or probe beam], a reconstructed image is obtained as the output signal. In the language of nonlinear optics, this process of simultaneous recording and reading of a phase pattern process is sometimes called real time holography, or optical wave front conjugation [91,94] and is discussed in more detail in Section 4.

From the point of view of nonlinear optics, OALCSLM is actually one of the most efficient and useful nonlinear optical devices ever made in terms of the refractive index change per unit of incident light intensity [albeit with the help of the ac bias field]. In typical SLM operation, a writing beam optical intensity I of the order of $500 \mu\text{W}/\text{cm}^2$ is used and the induced diffraction grating generates a first order diffraction efficiency of 10%. Since it is a thin grating ($\lambda d \ll \Lambda^2$ where $\lambda = \text{wavelength}$, $d = \text{thickness}$ and $\Lambda = \text{grating constant}$), the diffraction is of the Raman–Nath type. The first order diffraction efficiency is $\eta \sim J_1^2 \left(\frac{2\pi \Delta n d}{\lambda} \right)$. Also, for small index grating amplitude, i.e. $(\pi \Delta n d / \lambda) \ll 1$, $\eta \propto \left(\frac{\pi \Delta n d}{\lambda} \right)^2$. Writing $\delta\phi = \Delta n \pi d / \lambda = n_2 I \pi d / \lambda$, and noting the typical SLM liquid crystal layer thickness d is $\sim 5 \mu\text{m}$, one can deduce that the nonlinear coefficient n_2 is on the order of $10 \text{ cm}^2/\text{W}$ at the optical wavelength $\lambda = 0.5 \mu\text{m}$. This puts a LCSLM in the realm of supra-optical nonlinearity.

Many investigators have succeeded in incorporating photosensitivity in nematic liquid crystals by fabricating photosensitive thin films or nanoparticulates onto the cell wall, or by suspending photorefractive nanocrystals in the bulk,

and have observed greatly enhanced nonlinear optical responses for spatial light modulators [95–102]. With the rapid advances currently being made in nanosciences and technologies, more specially engineered liquid crystalline materials, in various forms, shapes, and cell geometries will likely emerge in the near future, and enlarge the ‘arsenal’ of liquid crystalline systems for linear as well as nonlinear optical studies and applications.

3. Optical nonlinearities of nematic liquid crystals

Nonlinear optics processes are often described in terms of induced polarizations \mathbf{P} of the material under the action of an optical electric field \mathbf{E} . In general, \mathbf{P} consists of a linear term $\mathbf{P}_L \sim \varepsilon_0 \chi^{(1)} \mathbf{E}$ and a nonlinear polarization of the form $\mathbf{P}_{NL} \sim \chi^{(2)} \mathbf{EE} + \chi^{(3)} \mathbf{EEE} + \dots$ where $\chi^{(1)}$, $\chi^{(2)}$ and $\chi^{(3)}$ are the linear, second and third order nonlinear susceptibilities [8]. The linear term is usually ‘absorbed’ in the definition of the dielectric constant of the material $\varepsilon(\mathbf{r}) = \varepsilon_0 + \varepsilon_0 \chi^{(1)}$; similarly the corresponding magnetic counterpart is included in the magnetic permeability $\mu(\mathbf{r})$ of the material. As pointed out in previous sections, the design, synthesis and fabrication of materials or metamaterials with the appropriate choice of $\varepsilon(r)$ and $\mu(r)$ are keys to realizing novel liquid crystals with the desired refractive indices and birefringence to control their interrelated linear and nonlinear light scattering properties. This section deals with the various mechanisms responsible for the extraordinary optical nonlinearities of nematic liquid crystals.

The propagation of the optical fields through the nonlinear medium is described by the Maxwell Wave equation:

$$\left(\nabla^2 - \mu(r) \varepsilon(r) \frac{\partial^2}{\partial t^2} \right) \mathbf{E}(\vec{r}, t) = \mu(r) \frac{\partial^2 \mathbf{P}_{NL}(\vec{r}, t)}{\partial t^2}. \quad (3.1)$$

As the optical electric fields $\mathbf{E} \sim e^{i(\mathbf{k} \cdot \mathbf{r} - \omega t)}$ contain both temporal (ω 's) and spatial frequencies (wave vectors \mathbf{k}), the mixings of these electric fields through the nonlinear polarization responses $\chi^{(2)} \mathbf{EE}$, $\chi^{(3)} \mathbf{EEE}$ give rise to new temporal and spatial frequency components. The temporal frequency mixing effects are usually called *sum and difference frequency* wave mixing, exemplified best by second (2ω), third (3ω), and higher harmonic generations of an input monochromatic laser. These and other sum and difference frequency wave mixing effects are mediated by electronic optical transitions in the molecules, c.f. Section 2.1; the susceptibilities that characterize these responses are often termed electronic susceptibilities $\chi_{el}^{(2)}, \chi_{el}^{(3)}, \dots$ etc. Generally, in bulk materials that possess centro-symmetry, $\chi_{el}^{(2)}$ vanishes. The centro-symmetry can be ‘broken’ by an applied field [usually an electric field]; on surfaces, centro-symmetry is also naturally broken. Accordingly, second order processes such as second harmonic generation have been conducted in (electrically) poled materials or surfaces. The spatial frequency counterparts are often called *degenerate four-wave mixing*, or simply self-diffraction in which the incident and diffracted beams are usually of the same temporal frequency, but emerge in different directions, i.e. different \mathbf{k} 's. The physical mechanisms responsible for such wave mixing phenomena include space charge fields, thermal, density, orientation, and order parameter changes as well as refractive index changes induced by the optical fields in the medium.

3.1. An introduction to nematogen theories – Order parameter, free energies and optical dielectric constants

A laser will induce in nematic liquid crystals changes in the populations of the electronic energy states, density, temperature, order parameter, and director axis orientation. All of these mechanisms result in changes in the refractive index or the electronic polarizability of the material, giving rise to nonlinear optical phenomena. Among the various phases of liquid crystals discovered to date, the nematic phase best exemplifies the dual nature of liquid crystals—fluidity and crystalline structure, and the extraordinary sensitivity to perturbations by optical fields are intriguingly tied to this unique aspect of liquid crystals.

The optical physics of nematic liquid crystals has been standardized for many years now by the work of deGennes, Maier-Saupe, and others [3–6]. In an aligned liquid crystal, the molecules are, on the average, aligned along the direction defined by the director axis, which is analogous to the crystalline *c*-axis in photorefractive crystals. Most nematic liquid crystals are uniaxial, characterized by a tensorial order parameter [103]:

$$S_{\alpha\beta}(\vec{r}) = S(T) \left[\hat{n}_\alpha(\vec{r}) \hat{n}_\beta(\vec{r}) - \frac{1}{3} \delta_{\alpha\beta} \right]. \quad (3.2)$$

The order parameter gives a measure of the degree of ordering in the director axis orientation; its magnitude varies from nearly unity in the crystalline phase to zero in the isotropic phase, c.f. Fig. 3.1 which illustrates the order parameter as the temperature is decreased and the liquid crystal changes from the solid, through Smectic-A and nematic to the isotropic phase.

Upon application of an external perturbation field, a nematic liquid crystal will undergo one or more of the three possible forms of deformations shown in Fig. 3.2(b)–(c), just as a solid, but with orders of magnitude smaller energies required to effect such distortions. A good example is the twist deformation shown in Fig. 3.1(c), which is a frequently employed deformation for electro-optical switching applications [104]. In ordinary solids this would create a very large torsional stress associated with the molecules being translationally displaced. In nematic liquid crystals, however, owing to the fluidity of the molecules, such *twist* deformations in liquid crystals simply involve a rotation of the molecules in the direction of the

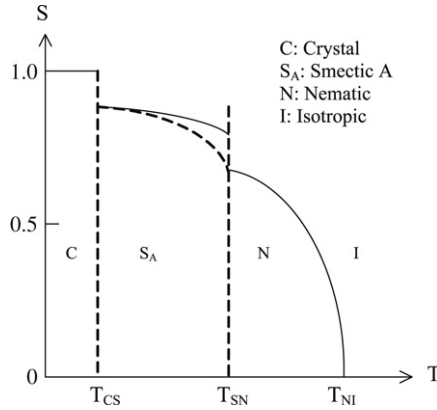


Fig. 3.1. Schematic depiction of the order parameter in the various phases of a thermotropic liquid crystal exhibiting the Smectic-A and nematic mesophases; T_{CS} , T_{SN} , T_{NI} are the respective transition temperatures from the crystal to smectic, smectic to nematic and nematic to isotropic.

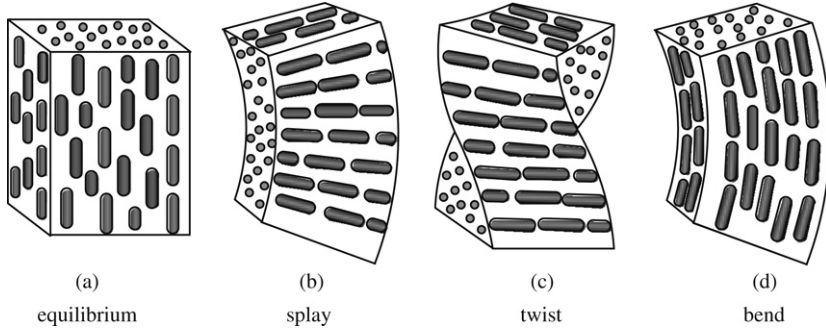


Fig. 3.2. An aligned nematic liquid crystal (a) at equilibrium and (b)–(c) undergoing splay, twist and bend deformations, respectively.

torque; there is no translational displacement of the center of gravity of the molecules, and thus the elastic energy involved is quite small.

Similarly, other types of deformations such as *splay* and *bend* deformations as shown in Fig. 3.2 involve mainly changes in the director axis $\hat{n}(\vec{r})$, and incur much less elastic energies than their counterparts in ordinary solids.

These considerations explain the easy susceptibility of the nematic director axis to reorientation by external fields (ac, dc, magnetic and optical), and the resulting extraordinary electro-optical and nonlinear optical responses. The free-energy densities (in units of energy per volume) associated with these deformations are given by [3]:

$$\text{splay: } f_1 = \frac{1}{2} K_1 (\nabla \cdot \hat{n})^2, \quad (3.3a)$$

$$\text{twist: } f_2 = \frac{1}{2} K_2 (\hat{n} \cdot \nabla \times \hat{n})^2, \quad (3.3b)$$

$$\text{bend: } f_3 = \frac{1}{2} K_3 (\hat{n} \times \nabla \times \hat{n})^2, \quad (3.3c)$$

where K_1 , K_2 , and K_3 are the respective Frank elastic constants. Typically, they are on the order of 10^{-6} dyne in cgs units (or 10^{-11} N in mks units).

In the study of electro-optical and nonlinear optical processes involving the reorienting action of the applied fields and torques, it is often necessary to invoke molecular fields arising from these distortion free energies via the Lagrange equation:

$$f_\alpha = \frac{-\partial F}{\partial n_\alpha} + \sum_\beta \frac{\partial}{\partial x_\beta} \frac{\partial F}{\partial g_{\alpha\beta}} \quad (3.4a)$$

$$g_{\alpha\beta} = \frac{\partial n_\alpha}{\partial x_\beta}. \quad (3.4b)$$

Accordingly, the molecular fields associated with splay, twist, and bend deformations are:

$$\text{splay: } \vec{f}_1 = K_1 \nabla (\nabla \cdot \hat{n}), \quad (3.5a)$$

$$\text{twist: } \vec{f}_2 = -K_2 (A \nabla \times \hat{n} + \nabla \times (A \hat{n})) , \quad (3.5b)$$

$$\text{bend: } \vec{f}_3 = K_3 (\vec{B} \times (\nabla \times \hat{n}) + \nabla \times (\hat{n} \times \vec{B})) , \quad (3.5c)$$

with $A = \hat{n} \cdot (\nabla \times \hat{n})$ and $\vec{B} = \hat{n} \times (\nabla \times \hat{n})$.

If all three forms of deformation are created, the total distortion free-energy density is given by:

$$F_d = \frac{1}{2} K_1 (\nabla \cdot \hat{n})^2 + \frac{1}{2} K_2 (\hat{n} \cdot \nabla \times \hat{n})^2 + \frac{1}{2} K_3 (\hat{n} \times \nabla \times \hat{n})^2 . \quad (3.6)$$

In many situations, this expression, and the resulting equations of motion and analysis, can be greatly simplified if one makes the so-called one-constant approximation ($K_1 = K_2 = K_3 = K$). In this case (3.6) becomes

$$F_d = \frac{1}{2} K [(\nabla \cdot \hat{n})^2 + (\nabla \times \hat{n})^2] . \quad (3.7)$$

A complete description should include also the surface interaction energy at the nematic liquid crystal cell boundaries, and thus the total free energy density of the system becomes:

$$F'_d = F_d + F_{\text{surface}} . \quad (3.8)$$

Under the so-called “hard-boundary” condition, in which the liquid crystal molecules are strongly anchored to the boundary and do not respond to applied perturbation fields, the surface energy may thus be regarded as a constant, and the surface interactions do not enter into the dynamical equations describing the field induced effects. On the other hand, if the molecules are not strongly anchored to the boundary, that is, the so-called “soft-boundary” condition, an applied field will perturb the orientation of the molecules at the cell boundaries. In this case a quantitative description of the dynamics of the field induced effects must account for these surface energy terms. Such surface effects are particularly important in many nonlinear optical studies involving specially engineered surfaces or surfaces with photosensitive materials, e.g. liquid crystal spatial light modulators [91,95]; these surface mediated effects are also responsible for the extraordinarily large optical nonlinearities observed in nematic liquid crystals [7,24,105–108].

In the presence of an applied (dc, low frequency, or optical) electric field \vec{E} , the displacement \vec{D} becomes:

$$\vec{D} = \varepsilon_{\perp} \vec{E} + (\varepsilon_{\parallel} - \varepsilon_{\perp}) (\hat{n} \cdot \vec{E}) \hat{n} \quad (3.9)$$

where ε_{\parallel} and ε_{\perp} are the (dc, low frequency, or optical) dielectric constants parallel and perpendicular to the director axis, respectively. In the dc or low frequency ac regime, ε_{\parallel} is $\sim 15\varepsilon_0$ and ε_{\perp} is $\sim 5\varepsilon_0$, i.e. $\varepsilon_{\parallel} - \varepsilon_{\perp} = \Delta\varepsilon \sim 10\varepsilon_0$. In negative uniaxial, nematic liquid crystals, $\Delta\varepsilon < 0$; dual frequency nematic liquid crystals $\Delta\varepsilon$ can be positive or negative depending on the frequency of the applied (low frequency ac) field [5,6].

In the optical regime, ε_{\parallel} is usually larger than ε_{\perp} . For 5CB, for example, ε_{\parallel} is $\sim 2.89\varepsilon_0$ and ε_{\perp} is $\sim 2.25\varepsilon_0$ corresponding to refractive indices $n_{\parallel} = 1.7$ and $n_{\perp} = 1.5$. In terms of the isotropic phase dielectric constant ε_l , ε_{\parallel} and ε_{\perp} can be expressed as [109,110]:

$$\varepsilon_{\parallel} = \varepsilon_l + \frac{2}{3} \Delta\varepsilon \quad (3.10a)$$

$$\varepsilon_{\perp} = \varepsilon_l - \frac{1}{3} \Delta\varepsilon . \quad (3.10b)$$

Here

$$\varepsilon_l = 1 + C_1 \rho \quad (3.10c)$$

$$\begin{aligned} \Delta\varepsilon &= \left(\frac{N}{3\varepsilon_0} \right) [\alpha_l K_l - \alpha_t K_t] S \\ &= \frac{N_A \rho}{\varepsilon_0 M} (\alpha_l K_l - \alpha_t K_t) \propto \rho S . \end{aligned} \quad (3.10d)$$

Here N_A is Avogadro's number, ρ is the density, and M is the mass number, α_l, α_t and K_l, K_t are the longitudinal and transverse component of the molecular polarizability and local field correction factors, respectively [5]; S is the scalar order parameter.

Central to the studies of nonlinear optics are the extraordinary and ordinary refractive indices $n_{\parallel} = (\varepsilon_{\parallel})^{1/2}$ and $n_{\perp} = (\varepsilon_{\perp})^{1/2}$. Clearly both refractive indices are functions of the density ρ and, more importantly, the order parameter S , and exhibit similar critical dependence on the temperature near the nematic-isotropic phase transition, c.f. Fig. 3.3.

$$n_{\parallel} = n_{\parallel}(\rho, S); \quad n_{\perp} = n_{\perp}(\rho, S) . \quad (3.11a)$$

There are two principal ways that an optical field can create changes in the refractive indices – the underpinning mechanism for nonlinear optics: One is to affect director axis orientation, which changes the extraordinary refractive index

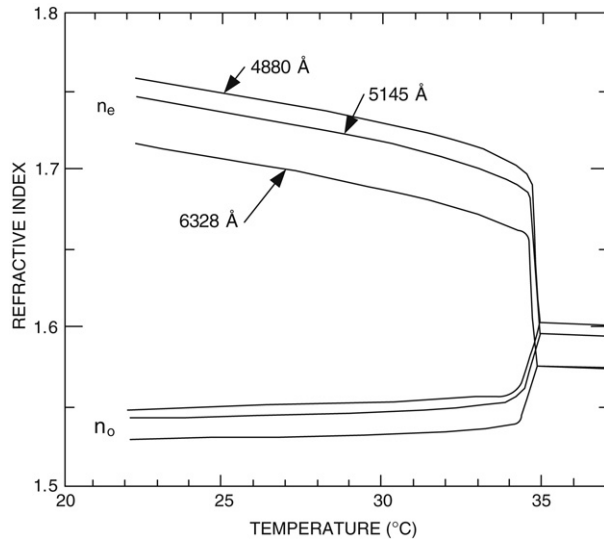


Fig. 3.3. Temperature dependence of the refractive indices of the nematic liquid crystal 5CB for three different wavelengths in the visible region. Similar dependency holds in the near-IR and infrared regime [5].

experienced by the optical field. The other is to impart changes in the temperature, density or order parameter through some photoabsorption processes. For the latter, it is worthwhile to note that the corresponding temperature index gradients are of the form [109,5]:

$$\frac{dn_{\parallel}}{dT} = \frac{1}{n_{\parallel}} \left(C_1 \frac{d\rho}{dT} + \frac{2}{3} C_2 S \frac{d\rho}{dT} + \frac{2}{3} C_2 \rho \frac{dS}{dT} \right) \quad (3.11b)$$

$$\frac{dn_{\perp}}{dT} = \frac{1}{n_{\perp}} \left(C_1 \frac{d\rho}{dT} - \frac{1}{3} C_2 S \frac{d\rho}{dT} - \frac{1}{3} C_2 \rho \frac{dS}{dT} \right). \quad (3.11c)$$

In general, $\frac{dn_{\parallel}}{dT} < 0$ and $\frac{dn_{\perp}}{dT} > 0$ corresponding to a negative and positive n_2 , respectively. The order parameter dependent terms will 'diverge' as the temperature approaches the phase transition temperature T_c , increasing by more than two orders of magnitude (from a value of $\sim 10^{-4} \text{ K}^{-1}$ typical of ordinary liquids or solids to 10^{-2} K^{-1}). As a result, nematic liquid crystals exhibit enormous thermal nonlinearities near T_c . Since their large birefringence and thermal gradients hold throughout the entire optical spectrum from near UV to the infrared, nematic liquid crystals are ideal candidates for nonlinear optics involving visible as well as infrared lasers [109–121].

3.2. Laser induced molecular reorientations in the isotropic phase – Ordinary optical nonlinearity

In the isotropic phase the liquid crystal molecules are randomly oriented. As mentioned earlier, their thermal and density effects are typical of ordinary fluids. However, their constituent anisotropic molecules will respond to an intense laser field through the dipolar interaction, and tend to align the molecules highest polarizability tensor component along the optical electric fields, giving rise some degree of preferred orientation in an otherwise random system [122–131]. Studies of molecular motions reveal two distinctive components: individual and collective molecular reorientations. The individual molecular motion is characterized by a response time on the order of a few picoseconds, and fluctuations in these individual molecular motions give rise to a broad central peak in a Rayleigh scattering measurement; this is usually referred to as the Rayleigh wing scattering component, and it always exists in ordinary anisotropic liquids such as CS_2 .

Besides these molecular motions, an optical field could also induce nuclear reorientation anisotropy [122,127]. This process is sometimes referred to as the nuclear optical Kerr effect; it is characterized by a rise time of a few picoseconds and a decay time of about 10^2 ps and the magnitude of the associated optical nonlinearities associated are quite small.

In the context of nonlinear optics, the correlated molecular reorientation in the isotropic phase is of interest owing to its large magnitude and non-resonant nature. Such a reorientation process is characterized by a response time on the order of 10^1 to 10^2 ns. In the vicinity of the phase transition temperature T_{NI} , molecular correlations in liquid crystals give rise to interesting critical phenomena. These critical phenomena are described by the Landau-deGennes [3,11] theory of second order phase transition. In this case, the free energy per unit volume is of the form:

$$F = F_0 + \frac{1}{2} A Q_{ij} Q_{ji} - \frac{1}{4} \chi_{ij} E_i^* E_j \quad (3.12)$$

$$A = a(T - T^*) \quad (3.13)$$

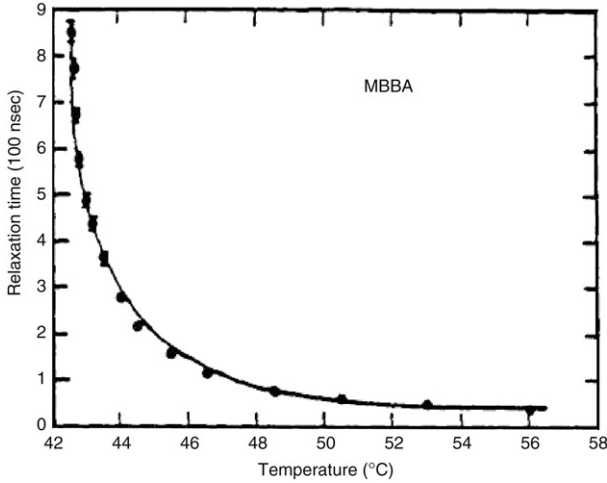


Fig. 3.4. Measured optical nonlinear susceptibility as a function of the temperature above T_c .

where Q_{ij} is a general order parameter tensor, and a and $T^*(\sim T_{NI})$ are constants. For simplicity of illustration, consider a linearly polarized laser (along the x direction for example) which produces the total induced polarization P_x of the form:

$$\begin{aligned} P_x &= \left(\varepsilon_0 \bar{\chi} + \varepsilon_0 \frac{2}{3} \Delta \chi Q \right) E_x \\ &= P_x^L + P_x^{NL} \end{aligned} \quad (3.14)$$

where $P_x^L = \varepsilon_0 \bar{\chi} E$ is the linear polarization, and $\bar{\chi}$ is the linear susceptibility. The nonlinear polarization arising from laser induced molecular reorientation is given by:

$$P_x^{NL} = \frac{2}{3} \varepsilon_0 \Delta \chi Q E.$$

From (3.12) the dynamical equation for Q_{ij} becomes:

$$\eta \frac{\partial Q_{ij}}{\partial t} + A Q_{ij} = f_{ij} \quad (3.15)$$

$$f_{ij} = \frac{1}{6} \Delta \chi \left(E_i^* E_j - \frac{1}{3} |E|^2 \delta_{ij} \right). \quad (3.16)$$

Here η is the viscosity coefficient in the isotropic phase.

The solution for Q_{ij} is

$$Q_{ij}(t) = \int_{-\infty}^t \left[\frac{f_{ij}(t')}{\eta} e^{-(t-t')/\tau} \right] dt'. \quad (3.17)$$

Here τ , the response time is given by:

$$\tau = \frac{\eta}{A} = \frac{\eta}{a(T - T^*)}. \quad (3.18)$$

Assuming for simplicity that the laser is a square pulse of duration τ_p , $f_{ij} = f_{ii} = \frac{1}{9} \Delta \chi E^2$ and we thus have:

$$Q_{ii} \sim \tau \Delta \chi E^2 (1 - e^{-\tau/\tau_p}) / 9\eta. \quad (3.19)$$

Eq. (3.18) shows that as T approaches T_c from the isotropic phase, the relaxation time constant τ will diverge. Accompanying such slowing down, however, the optical nonlinearity $P_x^{NL} \sim Q_{ii}$ associated with the reorientation experiences a dramatic enhancement, c.f. Fig. 3.4. These effects were observed in early studies of the reorientation Kerr effect [11] and optical wave front conjugation [130].

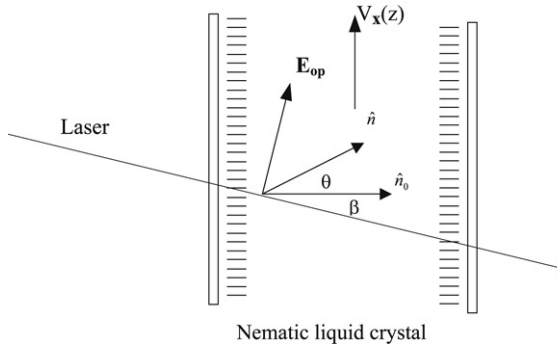


Fig. 3.5. Interaction of a linearly polarized (extraordinary wave) laser with a homeotropically aligned nematic liquid crystal film.

3.3. Steady State Laser induced molecular reorientations in the nematic phase – Giant optical nonlinearity

In an ordered phase such as the nematic phase, the total free energy of the system in the presence of an optical field consists of the distortion energy F_d in Eq. (3.6) and the optical dipolar interaction energy F_{op} ,

$$F_{op} = -\frac{1}{4\pi} \int \mathbf{D} \cdot d\mathbf{E} = -\frac{\varepsilon_\perp}{8\pi} E^2 - \frac{\Delta\varepsilon \langle (\hat{n} \cdot \mathbf{E})^2 \rangle}{8\pi}. \quad (3.20)$$

The angle bracket $\langle \rangle$ denotes a time average since the molecular reorientation response is slower than the optical period. Field induced reorientation of the director axis arises as a result of the total system's tendency to assume a new configuration with the minimum free energy. Since the first term on the right-hand side of (3.20) is independent of the director axis orientation, it may be ignored when we consider the reorientation process. The second term indicates that the system favors a realignment of the director axis along the optical field polarization since the dielectric anisotropy $\Delta\varepsilon$ is >0 in the optical frequency domain.

For illustration, consider the interaction geometry depicted in Fig. 3.5. A linearly polarized laser is incident on a homeotropically aligned nematic liquid crystal with the propagation wave vector \mathbf{K} making an angle $(\beta + \theta)$ with the optically perturbed director axis.

If the reorientation angle θ is small, then only one elastic constant K_1 (for splay distortion) is involved. A minimization of the total free energy of the system yields a torque balance equation:

$$K_1 \frac{d^2\theta}{dz^2} + \frac{\Delta\varepsilon \langle E_{op}^2 \rangle}{8\pi} \sin 2(\beta + \theta) = 0. \quad (3.21)$$

In the small θ approximation, this may be written as

$$2\xi^2 \frac{d^2\theta}{dz^2} + (2 \cos 2\beta) \theta + \sin 2\beta = 0 \quad (3.22)$$

where $\xi^2 = 4\pi K_1 / [\Delta\varepsilon \langle E_{op}^2 \rangle]$.

Because of the large birefringence of nematic liquid crystals, a small director axis reorientation angle θ will give rise to sufficiently large refractive index change to generate observable optical effects. In this case, using the so-called hard-boundary condition, i.e., the director axis is not perturbed at the boundary ($\theta = 0$ at $z = 0$ and at $z = d$), the solution of (3.22) is

$$\theta = \frac{1}{4\xi^2} \sin 2\beta (dz - z^2). \quad (3.23)$$

As a result of this reorientation, the incident laser (an extraordinary wave) experiences a z -dependent refractive index change given by

$$\Delta n = n_e(\beta + \theta) - n_e(\beta) \quad (3.24)$$

where $n_e(\beta + \theta)$ is the extraordinary ray index

$$n_e(\beta + \theta) = \frac{n_\parallel n_\perp}{[n_\parallel^2 \cos^2(\beta + \theta) + n_\perp^2 \sin^2(\beta + \theta)]^{1/2}}. \quad (3.25)$$

For small θ , the change in the refractive index Δn is proportional to the square modulus of the optical electric field, that is, $\Delta n = \alpha_2(z)I$ with $\alpha_2(z)$ given by

$$\alpha_2(z) = \frac{(\Delta\varepsilon)^2 \sin^2(2\beta)}{4Kc} (dz - z^2). \quad (3.26)$$

Note that, when $\alpha_2(z)$ is averaged over the sample thickness, it gives the effective refractive index coefficient, i.e. $\langle \alpha_2 \rangle \equiv n_2$. Using typical values of $d = 100 \mu\text{m}$, $\Delta\epsilon \sim 0.6$, $K = 10^{-6}$ dynes, $\beta = 45^\circ$, we have:

$$n_2 \sim 5 \times 10^{-3} \text{ cm}^2/\text{W}. \quad (3.27)$$

It is interesting to note that the optical nonlinearity associated with nematic director axis reorientation is proportional to the factor $\Delta\epsilon^2/K$, cf. Eq. (3.26). This is typical of orientational fluctuation induced light scattering processes, c.f. Eq. (1.2); although both $\Delta\epsilon$ and K are strongly dependent on the temperature, the combination $\Delta\epsilon^2/K$ is not [132,133]. This is because $\Delta\epsilon$ is proportional to the order parameter S , whereas K is proportional to S^2 . *This temperature independence of the orientation nonlinearity was verified in the experimental study of the temperature dependence of nonlinear diffraction (134).*

In the case of normal incidence, $\beta = 0$, Eq. (3.21) reduces to the familiar “inverted-top” problem:

$$K \frac{\partial^2 \theta}{\partial z^2} + \frac{\Delta\epsilon}{4\pi} E^2 \sin \theta \cos \theta = 0. \quad (3.28)$$

The relation between the reorientation angle and external field can be derived by integrating Eq. (3.28),

$$d = \int_0^{\theta_m} \left(c + \frac{\Delta\epsilon E^2}{8\pi K} \cos(2\theta) \right)^{-\frac{1}{2}} d\theta. \quad (3.29)$$

Here θ_m is the maximum reorientation angle and the constant c can be determined by minimizing the Free energy:

$$\frac{Ed}{2} \left(\frac{\Delta\epsilon}{4\pi K} \right)^{\frac{1}{2}} = \int_0^{\theta_m} \frac{d\theta}{(\sin^2 \theta_m - \sin^2 \theta)^{\frac{1}{2}}} = F(k). \quad (3.30)$$

The right-hand side of Eq. (3.30), $F(k)$ is an elliptic integral of the first kind, which is tabulated for values of $k = \sin \theta_m \leq 1$. For relatively small reorientation angles, the elliptic integral can be expanded as a series. To the second order, we have:

$$E = \left(\frac{4\pi K}{\Delta\epsilon} \right)^{\frac{1}{2}} \frac{\pi}{d} \left(1 + \frac{1}{4} \sin^2 \theta_m + \dots \right). \quad (3.31a)$$

Eq. (3.31a) shows that a deformation with $\theta_m \neq 0$ occurs only if the optical electric field exceeds the threshold E_F , the so-called *Optical Fredericksz Transition Threshold*

$$E_F = \left(\frac{4\pi K}{\Delta\epsilon} \right)^{\frac{1}{2}} \frac{\pi}{d}. \quad (3.31b)$$

Notice that the ‘voltage’ $V_F = E_F d = \left(\frac{4\pi K}{\Delta\epsilon} \right)^{\frac{1}{2}} \pi$ is independent of sample thickness.

3.3.1. More exact treatment – Plane wave and Gaussian laser beam; nonlocal dependence

A more quantitative treatment would need to account for the anisotropies of the elastic constants, the optical field propagation characteristics in the birefringent nematic film, and the mutual feedback between the field and the orientation [134,135]. For reorientation in the x - z plane, only the elastic energies associated with the splay (K_1) and bend (K_3) are involved. Writing $\hat{n} = \sin \theta'' \hat{x} + \cos \theta'' \hat{z}$, we have

$$(\nabla \cdot \hat{n})^2 = \sin^2 \theta'' \left(\frac{\partial \theta''}{\partial z} \right)^2 \quad (3.32a)$$

$$(\hat{n} \times \nabla \times \hat{n})^2 = \cos^2 \theta'' \left(\frac{d\theta''}{dz} \right)^2 \quad (3.32b)$$

where $\theta'' = \theta + \beta$. The Euler–Lagrange equation associated with a small director axis reorientation angle $\theta(z)$ is:

$$\frac{\partial F}{\partial \theta} - \frac{d}{dz} \frac{\partial F}{\partial \theta'} = 0 \quad (3.33)$$

where $\theta' = d\theta''/dz$.

The propagation of the optical field inside the nematic is described by the wave equation:

$$\nabla (\nabla \cdot \mathbf{E}_{op}) - \nabla^2 \mathbf{E}_{op} - \frac{\omega^2}{c^2} \bar{\epsilon} \mathbf{E}_{op} = 0 \quad (3.34)$$

$$\mathbf{E}_{op} = E_x \hat{x} + E_z \hat{z}. \quad (3.34)$$

Note that the dielectric tensor $\bar{\varepsilon}$ is dependent on the optical field \mathbf{E}_{op} as a result of the optical field induced director axis reorientation, and hence E_x and E_z remain to be calculated from Maxwell's equations in a self-consistent manner. In other words, (3.33) and (3.34) have to be solved in a self-consistent manner to yield $\theta(z)$ and $\mathbf{E}_{op}(z)$.

Again, for simplicity in illustration, and assuming the hard-boundary condition and ignoring the surface interaction term, Eqs. (3.32) and (3.33) yield:

$$\begin{aligned} & (K_1 \sin^2 \theta'' + K_3 \cos^2 \theta'') \frac{d^2 \theta}{dz^2} - (K_3 - K_1) \sin \theta'' \cos \theta'' \left(\frac{d\theta}{dz} \right)^2 \\ & + \frac{\Delta\varepsilon}{16\pi} \left[\sin 2\theta'' \left(|E_x|^2 - |E_y|^2 \right) + \cos 2\theta'' (E_x E_z^* + E_x^* E_z) \right] = 0. \end{aligned} \quad (3.35)$$

In the limit of very small director axis reorientation, that is, $\theta \ll 1$, Eq. (3.35) reduces to the simplified one given in (3.21). In general, solving for self-consistent solutions of \mathbf{E}_{op} and $\theta(z)$ from (3.34) and (3.35) is a very complex exercise, as these equations are highly nonlinear and are intricately coupled nonlocal dynamical equations; they also exhibit bistabilities, multi-stabilities and instabilities, especially when external feedbacks are introduced. The various nonlinear optical self-actions and mutual interactions in wave mixing processes associated with a laser induced director axis reorientation are discussed in the next section; we shall continue here with further examination of the material response.

Plane wave solutions of these coupled equations reveal the molecular correlation in the z -dimension, i.e. cell thickness. While this is the usual case in liquid crystal electro-optical devices where a spatially uniform electric field is applied across the cell, nonlinear optics experiments usually employ laser beams of finite beam size, and often focused laser beams. If the laser beam size ω_0 is comparable to or smaller than the film thickness, transverse correlation effects begin to manifest themselves; molecules situated within and outside the laser beam will exert torques on each other, and thereby influencing the resultant director axis reorientation profile. The torque balance equation describing these reorientation processes, e.g. Eqs. (3.21) and (3.35) are basically diffusion equations, where the elastic term plays the role of the diffusive mechanism. As a result of this diffusive nonlocal effect, as in many other physical processes, the spatial profile of the response is not the same as the excitation profile [136–142]. For an input Gaussian laser beam with a half-width ω_0 , the reorientation profile is not Gaussian, although it is still a bell-shaped function with a half-width ω_θ . In general, for the $\beta = 0$ case, the half-width ω_θ is always larger than ω_0 for all values of ω_0 , approaching ω_0 for large values of ω_0/d (cf. Fig. 3.6(a)). On the other hand, for the $\beta = 0$ case, ω_θ can be smaller than ω_0 , depending on whether ω_0 is smaller or larger than d (cf. Fig. 3.6(b)).

The detailed calculations given in [136] also show that in the case of a laser that is at normal incidence, i.e. $\beta = 0$, there is a threshold intensity for finite reorientation to occur. The threshold intensity depends on both the thickness of the film and the beam size ω_0 . For $\omega_0 \ll d$, the threshold intensity increases dramatically (compared with the value for a plane wave). There is no threshold intensity for field induced reorientation in the $\beta \neq 0$ case.

These nonlocal optical nonlinearities play crucial roles in many beam coupling, breakup and combining processes, spatial solitons formation and interactions in nematic liquid crystalline media (see for example [139–142]).

3.3.2. Director axis reorientation by pulsed lasers – Onset and relaxation dynamics

The dynamics of molecular reorientation are described by balancing all the prevailing torques acting on the director axis. For the interaction geometry given in Fig. 3.5, and assuming an elastic constant K and an effective viscosity coefficient γ for the viscous and elastic torques, the resulting equation becomes:

$$\gamma \frac{\partial \theta}{\partial t} = K \frac{\partial^2 \theta}{\partial z^2} + \frac{\Delta\varepsilon \langle E_{op}^2 \rangle}{8\pi} \sin(2\beta + 2\theta). \quad (3.36)$$

If θ is small, this becomes

$$\gamma \dot{\theta} = -\frac{K\pi^2}{d^2} \theta + \frac{\Delta\varepsilon \langle E_{op}^2 \rangle}{8\pi} \sin 2\beta + \theta \frac{\Delta\varepsilon \langle E_{op}^2 \rangle}{4\pi} \cos 2\beta. \quad (3.37)$$

Assuming that E_{op}^2 is a plane wave and strong anchoring at the boundaries, we may write $\theta(t, z) = \theta(t) \sin(\pi z/d)$, and substituting it into (3.37), we get

$$\gamma \dot{\theta} = -\frac{K\pi^2}{d^2} \theta + \frac{\Delta\varepsilon \langle E_{op}^2 \rangle}{8\pi} \sin 2\beta + \theta \frac{\Delta\varepsilon \langle E_{op}^2 \rangle}{4\pi} \cos 2\beta. \quad (3.38)$$

When the optical field is turned off, i.e. $E_{op} = 0$, we have

$$\begin{aligned} \gamma \dot{\theta} &= -\frac{K\pi^2}{d^2} \theta \\ \theta &= \theta_{\max} e^{-t/\tau_r} \\ \tau_r &= \gamma d^2 / K\pi^2. \end{aligned} \quad (3.39)$$

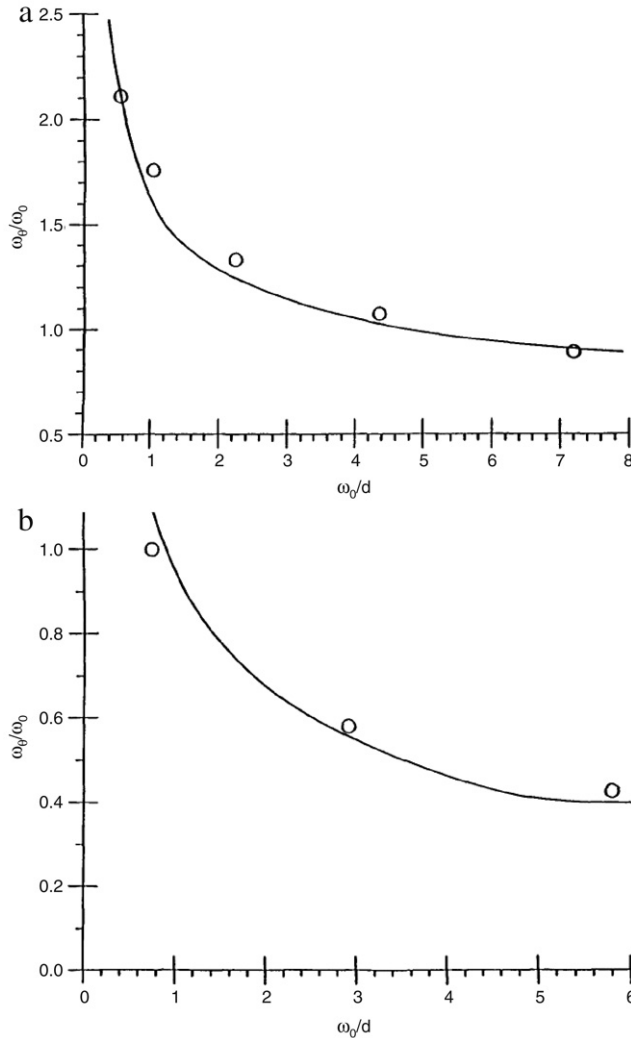


Fig. 3.6. Nonlocal transverse dependence of the director axis reorientation on the (Gaussian) laser's beam waist: (a) Plot of ω_θ/ω_0 as a function of ω_0/d for $\beta \neq 0$. (b) Plot of ω_θ/ω_0 as a function of ω_0/d for $\beta = 0$.

Here θ_{\max} is the director axis reorientation angle just before the laser pulse is turned off and τ_r is the director axis relaxation time constant. For typical cell thickness $d \sim 10 \mu\text{m}$, $\gamma = 0.1 \text{ P}$, and $K = 10^{-6} \text{ dyne}$, we have $\tau_r \approx 10 \text{ ms}$. Using a thinner cell of less viscous liquid crystals, the response time can be reduced further to 1 ms or even sub-milliseconds, but obviously this speed is not useful for fast modulation applications in digital data transmission, although it is satisfactory for image processing systems such as conventional displays.

On the other hand, the *rise time of the reorientation can be fast* since the process is dependent on the laser intensity. This fast response will be important for nonlinear optics applications involving one-way switching and will occur when the optical torque exerted by the intense laser field on the director axis is much larger than the elastic torque, i.e.

$$\left| \frac{\Delta\varepsilon \langle E_{op}^2 \rangle}{8\pi} \sin(2\beta + 2\theta) \right| \gg \left| K \frac{\partial^2 \theta}{\partial z^2} \right|. \quad (3.40)$$

In that case, the influence from the bulk and surface torques, and therefore the dependence on the cell thickness d is absent and the optical field needs to 'overcome' only the viscous drag. Eq. (3.38) then becomes, in the small angle approximation:

$$\begin{aligned} \dot{\theta} &= a + b\theta \\ \theta(t) &= \frac{a}{b} (\text{e}^{bt} - 1). \end{aligned} \quad (3.41)$$

Here $a = \Delta\varepsilon \langle E_{op}^2 \rangle \sin 2\beta / 8\pi \gamma$, and $b = \Delta\varepsilon \langle E_{op}^2 \rangle \sin 2\beta / 4\pi \gamma$.

Assuming for simplicity that the laser is a top-hat function of duration τ_p , we can see that if the laser intensity is sufficiently large such that $a\tau_p \sim \Delta\varepsilon E_{op}^2 \tau_p/\gamma$, it is possible to induce significant reorientation $\theta(\tau_p)$. Such an ultrafast responding director axis deformation in nematic as well as smectic liquid crystals has been demonstrated in early studies by Khoo and Normandin [143,144] using nanosecond laser pulses, and by Eichler et al. [145] using picosecond lasers. Accompanying such reorientations, these workers have also observed ultrasonic generation [145], and flow-reorientation coupling effects. The study [145] has also revealed the role played by the moment of inertia I_m of the liquid crystals; taking I_m into account, a general torque balance equation for the interaction geometry of Fig. 3.5 is of the form:

$$\text{Im} \frac{d^2\phi}{dt^2} + \gamma_1 \frac{d\phi}{dt} = [K_1 \sin^2 \phi + K_3 \cos^2 \phi] \frac{d^2\phi}{dz^2} + [(K_1 - K_3) \sin \phi \cos \phi] \left(\frac{d\phi}{dz} \right)^2 + [\alpha_2 \sin^2 \phi - \alpha_3 \cos^2 \phi] \frac{dv}{dz} + \varepsilon_0 \Delta\varepsilon E^2 \sin \phi \cos \phi \quad (3.42)$$

where $\phi = \theta + \beta$, v the flow velocity, γ_1, α_2 and α_3 are the viscosity coefficients (recalling that we need five viscosity coefficients to describe flow of nematic liquid crystals as anisotropic fluids [3,5]). These studies have demonstrated that indeed nematic liquid crystal reorientation process can be very fast under intense electric fields. Unlike dc or low frequency ac fields, however, optical frequency electric fields do not involve undesirable resistive or capacitive effects.

Although the spatially uniform applied field is common in electro-optical applications where an ac voltage is applied between the two cell windows, in nonlinear optics a more frequently employed geometry involved a sinusoidal optical intensity employed in various optical wave mixing or real time holography processes; the molecular correlation between molecules situated in the intensity maxima and minima is manifested in the form of a functional dependence on the grating constant Λ as well as the cell thickness d . Consider, for example, an optical intensity function of the form $\langle E_{op}^2 \rangle \sim E^2 (1 + \cos qy)$. The induced reorientational angle will have a corresponding modulation of the form:

$$\theta \sim \theta(t) \sin \left(\frac{\pi z}{d} \right) \cos qy. \quad (3.43)$$

The orientational relaxation dynamics when the optical field is turned off now becomes

$$\gamma \dot{\theta} = -K \left(\frac{\pi^2}{d^2} + q^2 \right) \theta. \quad (3.44)$$

The corresponding orientational relaxation time constant becomes:

$$\tau_r = \frac{\gamma}{K} \left(\frac{1}{\frac{\pi^2}{d^2} + q^2} \right). \quad (3.45)$$

Writing the wave vector q in terms of the grating constant $\Lambda = 2\pi/q$, we have

$$\tau_r = \frac{\gamma}{K} \left(\frac{1}{\frac{\pi^2}{d^2} + \frac{4\pi^2}{\Lambda^2}} \right). \quad (3.46)$$

For $\Lambda \ll d$, the orientational relaxation dynamics is dominated by the intermolecular torques whereas for $d \ll \Lambda$, the dynamics is decided by the boundary elastic torques. These nonlocal spatial dependencies play an important role in dictating the wave mixing efficiency and other nonlinear optical effects. In conjunction with other nonlocal physical processes such as ionic diffusion and space charge field formations in photorefractive effects [56], for example, they give rise to nonlocal refractive index changes, i.e. where the index grating function is phase shifted from the imparted optical intensity function. Such a nonlocal phase shift is responsible for various unique beam coupling effects. As in inorganic photorefractive crystals, this nonlocal diffusive nonlinear optical response in nematic liquid crystals gives rise to the existence of optimal conditions for cell thickness versus the grating spacing in the wave mixing efficiency (Fig. 3.7).

3.4. Giant, supra and colossal orientational optical nonlinearities in doped nematic liquid crystals

As pointed out in Section 1, the observations of purely optically induced director axis reorientation and the resulting optical nonlinearities ushered in the era of giant optical nonlinearities in the late 70s and early 80s. The nonlinear index coefficients n_2 associated with these processes are in the range 10^{-4} – 10^{-3} cm 2 /W. Usually, the liquid crystal cell thickness d is on the order of $100\text{ }\mu\text{m}$ (10^{-2} cm), and so in order to create a nonlinear optical phase shift $\delta = \Delta n d 2\pi/\lambda \sim \pi$ for visible light ($\lambda \sim 0.5\text{ }\mu\text{m}$), i.e. $\Delta n \sim 2.5 \times 10^{-3}$, a laser intensity on the order 1 W/cm^2 is required. This kind of intensity level is indeed frequently employed in studies involving director axis reorientation by a purely optical field through the dipolar interaction.

A number of mechanisms have been discovered in the last two decades, resulting in optical nonlinearities characterized by n_2 in the range $10^{-3} \rightarrow 10^3$ cm 2 /W. For $n_2 > 1\text{ cm}^2/\text{W}$, they have been called supra-optical nonlinearities, and for

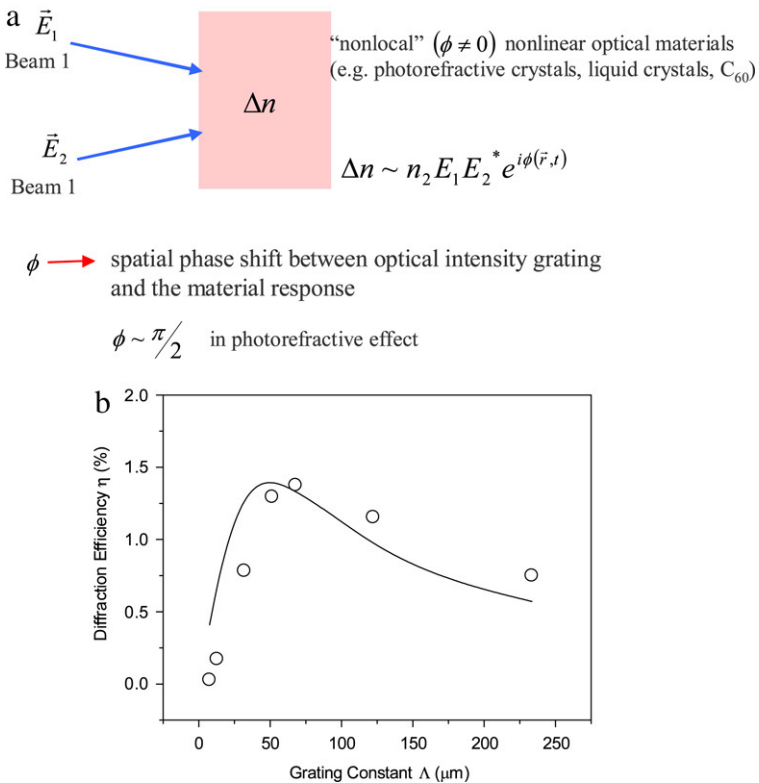


Fig. 3.7. Upper: schematic depiction of the nonlocal index modulation induced by mixing two coherent lasers in a nematic liquid crystal. Lower: exemplary experimental observation of the photorefractive self-diffraction efficiency as a function of the grating constant; maximum diffraction occurs at the predicted grating spacing $\Lambda = 2d$.

$n_2 > 1000 \text{ cm}^2/\text{W}$, they have been called colossal nonlinearities. In all cases, they involve introducing a photosensitive dye or molecular dopants to mediate, facilitate and enhance the reorientation process [7,24,53–66,146]. Corresponding to these dramatic improvements in n_2 , the laser power needed to create observable nonlinear optical effects have also dropped dramatically to the mW, μW and even nW levels!

In nematic liquid crystals doped with some absorbing dye molecules, studies [22,146] have shown that the excited dye molecules could exert an intermolecular torque $\tau_{\text{mol}} \sim \eta \tau_{\text{op}}$ on the liquid crystal molecules that could be stronger than the optical torque τ_{op} (η can be as large as 100). On the other hand, Gibbons et al. [146] have observed that, under prolonged exposure, dye doped liquid crystals (DDLCs) will align themselves in a direction orthogonal to the optical electric field and the propagation wave vector i.e., in the \hat{y} direction with reference to Fig. 3.8; Under suitable surface treatment conditions, such reorientational effects can be “locked” into place when the optical field is removed. The stored reorientation profile can be erased by the application of an ac field, for example, to realign the director axis to its original homeotropic state.

Khoo et al. [53] reported the observation of a large negative reorientational effect in some dye doped nematic cells. Using a variety of different polarization configurations between the pump and probe beam in the dynamic grating diffraction study, the authors have established that the negative change in the refractive index (i.e., negative nonlinearity) is associated with the liquid crystal director axis realigning towards the z direction. The efficiency of this reorientation process is governed by the types of dye molecules used as dopants. These observations then led to their discovery of supra- and colossal optical nonlinearities in methyl-red dye doped nematic liquid crystals (MRNLC) with refractive index coefficients $n_2 \gg 1 \text{ cm}^2/\text{W}$ [7, 24]. Studies of MRNLC also showed that the nonlinearities can be modulated by an applied ac electric field by changing the frequency; a low frequency [e.g. 300 Hz] ac field will enhance the reorientation nonlinearity, whereas a high frequency [30 kHz] ac field will quench the reorientation and ‘turn-off’ the optical nonlinearity, pointing to the possibility of dual frequency switching/modulation applications [147,148].

Studies of azobenzene liquid crystals (ALC) and ALC doped nematic liquid crystals have shown that this is also an effective mechanism for creating large optical nonlinearities [149–152]. In these materials, the ground state azodye molecules are in the trans-configuration that is oblong in shape and they conform to the alignment of the director axis. When photoexcited to the bent cis-configuration, they create disorder, i.e. induced a negative change in the order parameter ($-\Delta S$), resulting in a change in the refractive indices and birefringence. In some azodye molecules, such trans–cis isomerism can happen quite rapidly [in nanoseconds], and so the resulting order parameter and refractive index changes can be effected very rapidly [151],

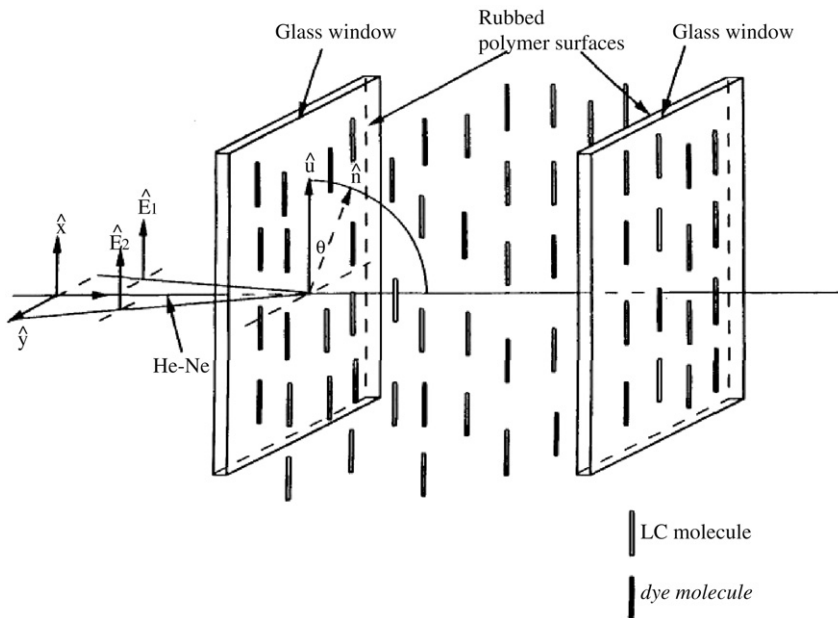


Fig. 3.8. Schematic diagram of the optical wave mixing of two coherent writing fields E₁ and E₂ in a planar aligned dye doped liquid crystal; E₃ is the probe beam.

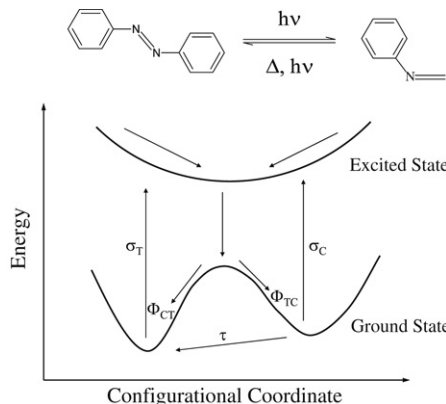


Fig. 3.9. [Upper] Molecular structural changes associated with Trans–cis isomerization of AZO molecules upon optical illumination. Lower diagram shows the excitation energy versus the molecular coordinate associated with these photoexcited processes and the various trans–cis cross-sections.

152]. A detailed discussion of such *fast optical nonlinearities* associated with laser induced temperature and order parameter modification is presented at the end of next section (Fig. 3.9).

3.5. Photorefractivity in nematic liquid crystals

In a previous section, we have discussed the operation of a Liquid Crystal Spatial Light Modulator where the responsible mechanism is the photoconduction generated by the incident optical field in the semiconductor layer adjacent to the liquid crystals sandwiched between two electrodes. A similar mechanism underlies the so-called photorefractive effect discovered by Khoo [56,57] and Sukhov et al. [55] in which the photoinduced charges and fields occur within the liquid crystal. In this case, a dc field is needed to mediate and augment the efficiency of the processes such as current flow and space charge buildup by anisotropic conductivities and dielectric constants [56,57]. This process of photo charge production and creation of local space charge fields that result in a refractive index change is analogous to the photorefractive (PR) effect occurring in electro optically active polymers [28] and inorganic crystals [29].

There is however an important difference between the inorganic photorefractive crystal and liquid crystal cases. In inorganic photorefractive crystals, such as BaTiO₃, the induced index change Δn is *linearly related* to the total electric field E present, the so-called Pockel cell effect, $\Delta n = \gamma_{\text{eff}} E$ where the sign and magnitude of the effective electro-optic coefficient γ_{eff} depends on the symmetry class of the crystal and the direction of the electric field. On the other hand, nematic liquid

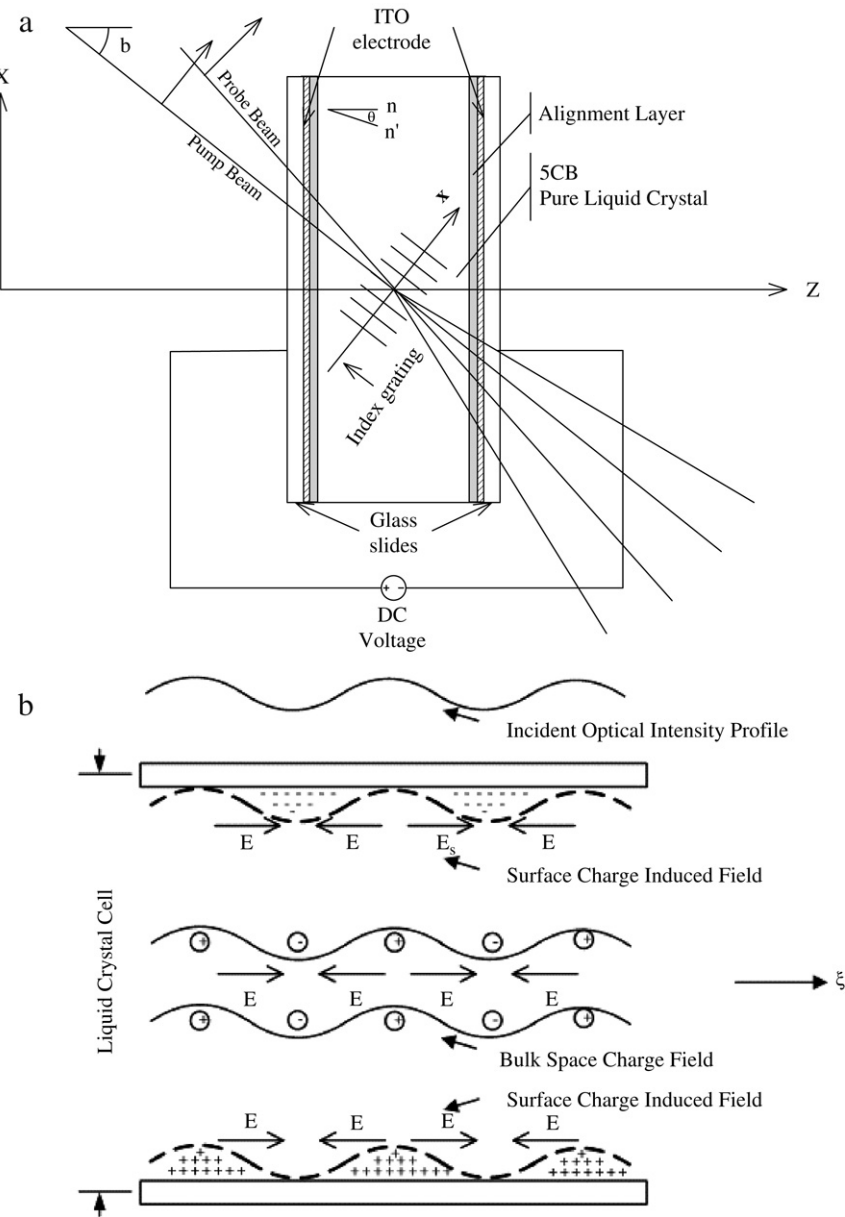


Fig. 3.10. (a) Schematic depiction of the optical wave mixing configuration for photorefractivity of nematic liquid crystal under a bias field. (b) Schematic showing various space charge fields involved in the orientational photorefractive effect in nematic liquid crystals. Note that the space charge field amplitude grating is $\pi/2$ phase shifted from the incident optical intensity grating function.

crystals possess centro-symmetry ($+\hat{n}$ is equivalent to $-\hat{n}$) and the field induced refractive-index change is quadratic in the total electric field, i.e., $\Delta n = n_2 E^2$, the so-called Kerr effect. Such quadratic dependence actually allows the mixing of the applied dc field with the space charge field for enhanced director axis reorientation effect, as various studies of photorefractivity in liquid crystals have demonstrated [55–57,153–161].

On the other hand, there is an interesting commonality. Just as in inorganic photorefractive crystals, an optical intensity grating acting on the nematic liquid crystals will produce an index grating that is phase shifted by $\sim \pi/2$ from the optical intensity as a result of the charge diffusion and space charge field build-up, c.f. Fig. 3.10. The $\pi/2$ phase shift gives rise to strong two beam coupling effects – for example a unidirectional flow of energy from one beam to the other.

The photorefractive effect best exemplifies the interplay between various applied fields and nematic liquid crystal material parameters. We therefore devote a special section here to illustrate the basic theories and mechanisms. In a typical experimental set-up as shown in Fig. 3.10, two linearly polarized coherent beams are overlapped at an oblique incident angle on an aligned liquid crystal cell with transparent conducting electrode coated windows. A small dc voltage (typically

a 2–3 V) is applied across the cell window. The total free energy of the system becomes:

$$F = \frac{K}{2} \left\{ \left[\vec{\nabla} \cdot n(\vec{r}) \right]^2 + \left[\vec{\nabla} \times n(\vec{r}) \right]^2 \right\} - \frac{\Delta\epsilon}{8\pi} \left[\vec{E} \cdot n(\vec{r}) \right]^2 - \frac{\Delta\epsilon_{op}}{8\pi} \left[\vec{E}_{op} \cdot n(\vec{r}) \right]^2. \quad (3.47)$$

Here $\Delta\epsilon$ is the dc field anisotropy and $\Delta\epsilon_{op}$ is the optical dielectric anisotropy. Denoting the reoriented director axis by $\hat{n} = (\sin\theta, 0, \cos\theta)$, and minimizing the Free energy with respect to the reorientation angle θ yields the well-known Euler–Lagrange equation for θ :

$$K \frac{d^2\theta}{dz^2} + K \frac{d^2\theta}{d\xi^2} + \frac{\Delta\epsilon}{4\pi} [\sin\theta \cos\theta (E_x^2 - E_z^2) + \cos(2\theta) E_x E_z] + \frac{\Delta\epsilon_{op} \cdot E_{op}^2}{8\pi} \sin 2(\beta + \theta) = 0. \quad (3.48)$$

In a nematic containing photo-charge producing impurities or dopants such as dyes, carbon nanotubes, fullerene C60, ...etc., three forms of space charge fields are created within the bulk of the cell [55–57]. One component is the so-called photorefractive-like space charge field E_{ph} [55]:

$$E_{ph} = E_{ph}^{(0)} \cos(q\xi) = \left[\frac{mk_B T}{2e} q v \frac{\sigma - \sigma_d}{\sigma} \right] \cos(q\xi) \quad (3.49)$$

where m is the optical modulation factor, k_B is Boltzmann constant, σ = conductivity under illumination, σ_d = dark state conductivity, and $v = (D^+ - D^-) / (D^+ + D^-)$, where D^+ and D^- are the diffusion constants for positive and negative ions, respectively, $q = 2\pi/\Lambda$ is the grating wave vector, with Λ the grating constant. Note that $E_{ph}[\sim \cos(q\xi)]$ is $\pi/2$ phase shifted from the imparted optical intensity grating $E_{op}^2 \sim \sin(q\xi)$.

The two other space charge field components $E_{\Delta\sigma}$ and $E_{\Delta\epsilon}$ come from the applied field E_{dc} along the z direction, in conjunction with the conductivity, dielectric anisotropies and the reoriented [by an angle θ] director axis. These space charge fields are of the form [56,57,162]:

$$E_{\Delta\sigma} = - \frac{[(\sigma_{||} - \sigma_{\perp}) \sin\theta \cos\theta]}{\sigma_{||} \sin^2\theta + \sigma_{\perp} \cos^2\theta} E_{dc}; \quad E_{\Delta\epsilon} = - \frac{[(\epsilon_{||} - \epsilon_{\perp}) \sin\theta \cos\theta]}{\epsilon_{||} \sin^2\theta + \epsilon_{\perp} \cos^2\theta} E_{dc}. \quad (3.50)$$

For the small angle approximation, the above equations can be linearized to yield,

$$E_{\Delta\sigma} \approx - \frac{\Delta\sigma}{\sigma_{\perp}} \theta E_{dc}; \quad E_{\Delta\epsilon} \approx - \frac{\Delta\epsilon}{\epsilon_{\perp}} \theta E_{dc}. \quad (3.51)$$

The total electric field in component form then becomes:

$$\begin{aligned} E_{\text{total}} &= \left[- \left(\frac{\Delta\sigma}{\sigma_{\perp}} + \frac{\Delta\epsilon}{\epsilon_{\perp}} \right) E_{dc} \theta \cos\beta - E_{ph} \cos\beta, 0, E_{dc} - \left(\frac{\Delta\sigma}{\sigma_{\perp}} + \frac{\Delta\epsilon}{\epsilon_{\perp}} \right) E_{dc} \theta \sin\beta - E_{ph} \sin\beta \right] \\ &= [- (E_{\Delta} \cdot \theta + E_{ph}) \cos\beta, 0, E_{dc} - (E_{\Delta} \cdot \theta + E_{ph}) \sin\beta] \end{aligned} \quad (3.52)$$

where $E_{\Delta} = \left(\frac{\Delta\sigma}{\sigma_{\perp}} + \frac{\Delta\epsilon}{\epsilon_{\perp}} \right) E_{dc}$.

The torque balance equation thus becomes:

$$K \frac{d^2\theta}{dz^2} + k \frac{d^2\theta}{d\xi^2} + \frac{\Delta\epsilon}{4\pi} [E_{\Delta} E_z \cos(\beta) \cdot \theta + E_z E_{ph} \cos(\beta)] + \frac{\Delta\epsilon \cdot E_{op}^2}{8\pi} [\sin(2\beta) + 2 \cos(2\beta) \cdot \theta] = 0. \quad (3.53)$$

Assuming that a “hard” boundary condition exists, a solution for θ is of the form,

$$\theta = \theta_0 \sin\left(\frac{\pi z}{d}\right) \cos(q\xi). \quad (3.54)$$

Eq. (3.53) then yields:

$$\theta_0 = \frac{\frac{\Delta\epsilon_{op} \cdot E_{op}^2}{8\pi} \sin(2\beta) + \frac{\Delta\epsilon \cdot E_{dc} E_{ph}^{(0)}}{4\pi} \cos(\beta)}{\left[\frac{\Delta\epsilon}{4\pi} E_{\Delta} E_{dc} \cos(\beta) + \frac{\Delta\epsilon_{op}}{4\pi} E_{op}^2 \cos(2\beta) \right] - \left[\left(\frac{\pi}{d} \right)^2 + q^2 \right] K}. \quad (3.55)$$

Or,

$$\theta_0 = \frac{\frac{1}{2} \frac{\Delta\epsilon_{op}}{\Delta\epsilon} E_{op}^2 \cdot \sin(2\beta) + E_{ph}^{(0)} E_{dc} \cos(\beta)}{\left[E_{\Delta} E_{dc} \cos(\beta) + \frac{\Delta\epsilon_{op}}{\Delta\epsilon} E_{op}^2 \cos(2\beta) \right] - E_F^2 \left[1 + \left(\frac{qd}{\pi} \right)^2 \right]}. \quad (3.56)$$

where $V_F = E_F^d = \pi \sqrt{\frac{K}{\varepsilon_0 \Delta \varepsilon}}$. Stable solutions are associated with a positive denominator in Eq. (3.56), i.e., we have

$$E_{dc} \geq E_F \left[\frac{\left[1 + (qd/\pi)^2 \right] - (\Delta \varepsilon_{op}/\Delta \varepsilon) (E_{op}/E_F)^2 \cos(2\beta)}{\left(\frac{\Delta \sigma}{\sigma_\perp} + \frac{\Delta \varepsilon}{\varepsilon_\perp} \right) \cdot \cos \beta} \right]^{\frac{1}{2}} = \alpha \cdot E_F. \quad (3.57)$$

This allows us to identify a threshold field E_{th} ,

$$E_{th} = \eta \cdot E_F = \left[\frac{\left[1 + (qd/\pi)^2 \right] - (\Delta \varepsilon_{op}/\Delta \varepsilon) (E_{op}/E_F)^2 \cos(2\beta)}{\left(\frac{\Delta \sigma}{\sigma_\perp} + \frac{\Delta \varepsilon}{\varepsilon_\perp} \right) \cdot \cos \beta} \right]^{\frac{1}{2}} \cdot E_F. \quad (3.58)$$

Since the optical intensity used is generally in the mW/cm² regime, $E_{op}/E_F \ll 1$, and the factor η is essentially independent of the optical intensity. For 5CB, we have $K \sim 10^{-11}$ N, the ac field dielectric constant $\Delta \varepsilon \sim 11$ ($\varepsilon_{||} \sim 16$, $\varepsilon_\perp \sim 5$) and $\Delta \sigma/\sigma_\perp \sim 0.5$. For typical wave mixing geometrical and optical parameters ($qd \sim 2\pi$, and the internal angle $\beta = 22.5^\circ$), we have $V_F \sim 1$ V, $\eta \sim 1.5$ and $V_{th} = \eta V_F \sim 1.5$ V. In general, because of various different boundary alignment layer materials used (some are photo-conducting, some are photorefractive, and some are charge carrier injectors), the observed thresholds vary considerably, but are all within the few V's range predicted with the bulk theories presented above. Nevertheless, in quantitative studies taking into account surface contributions, especially if these surfaces are capable of charge injections, photoconductive or photorefractive [see for example [153–163]]...etc., considerable deviations from these threshold values and optical field intensity dependence will arise.

3.6. Optical nonlinearities associated with order parameter changes, thermal and density effects

Under the action of an optical field of arbitrary duration, there are several mechanisms that will lead to changes in the refractive indices of the liquid crystals for a fixed director axis orientation. The total index change Δn is in general given by:

$$\Delta n = \left(\frac{\partial n}{\partial T} \right)_\rho dT + \left(\frac{\partial n}{\partial \rho} \right)_T d\rho^T + \left(\frac{\partial n}{\partial \rho} \right)_T d\rho^e + \left(\frac{\partial n}{\partial S} \right)_{T,\rho} dS. \quad (3.59)$$

The first term, $(\partial n/\partial T)_\rho dT$ on the RHS, arises from ‘internal temperature’ change in the molecules caused by a very short pulsed laser, which modifies the spectral dependence of the molecular absorption and emission process [164,165]. This term is usually quite small, and is not affected significantly by the ordering or molecular correlation present in the liquid crystalline phase. The second term on the RHS comes from a laser induced overall rise in temperature and the resulting change in the density. Again, this effect is typical of all materials and not specific to liquid crystals. The third term on the RHS is due to the electrostrictive effect in non-absorbing materials – the tendency of a material to move towards a region of high field strength. The only contribution unique to (nematic) liquid crystalline systems is the last term, which comes from the laser induced order parameter changes.

These thermal, density and order parameter changes occur on a faster time scale than director axis reorientation under moderate intensity laser illumination, and may be the preferred mechanism in some applications. We therefore discuss here the essential fundamentals and the interplays between laser induced temperature and density changes in liquid crystals; a more specific example of laser induced order parameter modification and nonlinear optical switching processes is discussed in detail in section IV. Consider again a wave mixing geometry where the impinging optical intensity is a sinusoidal intensity grating created by interfering two coherent co-polarized plane-wave laser beams. For equal intensity beams, we have $E^2 = 2E_0^2 \cos qy$ where $\mathbf{q} = \mathbf{k}_1 - \mathbf{k}_2$ is the grating wave vector. Correspondingly, $\Delta \rho$ and ΔT are of the form $\Delta \rho = \rho(t) \cos \mathbf{q} \cdot \mathbf{y}$; $\Delta T = T(t) \cos \mathbf{q} \cdot \mathbf{y}$ where $\rho(t)$ and $T(t)$ are the density and temperature grating amplitudes. The equations governing laser induced temperature and density changes are the coupled hydrodynamical equations (1,2):

$$-\frac{\partial^2}{\partial t^2} (\Delta \rho) + v^2 \nabla^2 (\Delta \rho) + v^2 \beta_T \rho_0 \nabla^2 (\Delta T) + \frac{\eta}{\rho_0} \frac{\partial}{\partial t} \nabla^2 (\Delta \rho) = \frac{\gamma^e}{8\pi} \nabla^2 (E^2) \quad (3.60a)$$

$$\rho_0 C_v \frac{\partial}{\partial t} (\Delta T) - \lambda_T \nabla^2 (\Delta T) - \frac{(C_p - C_v)}{\beta_T} \frac{\partial}{\partial t} (\Delta \rho) = \frac{u}{\tau} = \frac{\alpha n c}{4\pi} E^2 \quad (3.60b)$$

where ρ_0 is the unperturbed density of the liquid crystal, C_p and C_v the specific heats, λ_T the thermal conductivity, η the viscosity, v the speed of sound, γ^e the electrostrictive coefficient [$\gamma^e = \rho_0 (\rho \varepsilon / \partial \rho)_T$], β_T the coefficient of volume expansion, and η a viscosity coefficient and α the photo-absorption constant. Eq. (3.60a) describes the thermal expansion and electrostrictive effects on the density change, whereas (3.60b) describes the photo-absorption and the resulting temperature rise and heat diffusion process.

For $0 < t < \tau_p$, where τ_p is the duration of the laser pulse (assumed to be a square pulse), these grating amplitudes are shown to be of the form [111,112]:

$$T(t) = \left[\frac{\alpha c n E_0^2}{4\pi \rho_0 C_v \Gamma_R} \right] (1 - \exp(-\Gamma_R t)) \quad (3.61)$$

$$\rho(t) = \left[\frac{\gamma^e E_0^2}{4\pi v^2} \right] (1 - \exp(-\Gamma_B t) \cos \Omega t) - \left[\frac{\beta_T \alpha c n E_0^2}{4\pi C_v \Gamma_R} \right] (1 - \exp(-\Gamma_R t)). \quad (3.62)$$

The dynamics of the thermal grating amplitude is characterized by a response time constant $\tau_R = \Gamma_R^{-1} = \frac{\rho_0 C_v}{\lambda_T q^2}$ whereas the density grating is characterized by a Brillouin (acoustic) time constant $\tau_B = \Gamma_B^{-1} = \frac{2\rho_0}{\eta q^2}$. The sound frequency Ω is given by $\Omega = \sqrt{q^2 v^2 - \Gamma_B^2}$. In liquid crystals $n \sim 1.5$, $\eta = 7 \times 10^{-2} \text{ kg m}^{-1} \text{ s}^{-1}$, $v = 1540 \text{ m s}^{-1}$, $\rho_0 = 10^3 \text{ kg m}^{-3}$, $\lambda_T / \rho_0 C_v = 0.79 \times 10^{-7} \text{ m}^2/\text{s}$ [5]. For a grating constant ($\Lambda = 2\pi |\mathbf{k}_1 - \mathbf{k}_2|^{-1}$) of $20 \mu\text{m}$, we have $\tau_R \approx 100 \mu\text{s}$, and $\tau_B \approx 200 \text{ ns}$. These estimates are in very good agreement with actual experimental observations [109,111], where the widely different relaxation time constants of the thermal and density effects provide a means to distinguish their relative contributions in the nonlinear dynamic grating diffraction process.

The density change $\rho(t) = \rho^e(t) + \rho^T(t)$ as given in (3.62) comprises two distinct components:

$$\begin{aligned} \rho^e(t) &= \frac{\gamma^e E_0^2}{4\pi v^2} (1 - \exp(-\Gamma_B t) \cos \Omega t) \\ \rho^T(t) &= \frac{-\beta_T \alpha c n E_0^2}{4\pi C_v \Gamma_R} (1 - \exp(-\Gamma_R t)). \end{aligned} \quad (3.63)$$

One component $\rho^e(t)$ arises from the electrostrictive effect and is proportional to γ^e ; it is characterized by the Brillouin relaxation constant Γ_B and frequency Ω . The ρ^e component gives rise to a propagating wave. The other component $\rho^T(t)$ is the thermoelastic contribution (proportional to β^T) caused by thermal heating and is characterized by the thermal decay constant Γ_R ; it is non-propagative. These propagative and non-propagative components will therefore constructively and destructively interfere with one another, giving rise to an oscillatory (at the frequency Ω of the sound wave) diffraction from the probe beam. Since the magnitude of the wave vector $|\mathbf{k}_1 - \mathbf{k}_2|$ is known and the oscillation frequency Ω can be directly measured, these oscillations in the diffraction provide a means of determining sound velocities in a liquid crystal [109, 143, 144]. Similar thermal grating diffraction studies have ascertained the coupled thermal orientation and guest-host nonlinearities and dynamical characteristics in doped nematic liquids [166–168].

4. Nonlinear optical phenomena observed in liquid crystals

Almost all conceivable nonlinear optical phenomena have been observed in liquid crystals, in time scales spanning picoseconds (10^{-12} s) to hours ($> 10^3 \text{ s}$), involving visible-infrared lasers of powers ranging from MegaWatts (10^6 W) to nano-Watt (10^{-9} W) in bulk media, wave-guided geometries, optical resonators and cavities, and spatial light modulators or light valves. In addition to those discussed in preceding sections, a wide range of nonlinear optical phenomena such as stimulated scattering [169–174], self-phase modulation, -focusing and -defocusing [175–184], spatial soliton formation [185–191], nonlinear interface phenomena [192–197], passive optical switching [198–202], degenerate optical wave mixing and harmonic generation [203–209], beam coupling and beam combining [210–220], optical phase conjugation [221–231], coherent holography and image processing [232–238], and many more nonlinear optical effects [239–329] not grouped into the above categories, have been actively investigated under various conditions. From early observations aimed at unraveling the basic optical nonlinearities of liquid crystals to current studies centering on novel materials and nanostructures with unusual refractive indices [e.g. negative or zero refractive indices] and optical properties, liquid crystalline materials continue to provide a fertile ground for basic as well as application-oriented pursuits. Owing to space limitation, we shall limit our detailed discussion here to only a few exemplary nonlinear optical processes enabled by unique properties of liquid crystals.

4.1. Self-phase modulation, focusing, defocusing and spatial solitons

Self-action effects in which a single laser beam induces changes in the medium it traverses and in turn changes its own properties and characteristics such as frequencies, phase, amplitude, directions, polarizations, duration...etc., have been the mainstay of nonlinear optics ever since the dawn of the field in the 60s [239]. This broad class of processes include harmonic generation, stimulated scattering, self-focusing, self-phase modulation and self-guiding or spatial soliton formation, and self-limiting effects.

In early studies of isotropic phase liquid crystals discussed in Section 3, the nonlinearities involved were rather small, and thus all observations of self-phase modulation and self-focusing processes pertained to propagation effects accumulated over long interaction lengths, and lasers intensity levels on the order of MegaWatt/cm^2 , and were geared towards understanding the optical physics and material properties. The discoveries of giant- and supra-optical nonlinearity in nematic liquid crystals have ushered in the era of external self-focusing with laser power as low as micro- and nano-Watt

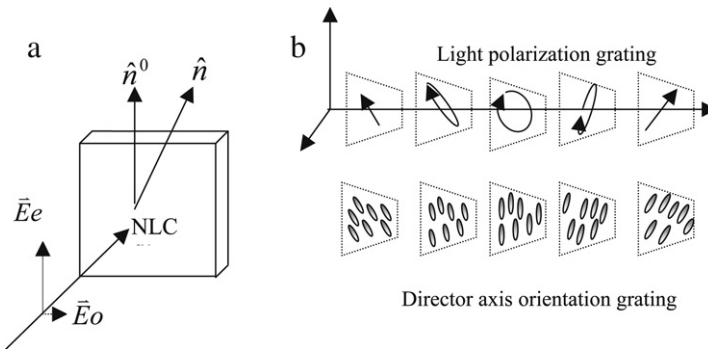


Fig. 4.1. (a) Scattering of a polarized laser by director axis fluctuations in a NLC (b) Optical polarization grating formed by coherent pump beam and the scattered orthogonal polarized component and the resulting director axis reorientation grating.

in some cases [200,201]. Because of the large nonlinearity, the necessary spatial intensity dependent phase shift required to overcome natural beam diffraction can be generated in 10's micron thin nematic liquid crystal cells [241–244]. In the far field diffraction zone, this phase shift is manifested by an increased beam divergence (defocusing) and the formation of spatial rings. Such studies were very actively pursued in the early development of NLC nonlinear optics mainly to understand the nonlinear response of nematics, and ‘external self-focusing’ and transverse bistability phenomena.

Self-phase modulation effects and the resulting modification of the beam’s spatial profile such as divergence and beam size become rather complex and intriguing when the interaction length is sufficiently long such that these processes occur within the liquid crystalline media, or if the exit fields are transferred back onto the media to provide mutual feedback. These complex phenomena have been actively investigated in the contexts of spatial solitons, self-starting pattern formation, bistabilities and instabilities [186–191,245–248]. In these studies, the millisecond response speed of liquid crystals allow convenient visual observations or recording of dynamical processes that are also encountered in other branches of physics, e.g. hydrodynamics, neural computing, ... etc. We will return to this subject in the next section dealing with similar laser induced director axis reorientation process; instead of a spatial redirection of light intensity, the process gives rise to complex dynamical energy exchanges between two orthogonal polarization states of the optical fields.

4.2. Stimulated orientation scatterings – Nonlinear dynamics

Stimulated Orientation Scattering (SOS) best exemplifies nonlinear optics with nematic liquid crystals, in which the director axis reorientations create wave mixing of the incident and its coherent scattered lights as they interact with the director axis and ‘feedback’ on each other, very much like the soliton studies mentioned above. In the case of liquid crystals, however, an interaction length of 100’s μm is sufficient for complete transfer of energy from one beam to another. The process involves dynamical coupling of the director axis reorientation and the nonlinear electromagnetic propagation and their feedback actions very much like those involved in other dynamical studies. Therefore it has served as a more user-friendly ‘test-bed’ for studying and simulating a rich array of similar dynamical processes.

Earlier observation [249] of transient SOS was conducted in the spirit of Stimulated Brillouin Scattering and involved a fairly high power pulsed ruby laser. The more interesting and practical cases, however, involve much lower power continuous-wave lasers [170–174,250,251]. Fig. 4.1 illustrates schematically the stimulated orientation scattering (SOS) processes caused by the director axis fluctuations. Without loss of physics, the incident laser at a frequency ω_1 is represented as a plane wave with its polarization along the x -axis, i.e. $\mathbf{E}(\text{incident}) = \mathbf{E}_e = \mathbf{e}_x E_e e^{i(k_e z - \omega_1 t)}$, i.e. the electric field is parallel to the director axis. Fluctuations in the director axis orientation give rise to orthogonally polarized noise components $\mathbf{E}(\text{scattered}) = \mathbf{E}_o = \mathbf{e}_y E_o^{(\text{noise})} e^{i(k_o z - \omega_2 t)}$ with a spectrum of frequencies ω_2 . Here \mathbf{e}_x and \mathbf{e}_y are unit vectors, E_e and E_o are electric field amplitudes and $k_e = (\omega/c)n_e$ and $k_o = (\omega/c)n_o$ are the wave vectors of the incident e - and scattered o -waves, respectively.

Since the scattered waves are in-phase with the incident wave, they add coherently to a resultant electric field polarization that carries a spatial modulation with a grating wave vector magnitude $q = \frac{2\pi}{\lambda}(n_e - n_o)$, and a temporal modulation with a frequency $\omega_1 - \omega_2$. The resulting torque exerted by the optical electric field’s polarization on the NLC-director is therefore also modulated with a grating wave vector q . It is important to note that these gratings are actually moving gratings, since they carry a factor of $\exp[-i(\omega_1 - \omega_2)t]$, and therefore they will mediate energy transfer from one frequency component to the other as in other stimulated processes such as SBS.

4.2.1. Steady-state SOS

To analyze this process quantitatively, the starting point is the Euler Lagrange equation for the Free energy f of the system of NLC film under an applied field:

$$\frac{\partial}{\partial x_j} \frac{\delta f}{(\partial U_m / \partial x_j)} - \frac{\delta f}{\delta U_m} - \frac{\delta R}{\delta \dot{U}_m} = 0. \quad (4.1)$$

Taking $\theta(z, t)$ as the independent variable, the equation governing the reorientation angle $\theta(z, t)$ becomes

$$\eta \frac{\partial \theta(z, t)}{\partial t} - K_2 \frac{\partial^2 \theta(z, t)}{\partial z^2} = \frac{1}{2} \varepsilon_a \left[\cos(2\theta(z, t)) (E_x E_y^* + E_y E_x^*) + \sin(2\theta(z, t)) (|E_y|^2 - |E_x|^2) \right]. \quad (4.2)$$

Writing $\theta(z, t) = \theta(z, t) e^{i(\vec{q} \cdot \vec{r} - \Omega t)} + c.c$ and using the slowly varying-envelop-approximation, i.e., $\frac{\partial^2 \theta(z, t)}{\partial z^2}$ and $q \frac{\partial \theta(z, t)}{\partial z}$ are negligibly small compared with the $q^2 \theta(z, t)$ term, the coupled equations for the electric field and director reorientation become:

$$\frac{dE_x(z)}{dz} = \frac{i\varepsilon_a}{2k_x} \left(-2|\theta(z)|^2 E_x(z) \frac{\omega_x^2}{c^2} + E_y(z) \frac{\omega_y^2}{c^2} \theta^*(z) \right) - \frac{\alpha}{2} E_x \quad (4.3)$$

$$\frac{dE_y(z)}{dz} = \frac{i\varepsilon_a}{2k_y} \left(2|\theta(z)|^2 E_y(z) \frac{\omega_y^2}{c^2} + E_x(z) \frac{\omega_x^2}{c^2} \theta(z) \right) - \frac{\alpha}{2} E_y$$

$$\left[K_2 q^2 - i\eta\Omega + \frac{1}{2} \varepsilon_a (|E_y|^2 - |E_x|^2) \right] \theta(z, t) = \frac{1}{2} \varepsilon_a E_x E_y^*. \quad (4.4)$$

In the small signal [$E_y \ll E_x, \theta \ll 1$] regime and assuming no pump depletion, i.e. $|E_y|^2 = \text{constant}$, the above equations yield:

$$I_o(z = L) = I_o^{(\text{noise})} e^{G L e^z} e^{-\alpha z} \quad (4.5)$$

$$G = f(\Omega) \frac{\pi \varepsilon_a^2}{2cn_e \lambda K_2 q^2} \quad (4.6)$$

$$f(\Omega) = \frac{2\Omega/\Gamma}{1 + \Omega^2/\Gamma^2}; \quad \Gamma = \frac{K_2 q^2}{\gamma}. \quad (4.7)$$

Here $\varepsilon_a = n_e^2 - n_o^2$ is the optical anisotropy of the NLC, K_2 is the nematic elastic constant, $\Omega = \omega_1 - \omega_2$ is the frequency difference between the pump and signal waves, and γ is the orientation viscosity. In Eq. (4.5) for the signal intensity, we have ‘tacked’ on a phenomenological loss factor $e^{-\alpha z}$ to account for the propagation loss of the o-wave.

These equations show that the noise component E_x will grow with an exponential constant $g |E_y|^2$ that is proportional to the intensity of the pump beam. In analogy to stimulated Raman or Brillouin scattering, a positive gain coefficient $G > 0$ is obtained, for $\Omega = \omega_1 - \omega_2 > 0$. Furthermore, G is maximum at $\Omega = \Omega_{\text{opt}} = \Gamma$, when $f = 1$ and $G = G_m$:

$$G_m (\text{cm W}^{-1}) = \frac{(n_e + n_o)^2 \lambda}{8\pi cn_e K_2}. \quad (4.8)$$

It is important to point out at this juncture that the above analysis applies equally well for the case of an incident o-wave pump beam, since the energy coupling effect, i.e. positive flow of energy from the pump beam at ω_1 to the signal beam at ω_2 is dictated only by the frequency difference $\Omega = \omega_1 - \omega_2 > 0$. Experimentally, SOS processes have been observed with both e- and o-wave pump beams [see for example [172–174]].

For a visible wavelength $\lambda \approx 0.5 \mu\text{m}$, and typical NLC parameters [5]: $n_o \approx 1.54$, $n_e \approx 1.75$, [i.e. $\varepsilon_a = n_e^2 - n_o^2 \approx 0.6$, $\Lambda \approx 2.5 \mu\text{m}$], $K_2 \approx 3 \times 10^{-7}$, one gets $G_m \sim 1 \times 10^{-2} \text{ cm/W}$. For a typical NLC cell scattering loss $\alpha \sim 4.6 \text{ cm}^{-1}$, a laser intensity $I_{op} > 10^3 \text{ W/cm}^2$ will generate enough gain to overcome the loss per pass to stimulate the spontaneously scattered component to become an intense coherent beam. Furthermore, since the birefringence $(n_e - n_o)$ remains sizeable throughout the visible-near-IR regime, and the gain coefficient G_m is only weakly dependent on the wavelength, SOS can be realized with visible as well as infrared lasers [170–174]. In the near-IR spectral regime (e.g. $1.31 \mu\text{m}$ and $1.55 \mu\text{m}$ and $2-5 \mu\text{m}$), the scattering loss is much less than that in the visible since the scattering loss scales as λ^{-n} ($n \geq 2$) [5] and hence allows longer interaction lengths. Such agile frequency versatility clearly deserves further attention in nonlinear optical studies outside the visible spectrum where highly nonlinear optical materials are scarce.

In order to account for the severe pump depletion associated with high conversion efficiency, quantitative self-consistent solutions of the coupled dynamical equations (4.3) and (4.4) are required, and have been investigated in [225,173]. These theories have also been extended and applied to describe self-starting optical phase conjugation based on stimulated orientational and thermal scattering. We remarked here on some of the salient features of SOS. Fig. 4.2, for example, shows some typical computed output e- and o-waves for the near-IR communication channel wavelength ($\lambda = 1.55 \mu\text{m}$). The parameters used were: sample thickness = $400 \mu\text{m}$; $n_e = 1.75$, $n_o = 1.54$; $K_2 = 3.0 \times 10^{-12} \text{ N}$; $\eta = 0.07 \text{ poise}$, laser focused beam spot diameter of $80 \mu\text{m}$. For these parameters, the optimum gain coefficient $G_r (\Omega \tau_r = 1)$ occurred at a Stoke

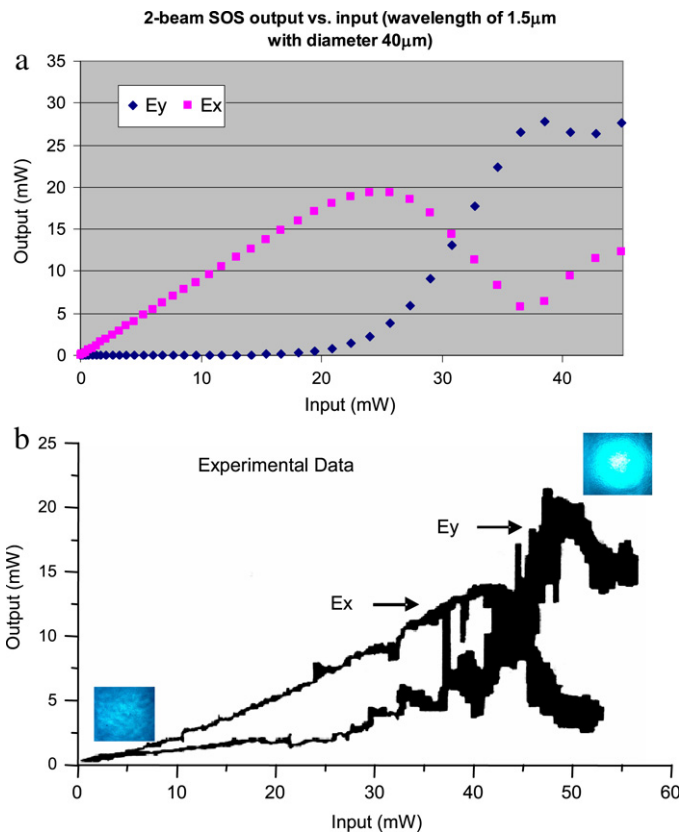


Fig. 4.2. (a) Calculated output e- and o-wave as functions of input e-wave power for near IR ($1.55\text{ }\mu\text{m}$) wavelengths. (b) Experimental observation of the transmitted e- and o-waves as a function of the input laser power; photos show the spontaneous noise at low power grows turning into an intense coherent beam with the SOS effect.

shift $\Omega = (\omega_1 - \omega_2) = 31\text{ Hz}$, and the grating constant $\Lambda = 7.38\text{ }\mu\text{m}$ (for $\lambda = 1.55\text{ }\mu\text{m}$). The threshold intensities, their dependence on the wavelength and the general growth pattern of the signal wave with the pump power are in good agreement with experimental observations. In particular, the threshold needed for $1.55\text{ }\mu\text{m}$ is lower than that for the visible, and the threshold intensities are generally in the 10's of mW range [for a focused laser spot diameter of $\sim 80\text{ }\mu\text{m}$].

Beyond the maximum conversion point, the strong o-wave signal beam (at frequency $\omega_1 - \Omega$) will act as a pump beam to its own spontaneously scattered e-wave noise, and stimulate the generation of a coherent e-wave signal at its Stoke frequency of $\omega_1 - 2\Omega$, which in turn generates an o-wave at $\omega_1 - 3\Omega$, then an e-wave at $\omega_1 - 4\Omega$ and so on.... similar to Stimulated Raman-Stokes cascading process. At the output end, the detection of either polarization component (e-wave at $\omega_1, \omega_1 - 2\Omega, \omega_1 - 4\Omega \dots$ or o-waves at $\omega_1 - \Omega, \omega_1 - 3\Omega, \omega_1 - 5\Omega \dots$ and so on) will eventually lead to an almost even distribution of the laser power into the two polarization components. This was indeed observed [252], c.f. Fig. 4.3, which vividly depicts the back and forth transfer of energy from one polarization state to the other as their energies rise and fall in time.

4.2.2. Stimulated orientational scattering – Nonlinear dynamics

Dynamically coupled oscillators and collective phenomena have been studied extensively in various material and optical systems; liquid crystals with their plethora of unique crystalline and fluid properties are no exceptions [247,248,250, 251,253–265]. These studies have provided valuable insights into how seemingly incoherent ‘noise’ would by mutual interactions and feedback evolve into an ordered system or conversely, how coherent interactions could lead to chaotic oscillations, with implications in areas as diverse as optics, hydrodynamics and neural network modeling.

SOS in nematic liquid crystals provides a natural typical setting to explore and gain further understanding of nonlinear dynamically coupled oscillator systems and other collective phenomena; the scattering of an input driving optical field by the director axis fluctuations into a whole spectrum of frequency components, their mutual interactions and feedback and the resulting collective outputs are analogous to the coupled nonlinear oscillator neural network model for describing associated memory [253], c.f. Fig. 4.4.

To treat similar dynamical processes, the molecular and optical parameters appearing in the coupled electromagnetic waves and director axis reorientation equations for SOS are expressed as spatial-temporal variables [257–262], i.e. $E_x = E_x(z, t)$ and $E_y = E_y(z, t)$ and $\theta = \theta(z, t)$. Furthermore, the director axis reorientation angle $\theta(z, t)$ is expanded in terms of

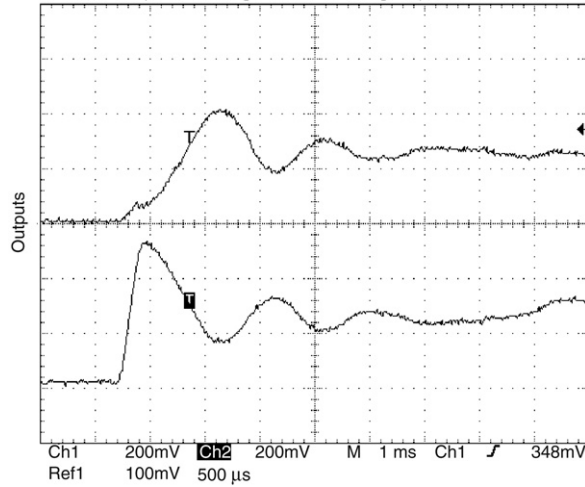


Fig. 4.3. Oscilloscope traces depicting polarization conversion via SOS in a planar 300 μm thick aligned nematic liquid crystal (E7) with visible laser wavelength $\lambda = 488 \text{ nm}$. Upper trace: transmitted signal wave; Lower trace: transmitted pump wave.

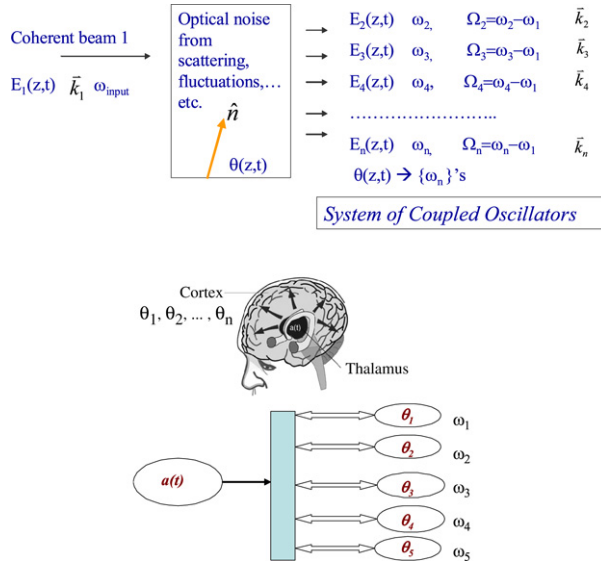


Fig. 4.4. Schematic depiction of the interaction of the input laser with its scattered components as coupled nonlinear oscillator similar to neural network model.

its longitudinal modes as $\theta(z, t) \equiv \sum_n A_n(t) \sin\left(\frac{n\pi z}{L}\right)$. The torque balance equation then becomes [250]:

$$\begin{aligned} \frac{dA_n}{dt} = & \left[i\Omega - \frac{K_2}{\eta} \left[q^2 + \left(\frac{n\pi}{L} \right)^2 \right] \right] A_n + \frac{\varepsilon_a}{\eta L} \int_0^L \theta_s \sin\left(\frac{n\pi z}{L}\right) \left(|E_y|^2 - |E_x|^2 \right) dz \\ & + \frac{\varepsilon_a}{\eta L} \int_0^L \sin\left(\frac{n\pi z}{L}\right) \left(E_x E_y^* - \frac{1}{2} \theta_s^2 E_x^* E_y - |\theta_s|^2 E_x E_y^* \right) dz. \end{aligned} \quad (4.9)$$

The propagation equations for the fields E_x and E_y , and the field-driven equations for the director angular expansion coefficients A_n were solved for the case of a continuous wave input laser. It is interesting to note that with a constant intensity input laser driving field, the output signal beams exhibit many dynamical behaviors such as periodic and chaotic oscillations, c.f. Fig. 4.5 (see also Fig. 4.2(b)). These dynamical behaviors are the temporal equivalent of those complex spatial pattern formation caused by a spatially uniform input beam [247,248]; they both originate from the nonlinear dynamical interaction between the driving optical field and the nematic director axis.

Detailed measurements of the Fourier spectra of the oscillatory output signals in this regime, and their intensity dependencies have been found to be in good agreement with the theoretical predictions [251]. Some exemplary

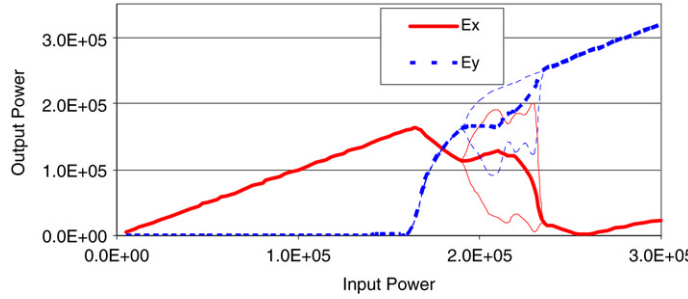


Fig. 4.5. Computed output x - and y -polarized beam as a function of the input beam power. Above the SOS threshold, marked by thinner lines, the generated signal beam exhibits periodic as well as ‘chaotic’ oscillations.

experimental observations of the dynamical energy exchanges and the spectral contents of the oscillations are shown in Fig. 4.6(a) and (b).

Another interesting feature of SOS with nematic liquid crystals is that it can be modulated by an applied ac control field of appropriate frequency. In particular, if the applied frequency is ‘resonant’ with the frequency difference for optimal signal gain, it has been observed that the stimulated scattering efficiency will be enhanced and accompanied by the generation of new frequency harmonics, c.f. Fig. 4.6(c).

4.2.3. Stimulated thermal scattering (STS)

In analogy to the SOS discussed above, laser induced thermal index changes in liquid crystals could also mediate energy transfer between an incident [pump] beam and its scattered noise [170,225]. Since the process requires absorption of light energy, i.e. an intensity grating, the pump beam and its scattered noise should be co-polarized, unlike the SOS process. By considering the mixing of two co-polarized light beams, the incident E_L and its scattered coherent noise E_S , an analogous set of equations can be derived.

In the small signal limit, again we have:

$$E_L(z) = E_L(0)e^{-\frac{\alpha}{2}z} \quad (4.10a)$$

$$\frac{dE_S}{dz} = \gamma_T e^{\alpha z} E_S - \frac{\alpha}{2} E_S \quad (4.10b)$$

$$\begin{aligned} \gamma_T &= i \frac{n_0 \omega^2}{k_{S2} c^2} \left\{ \frac{\alpha \frac{dn}{dT} \left(\frac{n^o}{8\pi}\right) |E_L|^2}{\rho c_p D q^2} \frac{1}{1 - i\Omega \tau_T} \right\} \\ &= i \frac{\omega \alpha \left(\frac{dn}{dT}\right) I_L}{c \rho c_p D q^2 \cos \frac{\Theta}{2}} \cdot \frac{1 + i\Omega \tau_T}{1 + (\Omega \tau_T)^2} = g_T + i\kappa_T \end{aligned} \quad (4.11a)$$

$$g_T = \text{Re}\{\gamma_T\} = \frac{\omega \alpha \left(\frac{dn}{dT}\right) I_L}{c \rho c_p D q^2 \cos \frac{\Theta}{2}} \cdot \frac{-2\Omega \tau_T}{1 + (\Omega \tau_T)^2} = G I_L. \quad (4.11b)$$

As in the case of SOS, the STS gain is maximum for a lower frequency noise at $\Omega \tau = -1$ [Note: In the notation of Ref. [170, 225], the frequency difference Ω is defined as $\Omega = \omega_S - \omega_L$ so that lower frequency noise than the pump means $\Omega < 0$]. For a wave mixing geometry which yields $q = 2k \sin\left(\frac{\Theta}{2}\right)$ where Θ is the crossing angle between the E_1 and E_2 , the maximum gain (at $\Omega \tau = -1$) is given by:

$$G_T = \frac{\omega \frac{dn}{dT} \alpha}{2c \rho c_p D q^2 \cos \frac{\Theta}{2}} = \frac{\lambda \frac{dn}{dT} \alpha}{16\pi \rho c_p D} \cdot \frac{1}{\sin^2 \frac{\Theta}{2} \cos \frac{\Theta}{2}}. \quad (4.12)$$

Using the following typical parameter set: density $\rho \approx 1 \text{ gm cm}^{-3}$, $C_p \approx 2 \text{ J gm}^{-1} \text{ }^\circ\text{K}^{-1}$, $D \approx 2 \times 10^{-3} \text{ cm}^2 \text{ s}^{-1}$, $dn/dT \approx 10^{-3}/^\circ\text{K}$, absorption $\alpha_a \approx 20 \text{ cm}^{-1}$ and the experimental parameters : $\lambda \approx 0.5 \mu\text{m}$, $\Theta = 1^\circ$, i.e., $\cos(\Theta/2) \approx 1$ and $\sin^2(\Theta/2) \approx \Theta^2/4 \approx (1.3 \times 10^4)^{-1}$ the intensity gain factor is estimated to be $2G_T = 1.3 \times 10^{-1} \text{ cm/W}$. This is an order of magnitude larger than $2G_m$ for SOS, implying much smaller threshold intensity for STS which is consistent with experimental observations [170,225].

4.3. Optical wave mixing and image processing

As pointed out in Section 3, the laser induced nonlinear polarization $\mathbf{P}_{NL} \sim \chi^{(2)} \mathbf{EE} + \chi^{(3)} \mathbf{EEE}$ give rise to various optical wave mixing phenomena resulting in the generation of various temporal and spatial frequencies in the output. The second order nonlinear effects associated with $\chi^{(2)}$ require that the materials do not possess centro-symmetry, while the third order

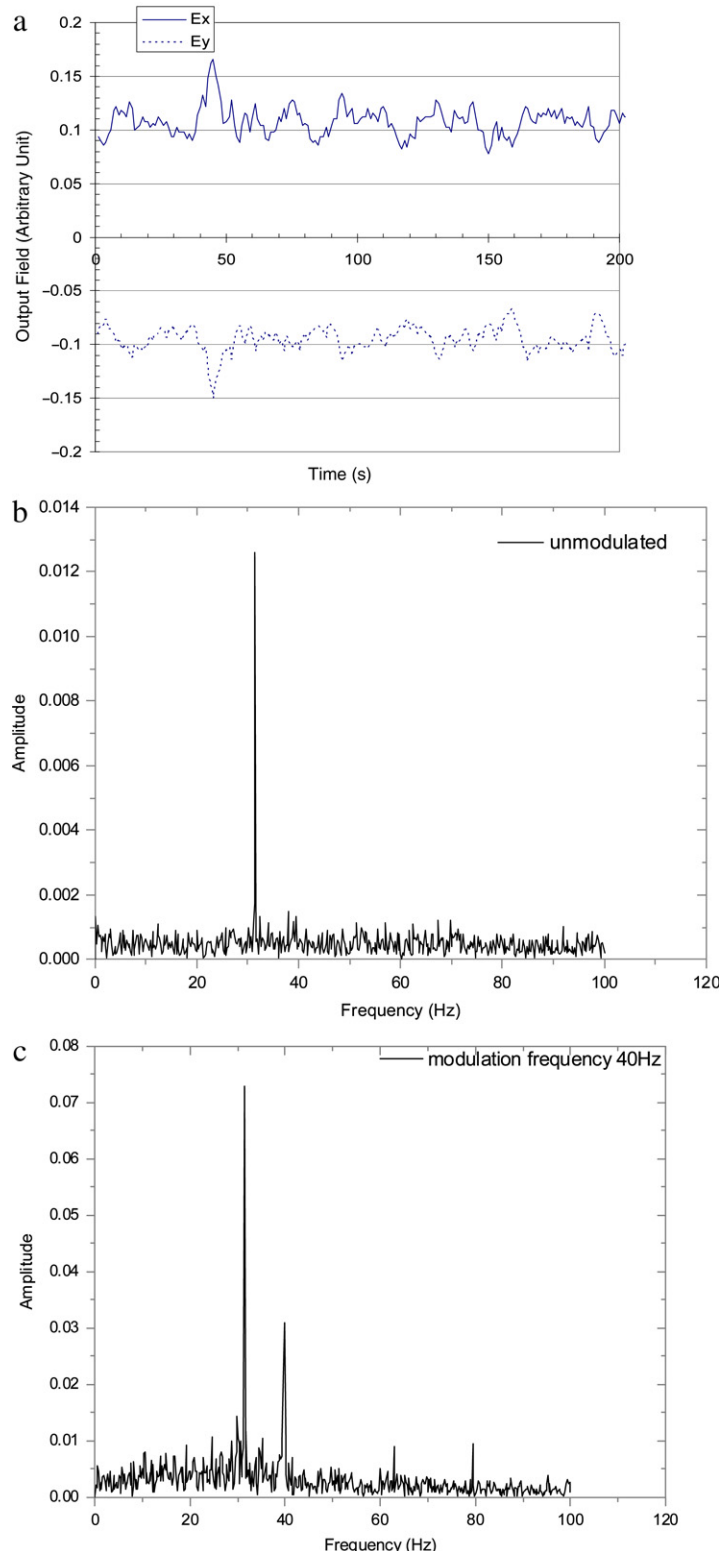


Fig. 4.6. (a) Energy flows between the two polarizations as a function of time above the stimulated scattering threshold. (b) Fourier analysis of the spectrum shows a spike at the frequency difference $\Omega_{opt} = \Gamma$ for maximum signal gain. (c) Spectrum of the oscillation in the presence of an ac modulation field applied transversely to facilitate the director axis fluctuation.

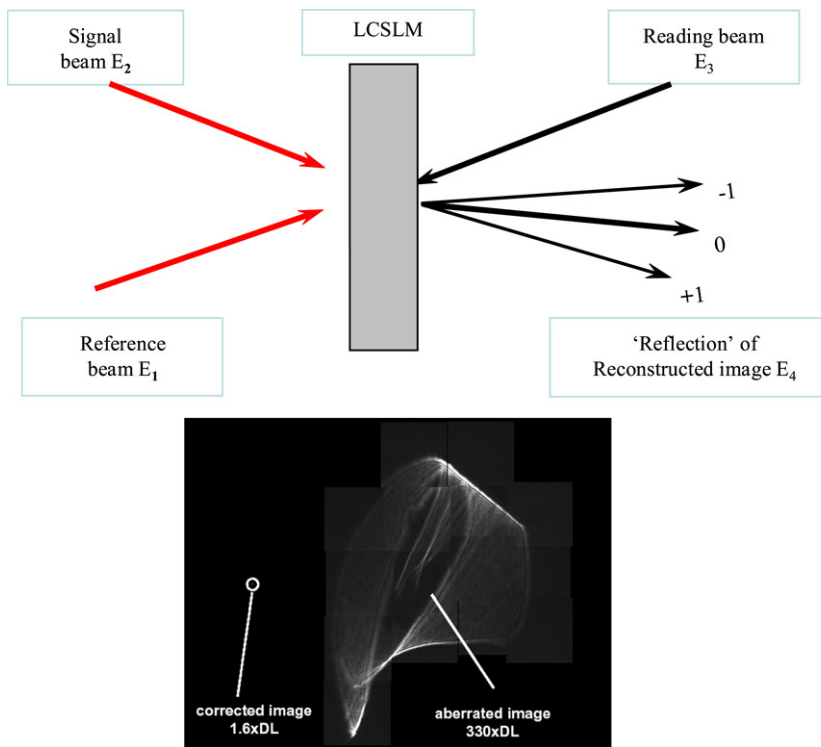


Fig. 4.7. Degenerate four-wave mixing mediated wave front conjugation with a liquid crystal spatial light modulator (LCSLM). Photograph shows the distorted image of a point source and the corrected image. [After Ref. [91]].

term occurs in all materials. Accordingly, second order processes have been observed in ferroelectric liquid crystals [which are not centro-symmetric because of the presence of a permanent dipole], in dc electric field poled nematic liquid crystals, and on surfaces [203–209]. Although the nonlinearities involved are small, these studies provide valuable information on material properties and the techniques employed there have evolved into valuable characterization tools.

Because most liquid crystals are centro-symmetric, the bulk of nonlinear optics of nematic liquid crystals is centered on their third order nonlinear susceptibilities, and particularly on the extraordinarily large orientational and thermal/density nonlinearities. As pointed out earlier, the major third order nonlinear polarizations are associated with an intensity dependent index change, i.e. $\chi^{(3)} \mathbf{EEE} \sim (n_2 \mathbf{I}) \mathbf{E}$. These nonlinearities and their response speed are competitive with respect to another class of highly nonlinear optical materials – inorganic photorefractive crystals [29]. In inorganic photorefractive crystals, although the nonlinear index change $\Delta n = n_2 \mathbf{I}$ is small, the long interaction length (a few millimeters to centimeters) of the crystals produce the nonlinear phase shift $\Delta\varphi = 2\pi \Delta n d / \lambda$ needed to effect substantial beam coupling and other wave mixing effects for coherent image processing applications. On the other hand, the beam coupling coefficient observed in nematic liquid crystals can be as large as 1000 cm^{-1} , and so even though the interaction length is short ($\sim 0.1 \text{ mm}$), the induced nonlinear phase shift and beam coupling effect is comparable to those obtainable from inorganic photorefractive crystals. The 'thin film' format of liquid crystals actually provides some advantages for imaging applications. As remarked earlier, a unique advantage of nematic liquid crystals is their broadband birefringence that spans the visible–infrared regime, and thus many of these coherent image processing techniques can be realized in spectral regimes not accessible by photorefractive crystals.

Because of their planar geometry, nematic liquid crystal cells and spatial light modulators are particularly suited for coherent as well as incoherent optical image processing applications [91–93,147,221–223,232–238,264–267]; operations such as infrared-visible conversion, contrast reversal, edge enhancement, image addition/subtraction, and aberration corrections have been demonstrated. In particular, optical wave front conjugation has been demonstrated to be an effective means for correcting aberrations in optical systems such as telescopes, laser resonators and amplifiers, atmospheric turbulence...etc [29,91]. For the case depicted in Fig. 4.7, the four-wave mixing process is mediated by the third order nonlinear polarization term $\mathbf{P} \sim \chi^{(3)} \mathbf{E}_1 \mathbf{E}_2^* \mathbf{E}_3$. This term describes the 'diffraction' of the reading beam \mathbf{E}_3 by the hologram or grating produced by the interference of the reference beam \mathbf{E}_1 and the signal beam \mathbf{E}_2 , and produces a reconstructed image beam \mathbf{E}_4 that propagates back along the direction of \mathbf{E}_2 , i.e. it is a conjugate ($\mathbf{E}_4 \sim \mathbf{E}_2^*$) that will cancel any phase aberration imparted on the signal beam \mathbf{E}_2 . In the case of a LCSLM operating in the reflective mode, \mathbf{E}_4 appears as the reflected +1 diffracted order. An example of the aberration correction capability of optical phase conjugation is shown in the photograph in Fig. 4.7, where a point image is recovered from a highly distorted input signal.

In studies using methyl-red doped NLC, this and other coherent image processing performance were also demonstrated. In [147], for example, studies have demonstrated that visible coherent images can be created with input beam intensity as low as $90 \mu\text{W}/\text{cm}^2$; the response time is intensity dependent and can be as short as a few milliseconds at an optical intensity of $\sim 1 \text{ mW}/\text{cm}^2$. Such sensitivity and performance are comparable to, but considerably less costly than those of liquid crystal spatial light modulators.

4.4. Passive optical switching – Laser hardening and optical limiting

We close this section with a discussion of some of the ongoing current work on passive optical switching with liquid crystals. As often repeated in this report, the broadband birefringence and transparency windows of nematic liquid crystal make them rather versatile and multi-functional materials for agile frequency sensor protection applications.

Pulsed and continuous-wave lasers are now extensively used in various settings where because of the sensitivity of the human eye or sensors, accidental or intentional exposures to laser radiation could cause temporary or severe permanent damages [268]. While fixed-wavelength filters offer effective protection from known laser sources, they are ineffective against agile frequency lasers, the wavelengths of which can be tuned anywhere in the UV to infrared. Consequently, there have been many intensive investigations of broadband nonlinear optical materials and active/passive optical switching and tunable filtering schemes for optical limiting action against agile frequency lasers. Besides the bandwidth issue, the temporal characteristics of the lasers are also important considerations. For sub-picosecond – nanosecond laser pulses, nonlinear absorbers such as reverse saturable absorbers [RSA] and two-photon [TPA] and multi-photon absorbers, including liquid crystals have been found to provide adequate performance characteristics [269–279]. These materials work by virtue of their (increasing) intensity-dependent multi-photon or multiple-photon absorption capabilities, c.f. Fig. 2.4 for example; the more intense is the laser, the more molecular states are involved in the absorption, and therefore the transmission can be ‘limited’. Nevertheless, these nonlinear absorbers become ineffective for longer pulses ($\sim 100 \text{ ns-ms}$ and longer) because of the reduced intensity for a given laser energy fluence.

For these longer time scales, nematic liquid crystals stand out as attractive candidate materials for such optical switching purposes owing to their ultra-broadband birefringence and/or extraordinary optical nonlinearities [279–282]. We discuss here details of one particularly exemplary study that illustrates the complex interplays between laser induced temperature fluctuations ΔT , order parameter S and the birefringence $\Delta n = (n_e - n_o)$ of nematic liquid crystals, thus complementing the SOS discussions which detail laser induced director axis reorientation.

Fig. 4.8 depicts a typical twist alignment nematic liquid crystal situated between two crossed polarizers commonly found in all liquid crystal display devices as an electro-optical switching pixel element. A linearly polarized input light at low power will obey the Mauguin law and its polarization will follow the director axis arrangement to the orthogonal direction reached at the exit end; the exit (transmitted) light intensity is thus maximal. Such a transmission process can be analyzed by the Jones Matrix method in which the liquid crystal cell is divided into N layers with thickness h ($h \ll$ the optical wavelength λ) [198,282]. The amplitude of the normalized transmitted light through the entire (polarizer + LCfilm + analyzer) set up is given by:

$$\Psi_{out}(d) = \begin{pmatrix} E'_x \\ E'_y \end{pmatrix} = P(\phi_{Exit}) \cdot \prod_{m=1}^M [S^{-1}(\phi_m) \cdot G \cdot S(\phi_m)] \cdot \begin{pmatrix} \cos \phi_{Ent} \\ \sin \phi_{Ent} \end{pmatrix} \quad (4.13)$$

where

$$P(\phi) = \begin{pmatrix} \cos^2 \phi & \cos \phi \sin \phi \\ \sin \phi \cos \phi & \sin^2 \phi \end{pmatrix}; \quad S(\phi_m) = \begin{pmatrix} \cos \phi_m & \sin \phi_m \\ -\sin \phi_m & \cos \phi_m \end{pmatrix}; \quad G = \begin{pmatrix} e^{i\frac{\gamma}{2}} & 0 \\ 0 & e^{-i\frac{\gamma}{2}} \end{pmatrix}. \quad (4.14)$$

$$\Delta n_m = \frac{n_e n_o}{\sqrt{n_e^2 \sin^2 \theta_m + n_o^2 \cos^2 \theta_m}} - n_o. \quad (4.15)$$

In these equations, $\gamma = \frac{2\pi h \Delta n_m}{\lambda}$ is the retardation associated with the m th LC layer, θ_m and ϕ_m are the tilt and twist angle of m th layer director axis and ϕ_{Ent} , ϕ_{Exit} are the axis of the entrance polarizer and exit analyzer, respectively ($\phi_{Ent} = 90^\circ$ and $\phi_{Exit} = 0^\circ$).

In conventional electro-optical devices, an ac electric field [on the order of a few volts/ μm] is applied between the two cell walls to reorient the director axis towards the homeotropic alignment, i.e. the director axis is perpendicular to both cell walls. This ‘destroys’ the polarization rotation process and the exit polarization is the same as the input polarization; its intensity is completely blocked by the exit polarizer. Obviously similar intensity switching effects can be realized with laser induced director axis reorientation. However, the equivalent optical electric field (from $\Delta \varepsilon_{op} E_{op}^2 = \Delta \varepsilon_{ac} E_{ac}^2$) would require an optical intensity on the order of kilowatts/ cm^2 . The response speed would also be slow, measured in the 10's of milliseconds or longer. As pointed out in a previous section, laser induced order parameter change is a much faster and efficient mechanism to ‘destroy’ the birefringence. In liquid crystals doped with absorbing dye or trans-cis molecules, these order parameter changes can be induced with orders of magnitude lower intensity lasers (mW/cm^2), and with orders of magnitude faster response speeds.

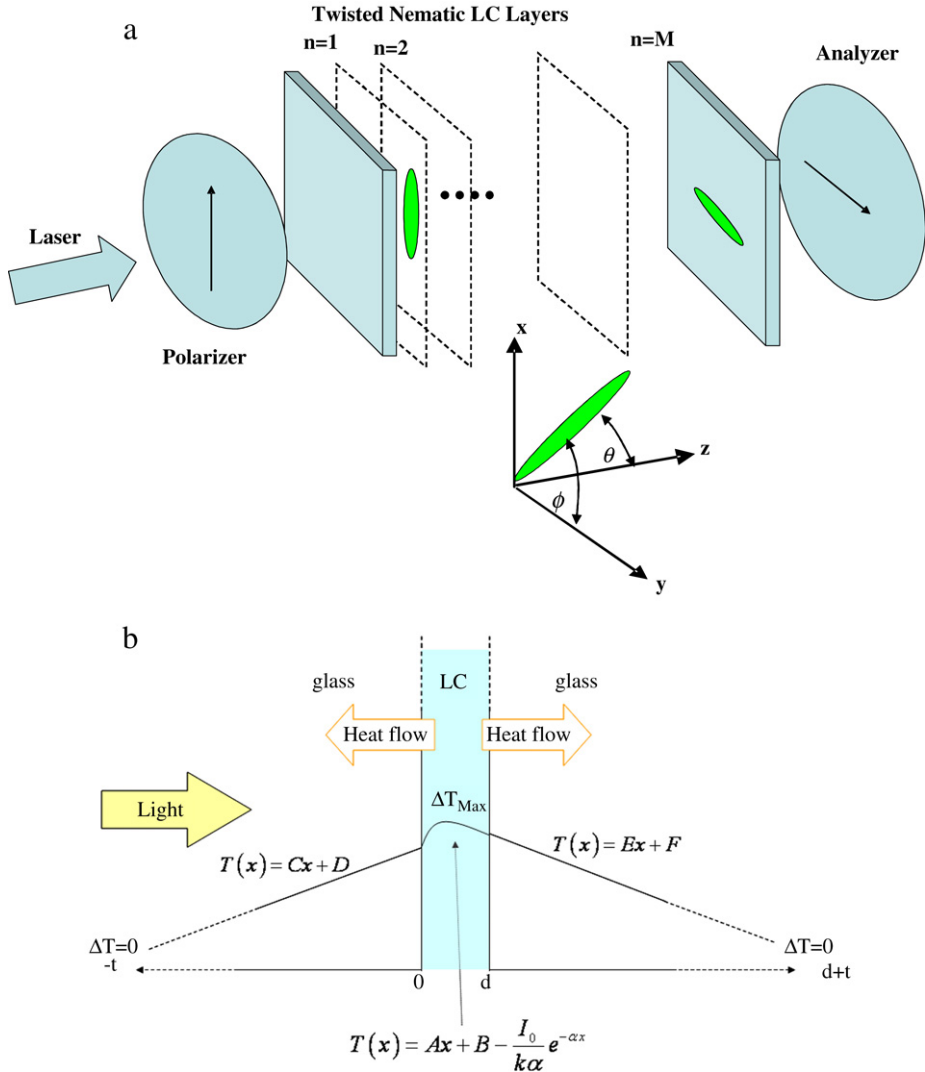


Fig. 4.8. Schematic depiction of the Jones Matrix approach for calculating the transmission through a 90° twist alignment nematic liquid crystal cell (TNLC). (b) 1D model for the laser induced temperature and order parameter changes in the TNLC.

Following the Landau-deGennes theory [283], the free energy density of the system with a temperature distribution $T(z)$ and order parameter $S(z)$ is given by:

$$f = a(T(z) - T^*)S(z)^2 + bS(z)^3 + cS(z)^4 + L\left(\frac{dS(z)}{dz}\right)^2 - g_1S_1 - g_2S_2. \quad (4.16)$$

In this expression, a , T^* , b , c and L are thermodynamic parameters, g_1 and g_2 are the surface potentials per unit volume and S_1 and S_2 are the surface order parameters. For typical nematic liquid crystal like 5CB [283], $a = 6.5 \times 10^4 \text{ J/m}^3 \text{ K}$, $b = -5.3 \times 10^5 \text{ J/m}^3$, $c = 9.8 \times 10^5 \text{ J/m}^3$, $T^* = 307.14 \text{ K}$ and $L = 4.5 \times 10^{-12} \text{ J m}^{-1}$.

At equilibrium, $S(z)$ is determined by minimization of the Free energy equation (4.16) which yields the Euler-Lagrange equation:

$$\frac{\partial f}{\partial S} - \frac{d}{dz} \left(\frac{\partial f}{\partial (\partial S / \partial z)} \right) = 0 \quad (4.17)$$

with the boundary conditions

$$-\left(\frac{\partial f}{\partial (\partial S / \partial z)} \right)_1 + \frac{\partial f_{S_1}}{\partial S_1} = 0, \quad \left(\frac{\partial f}{\partial (\partial S / \partial z)} \right)_2 + \frac{\partial f_{S_2}}{\partial S_2} = 0. \quad (4.18)$$

For simplicity, we also assume $g_1 = g_2 = 0$, i.e. we ignore the surface terms as their relative contribution to the transmission switching is negligible compared to the bulk. In that case, Eqs. (4.16) and (4.17) yield:

$$2a(T(z) - T^*)S(z) + 3bS(z)^2 + 4cS(z)^3 - 2L\left(\frac{d^2S(z)}{dz^2}\right) = 0. \quad (4.19)$$

The equation for the order parameter distribution $S(z)$ can be solved once the temperature distribution $T(z)$ within the nematic cell is known. $T(z)$ depends on the rate of heat production and thermal diffusion within the nematic cell, which are critically dependent on the particular nematic liquid crystal and cell window used, the cell and interaction geometry, as well as the temporal characteristics of the incident laser.

In the recent study conducted with a methyl-red doped 90° twist alignment nematic liquid crystal cell, the incident focused laser spot diameter was much larger than the liquid crystal thickness and therefore the thermal build-up and distribution process can be approximated by a 1D model. Accordingly, the Jones matrix method mentioned above can be applied as well as the 1D heating and diffusion equation:

$$\frac{d}{dz}\left(k_{LC}\frac{dT}{dz}\right) + \dot{q} = 0. \quad (4.20)$$

Here k_{LC} ($= 0.15 \text{ W/mK}$) is the LC thermal conductivity. We also assume that the light absorption follows the regular exponential form, i.e. $I = I_0 \exp(-\alpha z)$, where α is the absorption coefficient of the doped LC, so that the heat generation rate per unit volume is

$$\dot{q} = -\frac{dI}{dz} = -\frac{d}{dz}(I_0 e^{-\alpha z}) = I_0 \alpha e^{-\alpha z}. \quad (4.21)$$

Eqs. (4.13), (4.19) and (4.20) have been numerically solved for several cell thicknesses, NLC/glass thermal conductivities, ambient temperature etc. The typical output versus input intensity dependence for several cell thicknesses is shown in Fig. 4.9(a). As expected, the cell exhibits linear transmission at low input laser powers; when the input power is high enough to induce sufficient changes in the order parameter ΔS and birefringence Δn to negate the Mauguin condition, the transmission of the laser begins to drop dramatically to vanishing value.

As noted before, the process of laser induced birefringence change mediated by order parameter modification in dye-doped nematics can be orders of magnitude faster (10's or 100's ns) in comparison to typical field induced director axis reorientation process (10's ms). This is again borne out in this study, c.f. Fig. 4.9(b). In general, for an abrupt (2 ns) turn on time of a continuous-wave input laser, the transmission exhibits a double-exponential decay following a fast initial transient rise to a peak value; the fast decay component is characterized by a response time τ_1 of a few μs or less, and the slower decay component by τ_2 of a few 10's of μs . The former is attributed to local instantaneous laser induced changes in the order parameter, whereas the latter slower component is due to the overall temperature rise when thermal diffusion begins to set in. The faster response time becomes shorter for higher and higher input power or increasing dye concentration, and could reach sub-microsecond levels (0.7 μs) at an input power of 150 mW, while the slower component remains relatively unchanged. Similar switching dynamics and performance are observed in Epolite-dye doped TNLC using near-infrared ($\lambda = 1550 \text{ nm}$) laser [198].

4.5. Concluding remarks and outlook

Although we have attempted to give a comprehensive overview of the NLC materials' optical nonlinearities and exemplary nonlinear optical processes and phenomena, the presentation is by no means an exhaustive account, due mainly to space limitations. There are numerous other noteworthy studies of processes conducted with liquid crystals that are not included in the above general classifications, venturing into hitherto relatively un-explored realms of negative refractive index and nanostructured metamaterials, or other phases with their unique physical and optical properties [284–328]. Examples (again, a partial list) include basic optical physics associated with angular momentum exchanges between light and the nematic axis rotation [289–292], nonlinear dynamics [293–297], optical tweezers and manipulations [298–303], fast and slow light [304,305], bistability and Fabry–Perot and micro-cavity nonlinear optics [306–313], nonlinear interface switching [314–317], laser oscillators [318–320], metamaterials, photonic crystals and waveguides [321–329], to name but a few.

Some of these studies are focused on general nonlinear optical physics, others have considered possible applications, and many have unveiled new mechanisms or material properties. Liquid crystals are wonderfully complex optical materials. With the advent of nanostructures and metamaterials and the parallel rapid development in laser sources, many novel, interesting and useful material science, processes, phenomena, and device possibilities are still awaiting further exploration.

Acknowledgements

The author acknowledges the contributions from all the graduates and current members of his research laboratory, and funding from the National Science Foundation, the Army research Office, the Air Force Office of Scientific Research and the Defense Advanced Research Projects Agency.

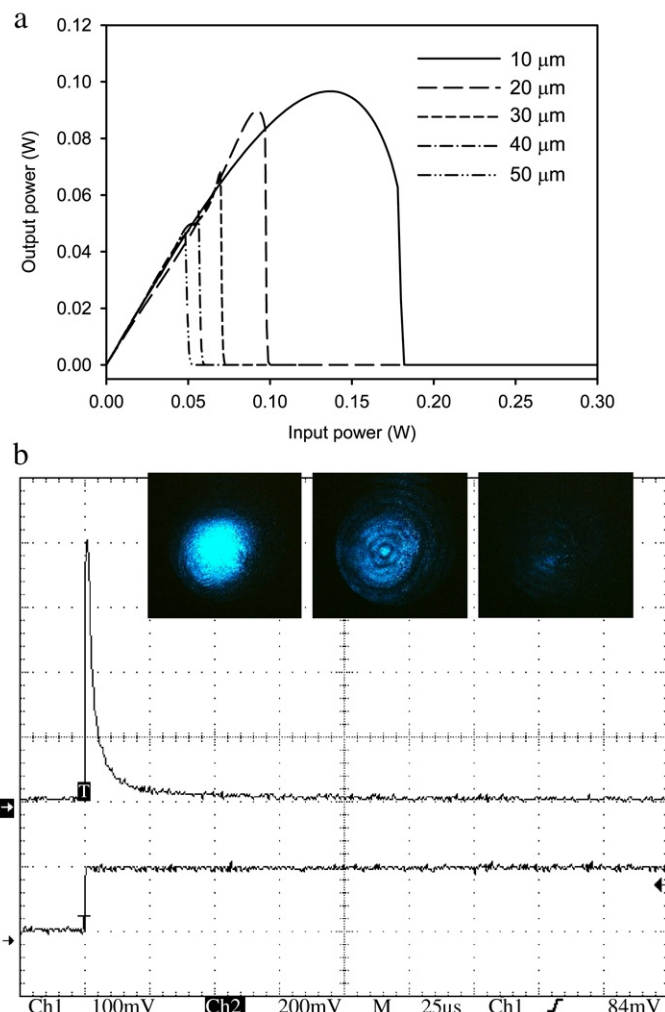


Fig. 4.9. (a) Theoretical plots of the transmitted power as a function of the input power for various sample thicknesses. Note that the transmission switching occurs at lower intensities for thicker sample. (b) Experimental observations of the transmission (upper trace) of a step-on input cw laser (lower trace) showing very fast switch off.

References

- [1] F. Reinitzer, Wiener Monatschr. Fur Chem. 9 (1888) 421–441.
- [2] Hiroisa Kawamoto, Proc. IEEE 90 (4) (2002) 500.
- [3] P.G. deGennes, *The Physics of Liquid Crystals*, Oxford Press, Clarendon, 1974.
- [4] S. Chandrasekhar, *Liquid Crystals*, 2nd edition, Cambridge University Press, Cambridge, 1992.
- [5] I.C. Khoo, *Liquid Crystals*, 2nd edition, Wiley, NJ, 2007.
- [6] I.C. Khoo, S.T. Wu, *Optics and Nonlinear Optics of Liquid Crystals*, World Scientific, Singapore, 1992.
- [7] I.C. Khoo, S. Slussarenko, B.D. Guenther, W.V. Wood, Opt. Lett. 23 (1998) 253–255. See also Ref. [233] where self-focusing of a cw laser beam was observed at a power level as low as 70 nW in such supra-nonlinear material.
- [8] R. Menzel, *Photonics – Linear and Nonlinear Interactions of Laser Light and Matter*, 2nd edition, Springer-Verlag, Berlin, Heidelberg, 2007.
- [9] F. Yang, J. Roy Sambles, Liq. Cryst. 30 (2003) 599–602.
- [10] D.V.G.L.N. Rao, S. Jayaraman, Phys. Rev. A 10 (1974) 2457. See also Ref. [243].
- [11] G.K.L. Wong, Y.R. Shen, Phys. Rev. A 10 (1974) 1277.
- [12] M.I. Barnik, L.M. Blinov, A.M. Dorozhkin, N.M. Shtykov, Sov. Phys. -JETP (Engl. Transl.) 54 (1981) 935.
- [13] I. Freund, P.M. Rentzepi, Phys. Rev. Lett. 18 (1967) 393.
- [14] G. Durand, C.H. Lee, Mol. Cryst. 5 (1968) 171.
- [15] R.M. Herman, R.J. Serinko, Phys. Rev. A 19 (1979) 1757.
- [16] I.C. Khoo, Shu-Lu Zhuang, Appl. Phys. Lett. 37 (1980) 3.
- [17] A.S. Zolotko, V.F. Kitaeva, N. Kroo, N.N. Sobolev, L. Chillage, JETP Lett. 32 (1980) 158–162.
- [18] B.Y. Zeldovich, N.F. Pilipetskii, A.V. Sukhov, N.V. Tabiryan, JETP Lett. 31 (1980) 263–269. See also Ref. [134] which also discuss smectic and cholesteric phases.
- [19] I.C. Khoo, Phys. Rev. A 23 (1981) 2077.
- [20] S.D. Durbin, S.M. Arakelian, Y.R. Shen, Phys. Rev. Lett. 47 (1981) 1411.
- [21] I.C. Khoo, Y.R. Shen, Opt. Eng. 24 (1985) 579–585.
- [22] I. Janossy, L. Csillag, A.D. Lloyd, Phys. Rev. A 44 (1991) 8410–8413.

- [23] R. Macdonald, P. Meindl, G. Chilaya, et al., Opt. Commun. 150 (1998) 195–200.
- [24] L. Lucchetti, M. Di Fabrizio, O. Francescangeli, F. Simoni, Opt. Commun. 233 (2004) 417.
- [25] S.D. Jacobs, K.A. Cerqua, K.L. Marshall, A. Schmid, M.J. Guardalben, K.J. Skerrett, J. Opt. Soc. Amer. B 9 (1988) 1962–1979.
- [26] J.L. Oudar, in: C. Flytzanis, J.L. Oudar (Eds.), Nonlinear Optics Materials and Devices, Springer, Berlin, 1986, p. 91.
- [27] D.S. Chemla, in: C. Flytzanis, J.L. Oudar (Eds.), Nonlinear Optics Materials and Devices, Springer, Berlin, 1986, p. 65.
- [28] O. Ostroverkhova, W.E. Moerner, Chem. Rev. 104 (2004) 3267–3314.
- [29] P. Gunter, J.P. Huignard (Eds.), Photorefractive Materials and Their Applications, vol. I and II, Springer-Verlag, Berlin, 1989.
- [30] R. Thoma, N. Hampp, C. Brauchle, D. Oesterhelt, Opt. Lett. 16 (1991) 651.
- [31] M. Sawamura, K. Kawai, Y. Matsuo, K. Kanie, T. Kato, e. Nakamura, Nature 419 (2002) 702–705.
- [32] G. Pelzl, S. Diele, W. Weissflog, Adv. Mater. 11 (1999) 707–724.
- [33] See for example Y. Amatatsu, M. Hosokawa, J. Phys. Chem. A 108 (2004) 10238–10244. See also Refs. [35,36] and references therein.
- [34] Q. Zhao, L. Kang, B. Du, B. Li, J. Zhou, H. Tang, X. Liang, B.Z. Zhang, Appl. Phys. Lett. 90 (2007) Article Number: 011112.
- [35] G.S. He, L.S. Tan, Q. Zheng, P.N. Prasad, Chem. Rev. 108 (2008) 1245–1330.
- [36] M. Albota, D. Beljonne, J.L. Bredas, J.E. Ehrlich, J.Y. Fu, A.A. Heikal, S.E. Hess, T. Kogej, M.D. Levin, S.R. Marder, D. McCord-Maughon, J.W. Perry, H. Rockel, M. Rumi, C. Subramaniam, W.W. Webb, X.L. Wu, C. Xu, Science 281 (1998) 1653–1656.
- [37] I.C. Khoo, M.V. Wood, B.D. Guenther, Min-Yi Shih, P.H. Chen, J. Opt. Soc. Amer. B 15 (1998) 1533–1540.
- [38] I.C. Khoo, H. Li, Appl. Phys. B 59 (1994) 573–780.
- [39] G.S. He, T.-C. Lin, P.N. Prasad, C.-C. Cho, L.-J. Yu, Appl. Phys. Lett. 82 (2003) 4717–4719.
- [40] O. Tsutsumi, A. Ohashi, T. Ikeda, S.R. Marder, J.W. Perry, Thin Solid Film 509 (2006) 118–122.
- [41] I.C. Khoo, A. Diaz, M.V. Wood, P.H. Chen, IEEE J. Sel. Topics Quantum Electron. 7 (5) (2001) 760–768.
- [42] U.A. Hrozhyk, S.V. Serak, N.V. Tabiryan, T. Bunning, J. Appl. Phys. 104 (2008) 063102.
- [43] S. Furumi, Appl. Phys. Lett. 84 (2004) 2491–2493.
- [44] V.I. Kopp, B. Fan, H.K.M. Vithana, A.Z. Genack, Opt. Lett. 23 (1998) 1707–1709.
- [45] P.J.W. Hands, S.M. Morris, T.D. Wilkinson, H.J. Coles, Opt. Lett. 33 (2008) 515–517.
- [46] Y.C. Yang, C.S. Kee, J.E. Kim, H.Y. Park, J.C. Lee, Y.J. Jeon, Phys. Rev. E 60 (1999) 6852–6854.
- [47] S. Meiboom, M. Sammon, Phys. Rev. A 24 (1981) 468–475.
- [48] P. Etchegoin, Phys. Rev. E 62 (2000) 1435–1437.
- [49] D.A. Coleman, J. Fernsler, N. Chattham, M. Nakata, Y. Takanishi, E. Koroblova, D.R. Link, R.F. Shao, W.G. Jang, J.E. MacLennan, O. Mondain-Monval, C. Boyer, W. Weissflog, G. Pelzl, L.C. Chien, J. Zasadzinski, J. Watanabe, M. Walba, H. Takezoe, N.A. Clark, Science 301 (2003) 1204–1211.
- [50] J.Y. Liu, M.G. Robison, K.M. Johnson, D.M. Wabba, M.B. Ros, N.A. Clark, R. Shao, D. Doroski, Opt. Lett. 15 (1990) 267.
- [51] J. Etxebarria, N. Pereda, C.L. Folcia, J. Ortega, Phys. Rev. E 57 (1998) 5634–5638.
- [52] I.D. Olenik, M. Copic, Phys. Rev. E 56 (1997) 581–591.
- [53] I.C. Khoo, H. Li, Y. Liang, IEEE J. Quant. Electron. 29 (1993) 1444–1447.
- [54] Hong Li, Yu Liang, I.C. Khoo, Mol. Cryst. Liq. Cryst. 251 (1994) 85.
- [55] E.V. Rudenko, A.V. Sukhov, JETP 78 (6) (1994) 875–882.
- [56] I.C. Khoo, H. Li, Y. Liang, Opt. Lett. 19 (1994) 1723.
- [57] I.C. Khoo, IEEE J. Quant. Electron. 32 (1996) 525–534.
- [58] I. Janossy, L. Szabados, Phys. Rev. E 58 (1998) 4598–4604.
- [59] D. Statman, E. Page, V.V. Werner, J.C. Lombard, Phys. Rev. E 75 (2007) Article Number: 021703.
- [60] L. Lucchetti, M. Gentili, Simoni, IEEE JQE 12 (2006) 422–430.
- [61] T.V. Truong, L. Xu, Y.R. Shen, Phys. Rev. E 72 (2005) Article Number: 051709.
- [62] I.C. Khoo, Opt. Lett. 20 (1996) 2137–2139.
- [63] G.P. Wiederrecht, B.A. Yoon, M.R. Wasielewski, Science 270 (1995) 1794–1797.
- [64] E. Buchnev, A. Dyadyusha, M. Kaczmarek, V. Reshetnyak, Y. Reznikov, J. Opt. Soc. Amer. B 24 (2007) 1512–1516.
- [65] I.C. Khoo, Kan Chen, Y. Zhang Williams, IEEE J. Selected Topics in Quantum Electronics 12 (3) (2006) 443–450.
- [66] X.D. Sun, F. Yao, Y. Pei, J. Appl. Phys. 102 (2007) Article Number: 013104.
- [67] I.C. Khoo, D.H. Werner, X. Liang, A. Diaz, B. Weiner, Opt. Lett. 31 (2006) 2592.
- [68] A. Diaz, J.H. Park, I.C. Khoo, JNOPM 16 (2007) 533–549.
- [69] I.C. Khoo, A. Diaz, Justin Liou, D. Werner, J.H. Park, Y. Ma, Junbin Huang, Mol. Cyrst. Liq. Cryst. (2009) (in press). Plenary paper presented at the 2nd Int. Workshop on Liquid Crystals for Photonics LCP 2008, Cambridge University, 21–23 July, 2008.
- [70] C.F. Bohren, D.R. Huffman, Absorption and Scattering of Light by Small Particles, Wiley, New York, 1983, pp. xiv, 530.
- [71] A.D. Rakic, A.B. Djuricic, J.M. Elazar, M.L. Majewski, Appl. Opt. 37 (22) (1998) 5271–5283 and references therein.
- [72] J.L. West, Mol. Cryst. Liq. Cryst. 157 (1988) 428.
- [73] P. Urzaic, J. Appl. Phys. 60 (1986) 2142.
- [74] V.P. Tondiglia, L.V. Natarajan, R.L. Sutherland, D. Tomlin, T.J. Bunning, Adv. Mater. 14 (2002) 187–191.
- [75] F. Vita, A. Marino, V. Tkachenko, G. Abbate, D.E. Lucchetta, L. Criante, F. Simoni, Rev. E 72 (2005) 011702.
- [76] R. Caputo, L. De Sio, A.V. Sukhov, A. Veltri, C. Umeton, Opt. Lett. 29 (2004) 1261.
- [77] G. Strangi, V. Barna, R. Caputo, A. de Luca, C. Versace, N. Scaramuzza, C. Umeton, R. Bartolino, Phys. Rev. Lett. 94 (2005) 63903.
- [78] A. Golemme, B.L. Volodin, E. Kippelen, N. Peyghambarian, Opt. Lett. 22 (1997) 1226–1228.
- [79] H. Ono, N. Kawatsuki, Jpn. J. Appl. Phys. 36 (1997) 6444–6448.
- [80] T. Ikeda, T. Sasaki, K. Ichimura, Nature 361 (1993) 428–430.
- [81] G. Anderson, I. Dahl, L. Komitov, S.T. Lagerwall, K. Skarp, B. Stebler, J. Appl. Phys. 66 (1989) 4983.
- [82] Thomas Tanggaard Larsen, Anders Bjarklev, David Sparre Hermann, Jes Broeng, Opt. Express 11 (2003) 2589–2596.
- [83] A. d’Alessandro, B. Nelline, D. Donisi, R. Beccerelli, R. Asquini, IEEE J. Quant. Electron. 42 (2006) 1084–1090.
- [84] E. Graugnard, J.S. King, S. Jain, C.J. Summers, Y. Zhang-Williams, I.C. Khoo, Phys. Rev. B 72 (2005) 233105 [4 pages].
- [85] K. Yoshino, Y. Shimoda, Y. Kawagishi, K. Nakayama, M. Ozaki, Appl. Phys. Lett. 75 (1999) 932–934.
- [86] A.E. Miroshnichenko, I. Pinkevych, Y.S. Kivshar, Opt. Express 14 (2006) 2839–2844.
- [87] T.K. Wu (Ed.), Frequency Selective Surface and Grid Array, Wiley & Sons, New York, 1995.
- [88] J.A. Bossard, X. Liang, L. Li, D.H. Werner, B. Weiner, P.F. Cristman, A. Diaz, I.C. Khoo, IEEE Trans. Antennas and Propagation 56 (2008) 1308–1320.
- [89] D.H. Werner, D.-H. Kwon, I.C. Khoo, A.K. Kildeshev, V.M. Shalaev, Opt. Express 15 (6) (2007) 3342–3347.
- [90] X. Wang, D.H. Kwon, D.H. Werner, I.C. Khoo, A. Kildeshev, V.M. Shalaev, Appl. Phys. Lett. 91 (2007) 143122.
- [91] Mark T. Gruneisen, James M. Wilkes, in: G. Burdge, S.C. Esener (Eds.), TOPS, vol. 14, 1997, pp. 220–226.
- [92] N. Konforti, E. Marom, S.T. Wu, Opt. Lett. 13 (1988) 251.
- [93] K. Komorowska, A. Miniewicz, J. Parka, F. Kajzar, J. Appl. Phys. 92 (2002) 5635–5641.
- [94] R.W. Hellwarth, J. Opt. Soc. Amer. 67 (1977) 1–3.
- [95] D.R. Evans, G. Cook, J.L. Carns, Mol. Cryst. Liq. Cryst. 488 (2008) 190–201.
- [96] Yu. Reznikov, O. Buchnev, O. Tereshchenko, V. Reshetnyak, A. Glushchenko, J. West, Appl. Phys. Lett. (2003) 1917–1919.
- [97] G. Cook, A.V. Glushchenko, V. Reshetnyak, A.T. Griffith, M.A. Saleh, D.R. Evans, Opt. Express 16 (2008) 4015–4022.
- [98] P. Aubourg, J.P. Huignard, M. Hareng, R.A. Muller, Appl. Opt. 21 (1982) 3706–3712.
- [99] F. Li, O. Buchnev, C. Il Cheon, A.A. Glushchenko, V.V. Reshetnyak, Y. Reznikov, T.J. Sluckin, J.L. West, Phys. Rev. Lett. 97 (2006) Article Number: 147801.
- [100] T.D. Wilkinson, X. Wang, K.B.K. Teo, W.I. Milne, Adv. Mater. 20, 363–366.

- [101] Andrew K. Kirby, Gordon D. Love, Opt. Express 12 (2004) 1470–1475.
- [102] B. Kiser, D. Pauluth, G. Gauglitz, Anal. Chim. Acta 434 (2001) 231–237.
- [103] S. Jen, N.A. Clark, P.S. Pershan, E.B. Priestley, J. Chem. Phys. 66 (1977) 4635–4661.
- [104] P. Yeh, C. Gu, Optics of Liquid Crystal Displays, Wiley, NY, 1999.
- [105] Małgorzata Kaczmarek, Andrey Dyadusha, Sergei Slussarenko, I.C. Khoo, J. Appl. Phys. 96 (2004) 2616–2623.
- [106] P. Pagliusi, G. Cipparrone, Phys. Rev. E 69 (2004) Article Number: 061708.
- [107] N.V. Tabiryan, C. Umeton, J. Opt. Soc. Amer. B15 (1998) 1912–1917.
- [108] I.C. Khoo, Mol. Cryst. Liq. Cryst. 282 (1996) 53–66.
- [109] I.C. Khoo, R. Normandin, IEEE J. Quant. Electron. 21 (1985) 329–335.
- [110] J. Li, S. Gauza, S.T. Wu, J. Appl. Phys. 96 (2004) 19–24.
- [111] I.C. Khoo, R.G. Lindquist, R.R. Michael, R.J. Mansfield, P. Lopresti, J. Appl. Phys. 69 (1991) 3853–3859.
- [112] I.C. Khoo, J.Y. Hou, G.L. Din, Y.L. He, D.F. Shi, Phys. Rev. A 42 (1990) 1001–1004.
- [113] I.C. Khoo, H. Li, Y. Liang, Opt. Lett. 18 (1993) 1490–1492.
- [114] R. Ramos-Garcia, I. Lazo-Martinez, I. Guizar-Iturbide, A. Sanchez-Castillo, M. Boffety, P. Ruck, Mol. Cryst. Liq. Cryst. 454 (2006) 179–185.
- [115] A.S. Kuzhelev, A.E. Dudelezak, J. Opt. A (2003) L5–L8.
- [116] F. Sanchez, P.H. Kayoun, J.P. Huignard, J. Appl. Phys. 64 (1988) 26.
- [117] L. Richard, J. Maurin, J.P. Huignard, Opt. Commun. 57 (1986) 365.
- [118] I.C. Khoo, S. Shepard, J. Appl. Phys. 54 (1983) 5491.
- [119] P.Y. Yan, I.C. Khoo, IEEE J. Quant. Electron. 25 (1989) 520.
- [120] R.P. Pan, C.F. Hsieh, C.L. Pan, C.Y. Chen, J. Appl. Phys. 103, Article Number: 2008.
- [121] J. Li, S.T. Wu, S. Brugioni, R. Meucci, S. Faetti, J. Appl. Phys. 97 (2005) Article Number: 073501.
- [122] F.W. Deeg, M.D. Fayer, Chem. Phys. 91 (1989) 2269.
- [123] J. Prost, J.R. Lalanne, Phys. Rev. A 8 (1973) 2090.
- [124] J.R. Lalanne, B. Martin, B. Pouliquen, Mol. Cryst. Liq. Cryst. 42 (1977) 153.
- [125] C. Flytzanis, Y.R. Shen, Phys. Rev. Lett. 33 (1974) 14.
- [126] G.K.L. Wong, Y.R. Shen, Phys. Rev. Lett. 30 (1973) 895–897.
- [127] G.D. Gottke, H. Cang, B.B. Bagchi, M.D. Fayer, J. Chem. Phys. 116 (2002) 6339–6347.
- [128] R. Muenster, M. Jarasch, X. Zhuang, Y.R. Shen, Phys. Rev. Lett. 78 (1997) 42–45.
- [129] K. Horii, K. Sakai, Phys. Rev. E 73 (2006) Article Number: 011709.
- [130] D. Fekete, J. Au Yeung, A. Yariv, Opt. Lett. 5 (1980) 51.
- [131] P.A. Madden, F.C. Saunders, A.M. Scott, IEEE J. Quant. Electron. QE-22 (1986) 1287.
- [132] P. Chatelain, Ada Crystallogr. 1 (1948) 315.
- [133] I.C. Khoo, Phys. Rev. A 27 (1983) 2747–2750.
- [134] N.V. Tabiryan, B.Ya. Zel'dovich, Mol. Cryst. Liq. Cryst. 69 (1981) 19–36.
- [135] H.L. Ong, R.B. Mayer, J. Opt. Soc. Amer. A 2 (1985) 198–201.
- [136] I.C. Khoo, P.Y. Yan, T.H. Liu, J. Opt. Soc. Amer. B 4 (1987) 115, and references therein.
- [137] E. Brasselet, A. Lherbier, L.J. Dube, J. Opt. Soc. Amer. B 23 (2006) 36–44.
- [138] E. Brasselet, B. Doyon, T.V. Galstian, L.J. Dub, Phys. Rev. E 69 (2004) Article Number: 021701.
- [139] J.J. Wu, S.H. Chen, J.Y. Fan, G.S. Ong, J. Opt. Soc. Amer. B 7 (1990) 1147–1157.
- [140] C. Conti, M. Peccianti, G. Assanto, Phys. Rev. Lett. 92 (2004) Article Number: 113902.
- [141] G. Demeter, D.O. Krimer, Phys. Rep. 448 (2007) 133–162.
- [142] X. Hutsebaut, C. Cambournac, M. Haelterman, J. Beeckman, K. Neyts, J. Opt. Soc. Amer. B 22 (2005) 1424–1431.
- [143] I.C. Khoo, R. Normandin, Appl. Phys. 55 (1984) 1416.
- [144] I.C. Khoo, R. Normandin, J. Appl. Phys. 55 (1984) 1416–1418.
- [145] H.J. Eichler, R. Macdonald, Phys. Rev. Lett. 67 (1991) 2666.
- [146] W.M. Gibbons, P.J. Shannon, S.-T. Sun, B.J. Swetlin, Nature (London) 351 (1991) 49–50.
- [147] I.C. Khoo, M.Y. Shih, M.V. Wood, B.T. Guenther, P.H. Chen, F. Simoni, S.S. Slussarenko, O. Francescangeli, L. Lucchetti, Proc. IEEE 87 (11) (1999) 1911–1987.
- [148] M. Kaczmarek, M.Y. Shih, R.S. Cudney, I.C. Khoo, IEEE J. Quant. Electron. 38 (2002) 451–457.
- [149] I.C. Khoo, M.Y. Shih, A. Shishido, P.H. Chen, M.V. Wood, Opt. Mater. 18 (2001) 85–90.
- [150] I.C. Khoo, P.H. Chen, M.Y. Shih, A. Shishido, S. Slussarenko, Mol. Cryst. Liq. Cryst. 358 (2001) 1–13.
- [151] A.T. Shishido, O. Tsutsumi, A. Kanazawa, T. Shiono, T. Ikeda, N. Tamai, J. Amer. Chem. Soc. 119 (1997) 7791–7796 and references therein. See also reference.
- [152] Y.L. Yu, T. Ikeda, J. Photochem. Photobiol. C – Photochem. Rev. 5 (2004) 247–265.
- [153] J. Mun, C.S. Yoon, H.-W. Kim, S.-A. Choi, J.-D. Kim, Appl. Phys. Lett. 79 (13) (2001) 1933–1935.
- [154] P. Pagliusi, G. Cipparrone, Appl. Phys. Lett. 80 (2) (2002) 168–170.
- [155] P. Pagliusi, G. Cipparrone, J. Appl. Phys. 92 (9) (2002) 4863–4869.
- [156] P. Pagliusi, G. Cipparrone, J. Appl. Phys. 93 (11) (2003) 9116–9122.
- [157] I.C. Khoo, Yana Zhang Williams, B. Lewis, T. Mallouk, Mol. Cryst. Liq. Cryst. 446 (2005) 233–244.
- [158] T. Sasaki, N. Moriya, N. Iwasaki, J. Phys. Chem. 111 (2007) 17646–17652.
- [159] M. Kaczmarek, A. Dyadusha, S. Slussarenko, I.C. Khoo, J. Appl. Phys. 96 (2004) 2616–2623.
- [160] X.D. Sun, F.F. Yao, Y.B. Pei, J.L. Zhang, Appl. Phys. Lett. 90 (2007) Article Number: 201115.
- [161] Y.P. Huang, T.Y. Tsai, W. Lee, W.K. Chin, Y.M. Chang, H.Y. Chen, Opt. Express 13 (2005) 2058–2063.
- [162] W. Helfrich, J. Chem. Phys. 51 (1969) 4092.
- [163] J. Zhang, V. Ostroverkhov, K.D. Singer, V. Reshetnyak, Y. Reznikov, Opt. Lett. 25 (2000) 414–416.
- [164] M.E. Mack, Phys. Rev. Lett. 22 (1969) 13.
- [165] H.J. Eichler, P. Gunter, D.N. Pohl, Laser Induced Dynamic Grating, Springer-Verlag, Berlin, 1986.
- [166] H. Hsiung, L.P. Shi, Y.R. Shen, Phys. Rev. A 30 (1984) 1453.
- [167] H. Ono, Y. Harato, J. Opt. Soc. Amer. B 16 (1989) 2195–2201.
- [168] I.C. Khoo, J. Modern Opt. 37 (1990) 1801.
- [169] B.Ya. Zeldovich, S.K. Merzlikin, N.F. Pilipetskii, A.V. Sukhov, JETP Lett. (Engl. Transl.) 41 (1985) 515.
- [170] I.C. Khoo, H. Li, Y. Liang, Opt. Lett. 18 (1993) 1490–1492.
- [171] P. Etchegoin, R.T. Phillips, Phys. Rev. E 54 (1996) 2637–2646.
- [172] I.C. Khoo, Y. Liang, H. Li, Opt. Lett. 20 (1995) 130–132. See also Ref. [225].
- [173] I.C. Khoo, J. Ding, Appl. Phys. Lett. 81 (2002) 2496–2498.
- [174] P. Etchegoin, R.T. Phillips, Phys. Rev. E 55 (1997) 5603–5612.
- [175] I.C. Khoo, S.L. Zhuang, S. Shepard, Appl. Phys. Lett. 39 (1981) 937.
- [176] I.C. Khoo, G. Finn, R.R. Michael, T.H. Liu, Opt. Lett. 11 (1986) 227.
- [177] R.P. Pan, S.M. Chen, C.L. Pan, J. Opt. Soc. Amer. B 8 (1991) 1065–1071.
- [178] I.C. Khoo, J.Y. Hou, T.H. Liu, P.Y. Yan, R.R. Michael, G.M. Finn, J. Opt. Soc. Amer. B 4 (1987) 886.
- [179] I.C. Khoo, R.R. Michael, G.M. Finn, Appl. Phys. Lett. 52 (1988) 2108–2110.

- [180] I.C. Khoo, M.V. Wood, B.D. Guenther, Min-Yi Shih, P.H. Chen, Zhaogen Chen, Xumu Zhang, Opt. Express 2 (12) (1998) 471–482.
- [181] E. Braun, L.P. Faucheuix, A. Libchaber, Phys. Rev. A 48 (1993) 611–622.
- [182] J.J. Wu, S.H. Chen, J.Y. Fan, G.S. Ong, J. Opt. Soc. Amer. B 7 (1990) 1147–1157.
- [183] P.P. Etchegoin, R.T. Phillips, Phys. Rev. E 54 (1996) 2637–2646.
- [184] I.C. Khoo, M.V. Wood, B.D. Guenther, Min-Yi Shih, P.H. Chen, Zhaogen Chen, Xumu Zhang, Opt. Express 2 (12) (1998) 471–482.
- [185] H. Vach, C.T. Seaton, G.I. Stegeman, I.C. Khoo, Opt. Lett. 9 (1984) 238–240.
- [186] M. Peccianti, A. De Rossi, G. Assanto, A. De Luca, C.P. Umeton, I.C. Khoo, Appl. Phys. Lett. 77 (2000) 7–9.
- [187] M.A. Karpierz, Phys. Rev. E 66 (2002) Article Number: 036603.
- [188] M. Peccianti, K.A. Brzakiewicz, G. Assanto, Opt. Lett. 27 (2002) 1460–1462.
- [189] A.A. Minzoni, N.F. Smyth, A.L. Worthy, J. Opt. Soc. Amer. B 24 (2007) 1549–1556.
- [190] P.D. Rasmussen, O. Bang, W. Krolikowski, Phys. Rev. E 72 (2005) Article Number: 066611.
- [191] A. De Luca, G. Coschignano, C. Umeton, M. Morabito, Opt. Express 14 (2006) 5548–5557.
- [192] I.C. Khoo, Appl. Phys. Lett. 40 (1982) 645–647.
- [193] I.C. Khoo, J.Y. Hou, J. Opt. Soc. Amer. B 2 (1985) 761–766.
- [194] F. Simoni, G. Cipparrone, C. Umeton, I.C. Khoo, Opt. Lett. 13 (1988) 886–888.
- [195] I.C. Khoo, P. Zhou, R.R. Michael, R.G. Lindquist, R.J. Mansfield, IEEE J. Quant. Electron. 25 (1989) 1755–1759.
- [196] I.C. Khoo, R.R. Michael, R.J. Mansfield, R.G. Lindquist, P. Zhou, G. Cipparrone, F. Simoni, J. Opt. Soc. Amer. B 8 (1991) 1464–1470.
- [197] I.C. Khoo, Ping Zhou, J. Opt. Soc. Amer. B 6 (1989) 884–888.
- [198] I.C. Khoo, Jae-Hong Park, Justin Liou, Appl. Phys. Lett. 90 (2007) Article Number: 151107.
- [199] L.G. Deng, H.K. Liu, Opt. Eng. 42 (2003) 2936–2941.
- [200] I.C. Khoo, M.V. Wood, B.D. Guenther, Min-Yi Shih, P.H. Chen, Zhaogen Chen, Xumu Zhang, Opt. Express 2 (12) (1998) 471–482.
- [201] I.C. Khoo, M.V. Wood, M.Y. Shih, P.H. Chen, Opt. Express 4 (11) (1999) 431–442.
- [202] I.C. Khoo, A. Diaz, S. Kubo, J. Liou, Mike Stinger, T. Mallouk, J.H. Park, Mol. Cryst. Liq. Cryst. 485 (1) (2008) 934–944.
- [203] Y.R. Shen, Liq. Cryst. 5 (1989) 635.
- [204] X. Zhuang, P.B. Miranda, D. Kim, Y.R. Shen, Phys. Rev. B 59 (1999) 12632–12640.
- [205] M. Oh-e, H. Yokoyama, S. Yorozuya, K. Akagi, M.A. Belkin, Y.R. Shen, Mol. Cryst. Liq. Cryst. 436 (2005) 1027–1035.
- [206] Z.-C. Ou-Yang, Y.-Z. Xie, Phys. Rev. A 32 (1986) 1189.
- [207] S.-J. Gu, S.K. Saha, G.K. Wong, Mol. Cryst. Liq. Cryst. 69 (1981) 287.
- [208] A.V. Sukhov, R.V. Timashev, (Engl. Transl.) 51 (7) (1990) 415.
- [209] J.Y. Liu, M.G. Robison, K.M. Johnson, D.M. Wabba, M.B. Ros, N.A. Clark, R. Shao, D. Doroski, Opt. Lett. 15 (1990) 267.
- [210] I.C. Khoo, P. Zhou, Phys. Rev. A 41 (1990) 1544.
- [211] I.C. Khoo, T.H. Liu, Phys. Rev. A 39 (1989) 4036.
- [212] I.C. Khoo, Phys. Rev. Lett. 64 (1990) 2273–2275.
- [213] I.C. Khoo, Hong Li, Yu Liang, IEEE J. Quant. Electron. 29 (1993) 12.
- [214] I.C. Khoo, Brett D. Guenther, M.V. Wood, P. Chen, Min-Yi Shih, Opt. Lett. 22 (1997) 1229–1231.
- [215] D.C. Jones, G. Cook, Opt. Commun. 232 (2004) 399–409.
- [216] W. Lee, S.L. Yeh, C.C. Chang, C.C. Lee, Opt. Express 9 (2001) 791–795.
- [217] I.C. Khoo, Min-Yi Shih, M.V. Wood, B.D. Guenther, P.H. Chen, F. Simoni, S. Slussarenko, O. Francescangeli, L. Lucchetti, IEEE Proc. 87 (11) (1999) 1897–1911.
- [218] I.C. Khoo, Brett D. Guenther, M.V. Wood, P. Chen, Min-Yi Shih, Opt. Lett. 22 (1997) 1229–1231.
- [219] U. Bortolozzo, S. Residori, J.P. Huignard, J. Appl. Phys. 41 (2008) Article Number: 224007.
- [220] A. Brignon, I. Bongrand, B.B. Loiseaux, J.P. Huignard, Opt. Lett. 22 (1997) 1855–1857.
- [221] I.C. Khoo, S.L. Zhuang, IEEE J. Quant. Electron. 18 (1981) 246.
- [222] A.S. Koujelev, A.E. Dzeluzak, Opt. Eng. 46 (2007) Article Number: 024001.
- [223] U. Bortolozzo, S. Residori, J.P. Huignard, Opt. Lett. 32 (2007) 829–831.
- [224] I.C. Khoo, R.R. Michael, P.Y. Yan, IEEE J. Quant. Electron. 23 (1987) 1344.
- [225] I.C. Khoo, Y. Liang, Phys. Rev. E 62 (2000) 6722–6733. See also Refs. [170,172].
- [226] O.L. Antipov, Opt. Commun. 103 (1993) 499.
- [227] O.L. Antipov, N.A. Dvoryaninov, V. Sheshkauskas, JETP. Lett. 53 (1991) 610.
- [228] L. Lucchetti, M. Di Fabrizio, M.M. Gentili, F. Simoni, Appl. Phys. Lett. 83 (2003) 5389–5391.
- [229] Y.R. Shen, H.K. Hsu, S.H. Chen, J. Opt. Soc. Amer. B 20 (2003) 65–72.
- [230] A.S. Koujelev, A.E. Dzeluzak, Opt. Eng. 46 (2007) Article Number: 024001.
- [231] J. Mysliwiec, S. Bartkiewicz, K. Janus, Opt. Commun. 276 (2007) 58–61.
- [232] I.C. Khoo, J. Ding, A. Diaz, Y. Zhang, K. Chen, Mol. Cryst. Liq. Cryst. 375 (2002) 33–44.
- [233] I.C. Khoo, R. Normandin, Appl. Phys. Lett. 47 (1985) 350.
- [234] K. Sayyah, U. Efron, Opt. Lett. 21 (1996) 1384–1386.
- [235] T.H. Barnes, T. Eiju, K. Matusda, N. Ooyama, Appl. Opt. 28 (1989) 4845–4852.
- [236] M.Y. Shih, I.C. Khoo, A. Shishido, M.V. Wood, P.H. Chen, Opt. Lett. 25 (2000) 978–980.
- [237] M.Y. Shih, A. Shishido, I.C. Khoo, Opt. Lett. 26 (2001) 1140–1142. See also Ref. [147].
- [238] C.S. Yelleswarapu, S.R. Kothapally, F.J. Aranda, D.V.G.L.N. Rao, Y.R. Vaillancourt, B.R. Kimball, Appl. Phys. Lett. 89 (2006) Article # 211116.
- [239] N. Bloembergen, Nonlinear Optics, Benjamin, New York, 1965.
- [240] G.K.L. Wong, Y.R. Shen, Phys. Rev. Lett. 32 (1974) 527–529.
- [241] S.D. Durbin, S.M. Arakelian, Y.R. Shen, Opt. Lett. 6 (1981) 411–413.
- [242] I.C. Khoo, Phys. Rev. A 25 (1982) 1636–1644.
- [243] E. Santamato, Y.R. Shen, Opt. Lett. 9 (1984) 564–566.
- [244] I.C. Khoo, J.Y. Hou, T.H. Liu, P.Y. Yan, R.R. Michael, G.M. Finn, J. Opt. Soc. Amer. B 4 (1987) 886–891.
- [245] F. Lederer, G.I. Stegeman, D.N. Christodoulides, G. Assanto, M. Segev, Y. Silberberg, Phys. Rep. 463 (2008) 1–126.
- [246] See for example the work featured in A. Buka, L. Kramer (Eds.), Pattern Formation in Liquid Crystals, Springer, New York, 1996.
- [247] E. Louvergneaux, Phys. Rev. E 87 (2001) Article Number: 244501.
- [248] F. Tito Arechi, Stefano Boccaletti, PierLuigi Ramazza, Phys. Rep. 318 (1999) 1–83.
- [249] B.Ya. Zeldovich, S.K. Merzlikin, N.F. Pilipetskii, A.V. Sukhov, JETP Lett. (Engl. Transl.) 41 (1985) 515.
- [250] I.C. Khoo, A. Diaz, Phys. Rev. E 68 (2003) 042701-1–042701-4.
- [251] Iam Choon Khoo, Jianwu Ding, Andres Diaz, J. Opt. Soc. Amer. B 22 (2005) 844–851.
- [252] Michael V. Stinger, Andres Diaz, Justin D. Liou, Iam-Choon Khoo, (unpublished).
- [253] F.C. Hoppensteadt, E.M. Izhikevich, Phys. Rev. Lett. 82 (1999) 2983–2986.
- [254] T.B. Simpson, J.M. Liu, A. Gavrielides, V. Kovanis, P.M. Alsing, Phys. Rev. A 51 (1995) 4181.
- [255] O. Sandfuchs, F. Kaiser, M.R. Belic, Phys. Rev. A 64 (2001) 063809.
- [256] G. D'Alessandro, W.J. Firth, Phys. Rev. Lett. 66 (1991) 2597.
- [257] V. Carbone, G. Cipparrone, C. Versace, C. Umeton, R. Bartolino, Phys. Rev. E 54 (1996) 6948–6951.
- [258] G. Cipparrone, V. Carbone, C. Versace, C. Umeton, R. Bartolino, F. Simoni, Phys. Rev. E 47 (1993) 3741.
- [259] G. Russo, V. Carbone, G. Cipparrone, Phys. Rev. E 62 (2000) 5036.

- [260] V. Carbone, G. Cipparrone, G. Russo, Phys. Rev. E 63 (2001) 051701.
- [261] G. Demeter, L. Kramer, Phys. Rev. E 64 (2001) 20701.
- [262] G. Demeter, Phys. Rev. E 61 (2000) 6678.
- [263] Y. Owechko, IEEE J. Quant. Electron. 25 (1989) 619–634.
- [264] C. Gorecki, B. Trolard, Opt. Eng. 37 (1998) 924–930.
- [265] K. Komorowska, A. Mineiwicz, J. Parka, F. Kajzar, J. Appl. Phys. 92 (2002) 5635–5641.
- [266] V.A. Berenberg, L.A. Beresnev, A.N. Chaika, M.T. Gruneisen, W. Haase, A.A. Leshchhev, A.P. Onokhov, M.V. Vasil'ev, V.Y. Venediktov, Ferroelectrics 246 (2000) 1153–1164.
- [267] V.A. Berenberg, A.P. Onokhov, J. Opt. Tech. 68 (2001) 672–676.
- [268] ANSI Standard Z136.1, American National Standard for the Safe Use of Lasers, American National Standards Institute, Inc., New York, 2000.
- [269] L.W. Tutt, T.F. Boggess, Prog. Quantum Electron. 17 (1993) 299–338.
- [270] C.W. Spangler, J. Mater. Chem. 9 (1999) 2013–2020.
- [271] R.L. Sutherland, M.C. Brant, D.M. Brandelik, P.A. Fleitz, D.G. McLean, T. Pottenger, Opt. Lett. 18 (1993) 858–860.
- [272] J. Barroso, A. Costela, I. Garcia-Moreno, J.L. Saiz, J. Phys. Chem. A 102 (1998) 2527–2532.
- [273] T. Xia, D.J. Hagan, A. Dogariu, A.A. Said, E.W. Van Stryland, Appl. Opt. 36 (1997) 4110–4122.
- [274] J.E. Ehrlich, X.L. Wu, I.Y.S. Lee, Z.Y. Hu, H. Rockel, S.R. Marder, J.W. Perry, Opt. Lett. 22 (1997) 1843–1845.
- [275] G.S. He, T.-C. Lin, P.N. Prasad, C.-C. Cho, L.-J. Yu, Appl. Phys. Lett. 82 (2003) 4717–4719.
- [276] I.C. Khoo, A. Diaz, M.V. Wood, P.H. Chen, IEEE J. Sel. Topics Quantum Electron. 7 (2001) 760–768.
- [277] I.C. Khoo, Andres Diaz, J. Ding, J. Opt. Soc. Amer. B 21 (2004) 1234–1240.
- [278] I.C. Khoo, IEEE J. Sel. Topics Quantum Electron. 14 (3) (2008) 946–951.
- [279] J.L. Carns, G. Cook, M.A. Saleh, S.V. Serak, N.V. Tabiryan, D.R. Evans, Opt. Lett. 31 (2006) 993–995.
- [280] S. Kurihara, K. Masumoto, T. Nonaka, Appl. Phys. Lett. 73 (1998) 160–162.
- [281] U. Urbas, J. Klosterman, V. Tondiglia, L. Natarajan, R. Sutherland, S. Tsutsumi, T. Ikeda, T. Bunning, Adv. Mater. 16, 1453–2004.
- [282] I.C. Khoo, J.H. Park, J.D. Liou, J. Opt. Soc. Amer. B 25 (2008) 1931–1937.
- [283] See for example Ping Sheng, Phys. Rev. A 26 (1982) 1610–1617.
- [284] T. Sasaki, N. Moriya, Y. Iwasaki, J. Phys. Chem. C 111 (2007) 17646–17652.
- [285] R.P. Lemieux, Soft Matter 1 (2005) 348–354.
- [286] D.S. Hermann, P. Rudquist, S.T. Lagerwall, L. Komitov, B. Stebler, M. Lindgren, M. Trollsas, F. Sahlen, A. Hult, U.W. Gedde, C. Orrenius, T. Norin, Liq. Cryst. 24 (1998) 295–310.
- [287] M. Lindgren, D.S. Hermann, J. Ortegren, P.O. Arntzen, U.W. Gedde, A. Hult, L. Komitov, S.T. Lagerwall, P. Rudquist, B. Stebler, F. Sahlen, M. Trollsas, J. Opt. Soc. Amer. B 15 (1998) 914–922.
- [288] V.S.U. Fazio, V. Zauls, S. Schrader, P. Busson, A. Hult, S.T. Lagerwall, H. Motschmann, Mol. Cryst. Liq. Cryst. 467 (2001) 4061–4070.
- [289] M. Kreuzer, E. Benkler, D. Paparo, G. Casillo, L. Marrucci, Phys. Rev. E 68 (2003) Article # 011701.
- [290] S. Juodkazis, S. Matsuo, N. Murazawa, I. Hasegawa, H. Misawa, Appl. Phys. Lett. 82 (2003) 4657–4659.
- [291] I. Janossy, Opt. Lett. 33 (2008) 2371–2373.
- [292] B. Piccirillo, A. Vella, A. Setaro, E. Santamato, Phys. Rev. E 73 (2006) Article # 062701.
- [293] E. Brasselet, L.J. Dube, Phys. Rev. E 73 (2006) Article # 021704.
- [294] E. Brasselet, B. Doyon, T.V. Galstian, L.J. Dub, Phys. Rev. E 67 (2003) Article # 031706.
- [295] E. Brasselet, T.V. Galstian, L.J. Dube, D.O. Krimer, L. Kramer, J. Opt. Soc. Amer. B 22 (2005) 1671–1680.
- [296] E. Brasselet, L.J. Dube, Mol. Cryst. Liq. Cryst. 453 (2006) 93–105.
- [297] A. Ashkin, Proc. Natl. Acad. Sci. USA 94 (1997) 4853–4860.
- [298] H.F. Gleeson, T.A. Wood, M. Dickinson, Philos. Trans. Roy. Soc. A (2006) 2789–2805.
- [299] N. Murazawa, S. Juodkazis, S. Matsuo, H. Misawa, Small 1 (2005) 656–661.
- [300] I.I. Smalyukh, A.N. Kuzmin, A.V. Kachynski, P.N. Prasad, O.D. Lavrentovich, Appl. Phys. Lett. 86 (2005) Article # 021913.
- [301] J.-I. Hotta, K. Sasaki, H. Masuhara, Appl. Phys. Lett. 71 (1997) 2085–2087.
- [302] D.K. Yoon, M.C. Choi, Y.H. Kim, M.W. Kim, O.D. Lavrentovich, H.T. Jung, Nature Mater. 6 (2007) 866–870.
- [303] See for example S. Residori, U. Bortolozzo, J.P. Huignard, Phys. Rev. Lett. 100 (2008) Article # 203603.
- [304] M. Pedersen, L. Rishøj, H. Steffensen, S. Xiao, N. Mortensen, Opt. Quant. Electron. 39 (2007) 903–911.
- [305] I.C. Khoo, Appl. Phys. Lett. 41 (1982) 909–911.
- [306] M.M. Cheung, S.D. Durbin, Y.R. Shen, Opt. Lett. 8 (1983) 39–41.
- [307] I.C. Khoo, J.Y. Hou, R. Normandin, V.C.Y. So, Phys. Rev. A 27 (1983) 3251–3257.
- [308] I.C. Khoo, J.Y. Hou, J. Opt. Soc. Amer. B 2 (1985) 761–766.
- [309] P.-Y. Wang, J.-H. Dai, H.-J. Zhang, Phys. Rev. A 41 (1990) 3250–3257.
- [310] M. Talarico, A. Golemme, Nature Mater. 5 (2006) 185–188.
- [311] G. D'Alessandro, A.A. Wheeler, Phys. Rev. A 67 (2003) Article # 023816.
- [312] S. Hoogland, J.J. Baumberg, S. Coyle, J. Baggett, M.J. Coles, H.J. Coles, Phys. Rev. A 66 (2002) Article # 055801.
- [313] A.E. Kaplan, JETP Lett. 24 (1976) 114.
- [314] I.C. Khoo, Appl. Phys. Lett. 40 (1982) 645–647.
- [315] I.C. Khoo, P. Zhou, Opt. Lett. 17 (1992) 1325–1327.
- [316] S.V. Serak, H.J. Eichler, A.A. Kovalev, T.A. Davidovich, Opt. Commun. 196 (2001) 269–280.
- [317] U. Bortolozzo, A. Montina, F.T. Arecchi, J.P. Huignard, S. Residori, Phys. Rev. Lett. 99 (2007) Article # 023901.
- [318] S. Residori, U. Bortolozzo, A. Montina, F.T. Arecchi, J.-P. Huignard, J. Nonlinear Opt. Phys. 16 (2007) 343–357.
- [319] A. Montina, U. Bortolozzo, S. Residori, J.P. Huignard, F.T. Arecchi, Phys. Rev. A 76 (2007) Article # 033826.
- [320] F.L. Zhang, Q. Zhao, D.P. Gaillot, X.P. Zhao, D. Lippens, J. Opt. Soc. Amer. B 25 (2008) 1920–1925.
- [321] S.V. Serak, N.V. Tabiryan, T.J. Bunning, J. Nonlinear Opt. Phys. Mater. 16 (2007) 471–483.
- [322] V.A. Belyakov, Mol. Cryst. Liq. Cryst. 467 (2007) 155–169.
- [323] A.E. Mirosnichenko, E. Brasselet, Y.S. Kivshar, Phys. Rev. A 78 (2008) Article # 053823.
- [324] N.V. Tabiryan, S.R. Nersisyan, Opt. Eng. 41 (2002) 2876–2889.
- [325] M. Marangoni, R. Osellame, R. Ramponi, M. Buscaglia, T. Bellini, F. Mantegazza, Appl. Phys. Lett. 81 (2002) 2337–2339.
- [326] T. Matsui, M. Ozaki, K. Yoshino, J. Opt. Soc. Amer. B 21 (2004) 1651–1658.
- [327] H. Ono, M. Ito, Jpn. J. Appl. Phys. Part 2 - Lett. 40 (2001) L206–L208.
- [328] A. d'Alessandro, D. Donisi, L. De Sio, R. Beccherelli, R. Asquini, R. Caputo, C. Umeton, Opt. Express 16 (2008) 9254–9260.
- [329] D.P. Gaillot, E. Graugnard, J.S. King, C.J. Summers, J. Opt. Soc. Amer. B 24 (2007) 990.